UNIVERSITEIT VAN PRETORIA
UNIVERSITY OF PRETORIA
YUNIBESITHI YA PRETORIA

PHYSICAL MODELLING OF A SOIL WALL REINFORCED WITH EXTENSIBLE AND INEXTENSIBLE REINFORCEMENT

SHAUN FRIEDRICH CRAMER

A dissertation submitted in partial fulfilment of the requirements for the degree of

MASTER OF ENGINEERING (GEOTECHNICAL ENGINEERING)

In the

FACULTY OF ENGINEERING, BUILT ENVIRONMENT AND INFORMATION TECHNOLOGY

UNIVERSITY OF PRETORIA

June 2022

DISSERTATION SUMMARY

PHYSICAL MODELLING OF A SOIL WALL REINFORCED WITH EXTENSIBLE AND INEXTENSIBLE REINFORCEMENT

SHAUN FRIEDRICH CRAMER

Supervisor: Professor SW Jacobsz

Department: Civil Engineering

University: University of Pretoria

Degree: Master of Engineering (Geotechnical Engineering)

Reinforced soil walls are structures that make use of reinforcement elements to retain soils at slopes for a variety of engineering applications. The reinforcement elements provide the necessary tensile strength to the soil body to resist shearing and failure within the soil. The reinforced soil principle was patented as recently as 1963 by inventor Henri Vidal, and various types of reinforcing materials have been the subject of investigation and research both in the laboratory and in the field. Steel and geosynthetics are the two most common reinforcement materials used in soil walls. Steel reinforcement is considered inextensible and geosynthetic reinforcement extensible due to the inherent elastic modulus of the materials.

Since the rise of geosynthetics in industry and the subsequent challenge posed to conventional steel reinforcement, it was pertinent to directly compare the performance of a soil wall reinforced with both types of reinforcement under surcharge loading. This was done by constructing four small-scale vertical soil walls, tested in the geotechnical centrifuge at the University of Pretoria with extensible (PVC) and inextensible (brass) reinforcement strips and applying a surcharge load onto the retained soil behind the walls at a centrifugal acceleration of 30 G. The models were constructed with metallic U-shaped facing panels and backfilled with fine silica sand. The horizontal displacement of the facing was measured with displacement transformers, the soil strain was captured using particle image velocimetry analysis, and the reinforcement strains were recorded with conventional strain gauges and fibre optic technology by means of fibre Bragg gratings.

The results of the experiments showed that the soil walls reinforced with inextensible reinforcement exhibited rigid behaviour during loading, deformation of the wall facing was

resisted with a wall stiffness four times larger than with extensible reinforcement, and low magnitudes of reinforcement strains were recorded. On the other hand, the soil walls reinforced with extensible reinforcement exhibited flexible behaviour as the facing displaced eight times more, and the reinforcement strains were one order of magnitude larger than the rigid counterpart. The results also showed the Coulomb tie-back wedge method to adequately describe the behaviour of the extensible reinforced soil wall as the reinforcement strains peaked at the theoretical maximum tension locations, or the Coulomb failure plane.

These conclusions indicate the significant role extensibility of reinforcement plays within the operation and performance of soil walls. The type of reinforcement material installed in a soil wall significantly affects the wall response to loading and must be selected carefully to ensure that safe soil walls are constructed for the appropriate applications.

DECLARATION

I, the undersigned hereby declare that:

- I understand what plagiarism is and I am aware of the University's policy in this regard;
- The work contained in this thesis is my own original work;
- I did not refer to work of current or previous students, lecture notes, handbooks or any other study material without proper referencing;
- Where other people's work has been used this has been properly acknowledged and referenced;
- I have not allowed anyone to copy any part of my thesis;
- I have not previously in its entirety or in part submitted this thesis at any university for a degree.

Signature of student: 

Name of student: **Shaun Cramer**

Student number: **10018825**

Date: **09/06/2022**

ACKNOWLEDGEMENTS

I wish to express my appreciation to the following organisations and persons who made this project dissertation possible:

a) Professor SW Jacobsz, my supervisor, for his guidance and continued support during the course of the study.

b) Mr L Maritz from Reinforced Earth (Pty) Ltd South Africa, for the financial support and opportunity to do the research.

c) Mr J Vermaak for his assistance in the laboratory during the construction and testing of the physical models.

d) My wife and family for their encouragement and support during the study.

e) The Lord my God for all the strength to complete the dissertation.

TABLE OF CONTENTS

LIST OF TABLES

LIST OF FIGURES

LIST OF SYMBOLS

K_a	Active lateral earth pressure coefficient
δ'	Angle of friction between soil and reinforcement
K_0	At rest lateral earth pressure coefficient
F	Axial force in reinforcement (N)
λ_B	Bragg wavelength (nm)
C_U	Coefficient of uniformity
a_r	Cross-sectional area of reinforcement (m^2)
ρ_w	Density of water (kg/m^3)
a_rE_r	Effective stiffness of the reinforcement (N)
b	Element width (mm)
n_{eff}	Fibre effective refractive index
ε_{fibre}	Fibre optic strain
T_f	Frictional resistance (N)
Λ	Grating periodicity
δh	Horizontal deformation
σ_h	Horizontal stress (Pa)
S_x	Horizontal spacing of reinforcement (m)
D_{10}	Largest sieve size through which 10% of the soil particles pass
D_{60}	Largest sieve size through which 60% of the soil particles pass
σ	Normal stress in soil (Pa)
E_r	Reinforcement elastic stiffness (N/m^2)
L_e	Reinforcement length in resistant zone (m)
τ	Reinforcement shear stress (Pa)
ε_r	Reinforcement strain
σ_r	Reinforcement stress (N/m2)
I_D	Relative density
z	Soil depth (m)
ρ_d	Soil dry density (kg/m^3)
ϕ'	Soil friction angle (°)
H	Soil wall height
G_s	Specific gravity of soil particles
K_ε	Strain coefficient
q	Surcharge (N/m^2)
K_T	Temperature coefficient
T	Tensile force in reinforcement (N)
T_w	Total tensile resistant force (N)
γ	Unit weight of soil (N/m^3)
δv	Vertical deformation
S_z	Vertical spacing of reinforcement (m)
σ_v	Vertical stress (Pa)

σ_z	Vertical stress at depth z (Pa)
e	Void ratio
λ	Wavelength
E	Young's modulus (Pa)

1 INTRODUCTION

1.1 BACKGROUND

The earliest examples of soil structures applying the reinforced soil principle are recorded in the Bible (Exodus 5, verses 6-9) where the ancient Egyptians used straw in the making of bricks for their pyramids. The Agar-Quf ziggurat was constructed over 3000 years ago in Iraq with clay bricks reinforced by layering woven mats of reed on sand and gravel (Bagir, 1944). The Great Wall of China also contains reinforced soil in the case of clay and gravel bricks reinforced with tamarisk branches. The same concepts are still applied to soil structures today and the reinforced soil principle was patented as Reinforced Earth® by the inventor Henri Vidal in 1963. Vidal found that dry sand could stand at a steeper slope after adding pine needles in horizontal layers to the sand and concluded that the composite material of granular soil and reinforcement was stronger due to the tensile strength of the reinforcement (Vidal, 1966).

Reinforced soil walls are soil structures that make use of reinforcement elements to construct walls that retain soils at slopes otherwise not possible. The primary working principle in soil walls is friction between the reinforcing elements and the soil particles. Hence, it follows that the pressure induced by the weight of the soil onto the reinforcement increases the frictional forces and therefore the overall strength of the structure (Ingold, 1982).

Soil walls are made up of three main components, namely the soil wall facing, the reinforcement, and the soil backfill. There exists a wide variety of each component available for the construction of a soil wall and the combination of soil wall components produces soil walls that greatly differ in performance and behaviour. The reinforcement elements chosen for a soil wall, and more specifically, the degree of extensibility of the reinforcement play a vital role in the functioning of a soil wall. In industry, the two most common types of reinforcement material are steel (considered inextensible) and geosynthetics (considered extensible). The recent increase in the development and use of geosynthetics in soil walls, where otherwise steel would have traditionally been used, raises the question concerning how well the geosynthetics compare to the conventional steel reinforcement. This gives rise to the purpose of the study presented in this dissertation: how does the performance of a soil wall reinforced with geosynthetic material compare to an equivalent steel reinforced soil wall with the same wall facing and soil backfill under a surcharge load applied to the retained soil? Furthermore, how do the reinforcement strains compare between the two types of soil walls? The increased understanding of the different reinforcement types will improve application of the soil walls in industry. These questions provide the context for the content of this study.

1.2 OBJECTIVES OF THE STUDY

The aim of this study is to investigate the effect of reinforcement extensibility in a soil wall. More specifically, the research question asks how the behaviour and response of a soil wall reinforced with extensible reinforcement compares to a soil wall reinforced with inextensible reinforcement. The objectives are described further as follows:

- To investigate the effect on horizontal displacement of the soil wall facing reinforced with extensible and inextensible reinforcement under loading applied to the retained soil;
- To compare the difference in horizontal soil strain of the two types of reinforced soil wall;
- To determine the amount and progression of reinforcement strains under loading;
- To define the magnitude of wall stiffness provided by the extensible and inextensible reinforcement; and
- Classification of the relative behaviour of the soil wall reinforced with extensible and inextensible reinforcement.

1.3 SCOPE OF THE STUDY

The scope of this study is related to the experimentation and analysis of reinforcement extensibility in small scale physical models of soil walls tested in the geotechnical centrifuge to ensure stress-strain similitude to the full-scale problem. The scope was limited to two types of reinforcement material, namely brass (inextensible) and geosynthetics (extensible) reinforcement. The wall facing and soil backfill components of the soil walls were kept constant in the experiments. The scope excluded numerical modelling and field studies of soil walls.

1.4 METHODOLOGY

Literature pertaining to the scope of this study was reviewed and used to inform and guide the experimental research undertaken in this study. The literature review presented the concept of the reinforced soil principle and current research related to the behaviour of vertical soil walls.

Two vertical soil wall load-displacement tests were conducted in the geotechnical centrifuge at an acceleration of 30 G. A surcharge load was applied to the top surface of the soil wall and the corresponding displacement of the soil wall facing was measured by four LVDTs: two near the top, and two near the bottom of the soil wall. The first soil wall was constructed with extensible reinforcement in the form of PVC strips and the second soil wall was reinforced with inextensible reinforcement, namely brass strips.

The soil walls were subjected to 100 kPa surcharge loads applied to the retained soil surface and the largest displacements were recorded by the soil wall reinforced with the extensible PVC reinforcement strips.

Two additional vertical soil wall stress-strain tests were conducted in the geotechnical centrifuge at an acceleration of 30 G. The surcharge load was applied to the retained soil surface behind the soil wall and the resulting strains that developed in the reinforcement elements were measured with strain instrumentation. The third soil wall was constructed with extensible reinforcement in the form of PVC strips and the fourth soil wall was reinforced with the brass strips.

The extensible reinforcement strips were instrumented with eight strain gauges and the inextensible reinforcement strips were instrumented with eight fibre Bragg gratings (FBGs). The strain instruments were fastened at 3 m, 5 m, and 7 m prototype soil wall heights and in three horizontal zones located along the lengths of the reinforcement strips.

The experimental results were compared, analysed, and summarised to present the conclusions of the findings. Recommendations were made for future work and for practice in industry.

1.5 ORGANISATION OF THE REPORT

The report consists of the following chapters and appendices:

- An introduction to the dissertation is presented in Chapter 1.
- Literature related to the scope of the study and a technical introduction to the work is presented in Chapter 2 as the Literature Review.
- The experimental methodology is presented in Chapter 3 for the two sets of experiments that were performed in the study.
- Chapter 4 presents the experimental results, analysis, and discussion of the load-displacement experiment. The chapter is titled Load-Displacement Response of Reinforced Soil Wall.
- Chapter 5 presents the experimental results, analysis, and discussion of the stress-strain experiment. The chapter is titled Stress-Strain Response of Reinforced Soil Wall.
- The conclusions and recommendations of the study are provided in Chapter 6.

2 LITERATURE REVIEW

2.1 INTRODUCTION

'Reinforced soil' is a general term given to any in-situ or placed soil that has been mechanically strengthened or stabilised with reinforcement elements. The reinforcement elements improve the stability of the soil by providing tensile strength to the soil body. Confinement of the reinforced soil mass, interface friction and interlocking between the reinforcement elements and the soil are the mechanisms through which the stability of soil is improved (Ziegler, 2016).

Reinforcement elements in soil structures are generally separated into two categories according to the type of material used: metallic elements and geosynthetic elements. Steel strips and steel grids are common examples of metallic reinforcement whereas geosynthetic strips, geogrids and geotextiles are examples of geosynthetic reinforcement (Da Silva, 2017). Metallic reinforcement elements are considered inextensible reinforcement elements due to the high stiffness and resistance to strain under loading. On the other hand, geosynthetic elements are considered extensible due to the low stiffness and high strains under loading (Bonaparte and Schmertmann, 1988). An example of a metallic reinforcement element in the form of a high tensile steel strip is shown in Figure 2-1. Likewise, an example of a geosynthetic reinforcement element in the form of a geosynthetic strap is shown in Figure 2-2. The geosynthetic straps are made of closely packed high-tenacity polyester fibres encased in a polyethylene sheet.

Of interest to this study is the influence of reinforcement extensibility on the performance of reinforced soil walls. An overview of the application and design of soil walls is presented in this chapter, followed by a review of literature related to the aspects affecting soil wall performance, particularly reinforcement extensibility. Finally, a summary of the literature review that guided the work carried out in this study is presented.

Figure 2-1. High tensile steel reinforcement strip.

Figure 2-2. Polyester geosynthetic reinforcement strap.

2.2 PRINCIPLE OF REINFORCED SOIL

The principle of reinforced soil is simple and yet with a closer look, becomes quite complex. Simply put, the reinforcement elements present in a soil body provide the necessary tensile strength that the soil does not inherently have. The reinforced soil mass now has tensile strength that resists horizontal deformation caused by vertical stresses and resists shear failure (Jones, 1985). The stresses and strains acting on a body of soil are shown in Figure 2-3.

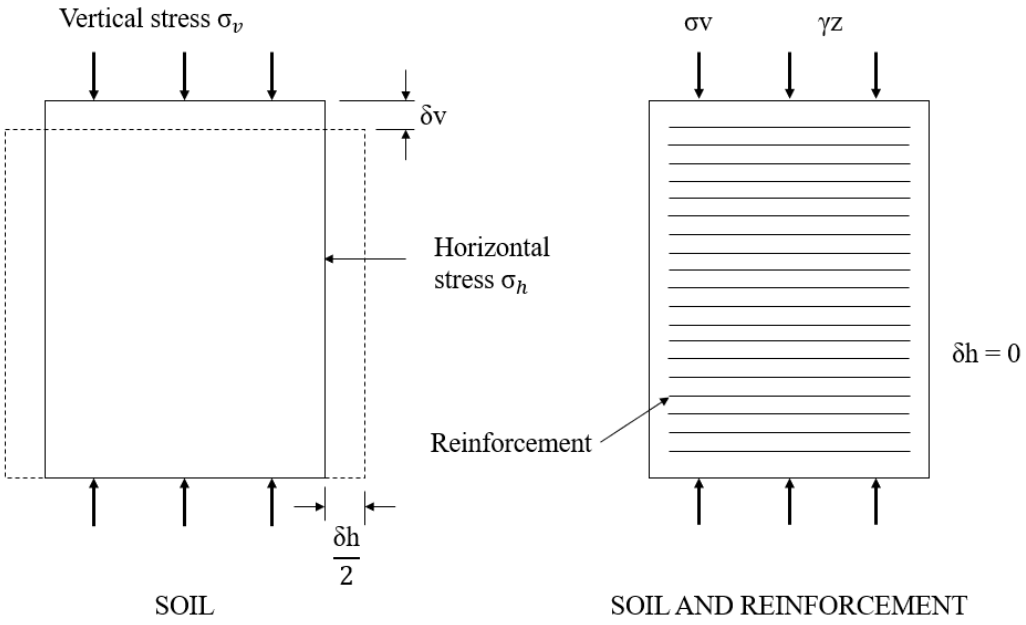

Figure 2-3. The stresses and strains on a body of soil and on a body of reinforced soil adapted from Jones (1985).

The vertical stress σ_v acting on the soil represents the soil weight and any surcharge placed on top of the body:

$$\sigma_v = \gamma z + q \qquad \text{(Equation 2-1)}$$

Where:

γ = unit weight of soil (N/m^3)

z = soil depth (m)

q = surcharge (N/m^2)

The horizontal stress acting on the soil is created by the vertical stress and represented by the lateral earth pressure coefficient K_a under active conditions. Using Terzaghi's Principle (Terzaghi, 1943) the horizontal pressure is determined as follows (Knappett & Craig, 2012):

$$\sigma_h = K_a \sigma_v \qquad \text{(Equation 2-2)}$$

Where:

$$K_a = \frac{\sigma_h}{\sigma_v} = \frac{1 - \sin\phi}{1 + \sin\phi}$$

ϕ = soil friction angle (°)

The resulting horizontal and vertical deformations, δh and δv respectively, are also shown in Figure 2-3. The soil mass with reinforcement experiences assumed zero horizontal strain and so it is assumed that the applied vertical pressure is transferred to the reinforcement through a certain mechanism to keep the soil body at rest. Therefore, the tensile stress acting on the cross-sectional area of the reinforcement is equivalent to the lateral stress in a unit of soil at rest:

$$\sigma_r = \frac{K_0 \sigma_v}{a_r} \qquad \text{(Equation 2-3)}$$

Where:

σ_r = reinforcement stress (N/m^2)

K_0 = lateral earth pressure coefficient at rest

a_r = cross-sectional area of reinforcement (m^2)

The strain in the reinforcement can then be determined:

$$\varepsilon_r = \frac{K_0 \sigma_v}{a_r E_r} \qquad \text{(Equation 2-4)}$$

Where:

ε_r = reinforcement strain

E_r = reinforcement elastic stiffness (N/m^2)

Jones describes the product, a_rE_r, as the effective stiffness of the reinforcement. The effective stiffness of the reinforcement is proven here to be inversely proportional to the reinforcement strain, ε_r, i.e., an increase in the stiffness of the reinforcement reduces the amount of reinforcement strain (Jones, 1985).

2.3 APPLICATIONS OF SOIL WALLS

Civil infrastructure development often requires soil bodies to be retained. The soil mass may need to be retained at various slope angles or vertically, and the soil may need to be retained permanently or only temporarily. Various kinds of retaining structures are therefore designed and constructed according to the specific requirements. Permanent retaining structures, for example, are installed in areas where unstable soil lies next to a road or where a section of ground needs to be elevated, and the durability of the materials used is essential for continued satisfactory performance. Conversely, temporary retaining structures are commonly used for excavations where services need to be installed, or for safe construction of foundations, and the durability of materials is of less importance. Temporary retaining structures are also used for stockpiling soil in an efficient and safe manner (Jones, 1985).

Soil retaining structures that make use of the reinforced soil principle have been used for dams, embankments, ground slabs, foundations and walls. The applications have been highly diverse, ranging from underground slabs over dolomitic cavities for roads (Steiner, 1975) to earthquake-resistant walls and embankments for bridges (Babu, 2007; Tatsuoka, 2019).

There are two types of retaining walls typically used to retain soil:

- The conventional reinforced concrete retaining wall or gravity wall and,
- The mechanically stabilised earth (MSE) wall or reinforced soil wall.

The gravity retaining wall is constructed with a large self-weight and uses its mass together with the law of gravity to retain soil. The gravity retaining wall resists movement and is stiff relative to the natural soil surrounding it. The MSE wall, on the other hand, is a reinforced soil wall that relies on strengthening the soil mass with reinforcement. Depending on the stiffnesses of materials used in the design, reinforced soil walls may be either stiff or highly flexible and can allow movement to take place. A relatively flexible reinforced soil wall is preferred in locations where seismic activity exists (Knappet and Craig, 2012; Tatsuoka *et al.*, 1997). It has also been shown that reinforced soil walls are more economical to construct than conventional concrete walls due to the use of soil instead of costly reinforced concrete (U.S. Department of Transport, 2001).

2.4 RESEARCH METHODOLOGY

Reinforced soil walls consist of three fundamental components, namely the wall facing, the soil back-fill, and the reinforcing elements. These components are illustrated in the soil wall cross-section shown in Figure 2-4 and are discussed further below.

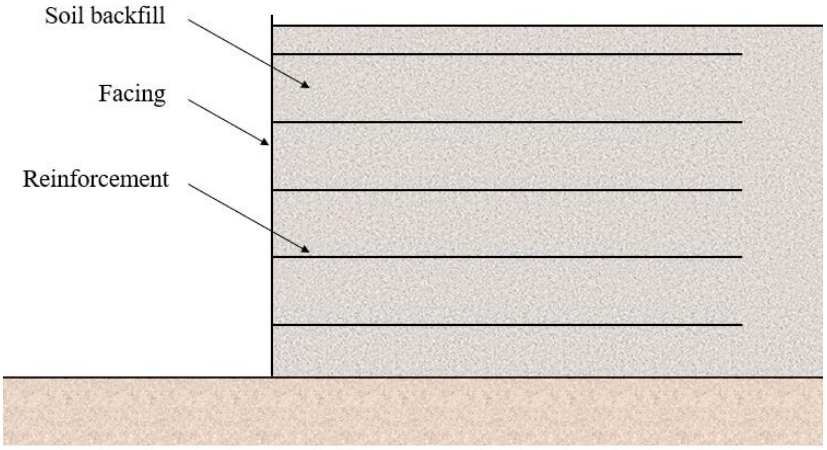

Figure 2-4. The three main components in a reinforced soil wall.

2.4.1 Wall facing

As recent as the early 1980s, the wall facing was still seen as a non-vital component to the performance of a soil wall with only two minor functions. The first was to prevent soil erosion, and the second was to provide an aesthetically acceptable external appearance (Ingold, 1982). Little was known relating to the role the facing plays in the performance of a soil wall; the fact that the facing resists horizontal pressures exerted by the backfill (depending on the material used), and how a stiff or flexible facing affects the translation of stresses to the reinforcement elements during construction (Tatsuoka *et al.*, 1997).

The two types of wall facings used in industry are classified as either “hard” or “soft” facing. The hard facings typically consist of reinforced concrete and are used for conventional retaining walls and for reinforced soil walls. In gravity walls, the concrete is normally poured on site, whereas, for reinforced soil retaining walls, precast concrete blocks and panels are assembled on site. Gabions and grout-filled bags are also known to have been used as facings (Okechukwu, 2016). The hard facing acts independently from the soil and acts against the active earth pressure of the backfill to resist overturning of the soil wall. (Tatsuoka *et al.*, 1997).

Soft facings are used in reinforced soil walls and typically consist of steel panels or steel meshes, timber, and geosynthetics. The soft facings have also been termed flexible facings due to the varying degrees of material flexibility that provide wall movement and settlement together with the soil (Ingold, 1982; Tatsuoka *et al.*, 1997).

2.4.2 Soil backfill

The soil that is selected to be used as backfill in reinforced soil walls depends on the application of the soil wall. A bridge abutment, for example, requires carefully designed backfill soil whereas improving the strength of waste material may need less consideration. Nonetheless, the ideal soil used for the backfill is a well-graded, cohesionless, granular material that is easily compacted to a high density and is non-corrosive to the reinforcement material. Generally, cohesive material has unfavourable corrosive properties such as the clay mineral illite that accelerate metal corrosion (Jones, 1985).

Poorly drained or cohesive soils delay the transfer of effective stress from the soil to the reinforcement material and result in reduced shear strength and slowed construction rates. Fine-grained soils may also exhibit plastic behaviour and cause long-term creep in the soil wall structure (McKittrick, 1978). Granular soils have high permeability and allow water to drain quickly out of the soil wall structure, preventing large build-up of unfavourable pore pressures in the structure.

A well-graded soil compacts easily and produces a high density that provides stability and strength through particle interlocking as the soil dilates under strain. The well-graded, granular soil also provides higher friction between the soil and reinforcement material (Okechukwu, 2016; Jones, 1985).

2.4.3 Reinforcement elements

A large variety of materials are used to reinforce soil. In essence, all that is required to construct reinforced soil is the insertion of material with tensile strength to the soil body. The two most common types of materials used in industry are steel and geosynthetic polymers (Saran, 2010). Steel and geosynthetics both provide tensile strength to reinforced soil walls but differ in stiffness. Steel reinforcement has large stiffness relative to geosynthetics due to the large inherent elastic modulus property. Consequently, geosynthetic reinforcement of a certain size undergo larger strains under load than the equivalent sized steel reinforcement. Steel reinforcement is therefore considered inextensible and exhibit brittle behaviour at failure relative to geosynthetic reinforcement, whereas geosynthetic reinforcement is considered extensible and exhibit ductile behaviour at failure.

Geosynthetic material is non-corrosive and highly durable, whereas steel is more susceptible to corrosion and therefore less durable. Another difference is geosynthetics are lighter and therefore easier to transport and quicker to construct on site compared to steel, which may lead to greater cost-effectiveness (Saran, 2010).

Common forms of reinforcement are strips, sheets, grids, bars, and anchors. The type of backfill soil used in the soil wall determines the form of reinforcement that is selected. The strips, sheets and bars rely on the friction to develop bonds between the reinforcement and the soil particles. The grids and anchors, however, produce soil-reinforcement interlock by causing blocks of soil to resist movement (Jones, 1985).

2.5 REINFORCED SOIL WALL DESIGN PRINCIPLES

2.5.1 South African and British Standard

In South Africa, reinforced soil walls are designed for stability using limit state design principles from the *SANS 207:2011* standard which is based on the British standard *BS8006:2010* (SABS, 2011; BSI, 2010). The limit state principles consist of two analyses namely the ultimate limit state (ULS) and serviceability limit state (SLS). The ultimate limit state pertains to the failure of the soil wall structure or the failure of an element within the structure. The serviceability limit state prescribes the allowable deformation of the soil wall that keeps the structure within the proper serviceability limits.

The ultimate and serviceability limit states are considered for both external and internal stability of the soil wall in the following ways:

1. External stability:
    - Foundation soil bearing resistance failure resulting in tilting of the soil wall (ULS),
    - Sliding between the reinforced soil mass and the foundation soil (ULS),
    - The development of a deep slip surface (ULS),
    - Excessive wall deformation and settlement (SLS).
2. Internal stability:
    - Tensile rupture of reinforcement element (ULS),
    - Reinforcement tensile axial strain limit (SLS),
    - Facing-reinforcement joint/connection failure (ULS),
    - Pull-out of reinforcement elements due to inadequate friction between elements and soil (ULS),
    - Local slipping due to inadequate friction between reinforcement elements and soil (SLS).

Of particular interest to this study is the internal stability of the reinforced soil mass relating to the stresses and strains acting on the reinforcement elements. There are two semi-empirical methods that are commonly used for reinforcement tensile force analysis, namely the tie-back wedge method and the coherent gravity method. The tie-back wedge method is used for soil walls with reinforcement elements of high extensibility, such as geosynthetics, and the coherent gravity method for walls with reinforcement of relatively low extensibility such as steel strips. Both methods are based on Equation 2-5 whereby the tensile forces exerted on the reinforcement elements from the overburden stresses are determined. The equation is set out as follows (Knappet and Craig, 2012):

$$T = K\sigma_z S_x S_z \qquad \text{(Equation 2-5)}$$

Where:

T = tensile force in reinforcement (N)

K = lateral earth pressure coefficient

σ_z = vertical stress at depth z (Pa)

$S_x S_z$ = horizontal and vertical spacing of reinforcement (m)

Assuming a friction angle ϕ' of 37° for the backfill soil, the active (K_a) and at-rest (K_0) earth pressure coefficients are determined as follows:

$$K_a = \frac{1 - sin\phi'}{1 + sin\phi'} = 0.25$$

$$K_0 = 1 - sin\phi' = 0.40$$

The main differences between the two methods are the region where the respective earth pressure coefficients are applied, and the mode of failure expected. The tie-back method is an extension of Coulomb's method as it considers the forces acting on a wedge of soil. The active state is assumed throughout the entire depth of the reinforced soil mass due to the large strains that take place between the reinforcement and the soil. The active earth pressure coefficient is therefore applied for the entire depth of soil and the failure surface is assumed to occur along the plane AB inclined at an angle equal to 45°+ $\phi'/2$ as indicated in Figure 2-5, adapted from Knappett and Craig (2012).

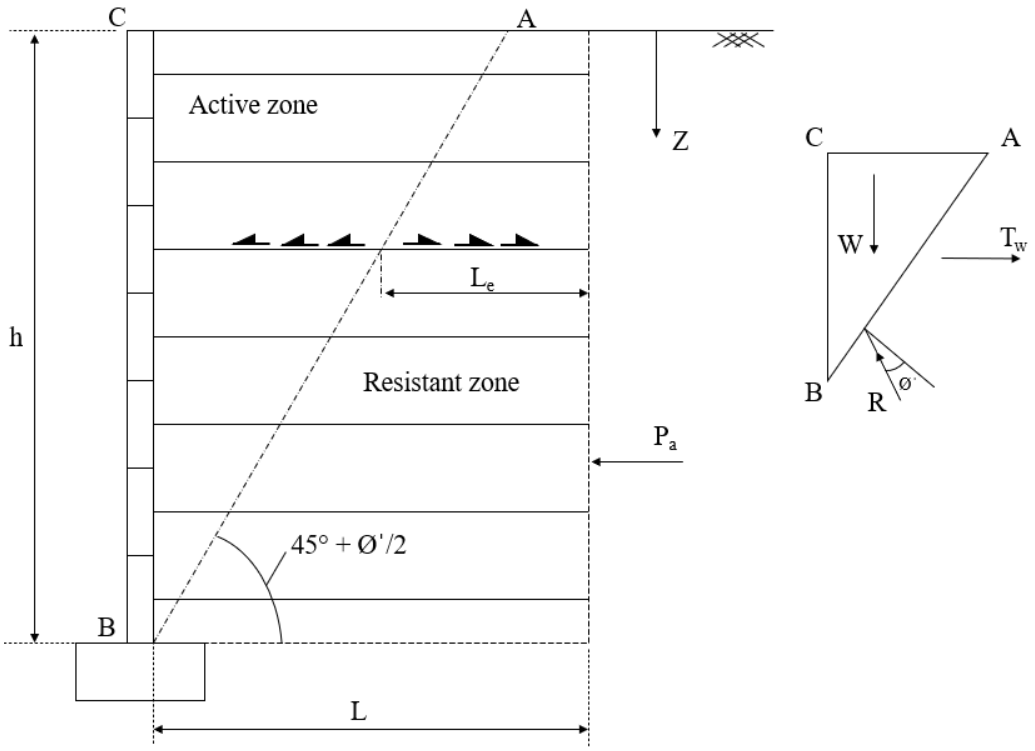

Figure 2-5. The tie-back wedge method after Knappett and Craig (2012).

The failure surface divides the reinforced soil mass into the active and resistant zones wherein the shear stresses on the reinforcing elements work outwards, towards the facing, and inwards respectively. The failure surface indicates the plane of collapse and therefore the tie-back method relates to the ultimate limit state rather than the serviceability limit state.

Bond failure between the reinforcement elements and the soil is determined by calculating the frictional resistance, T_f, available on the top and bottom of the reinforcement surfaces with the following equation:

$$T_f = 2bL_e\sigma_z tan\delta' \quad \text{(Equation 2-6)}$$

Where:

b = element width

L_e = reinforcement length in resistant zone

δ' = angle of friction between soil and reinforcement

The design requirement, to prevent sliding between the reinforced fill and the soil, is the sum of all the tensile forces in the reinforcement elements that are enabled by the frictional resistances to be greater or equal to the total tensile resistant force, T_w. The total resistant force is determined by checking the stability of the wedge, ABC. The forces acting on the wedge are the weight of the wedge, W, the resultant of the normal and shear forces, R, that acts at angle Ø' to the normal, and the total resistant force, T_w (Knappett and Craig, 2012).

The coherent gravity method, on the other hand, assumes the mode of failure is progressive fracture of the reinforcement elements at the points of maximum tensile stress (Juran and Schlosser, 1978). The experimental work done by Juran and Schlosser (1978) show the tensile stresses along the length of the reinforcement strips follow the general shaded region, σ_t, as shown in Figure 2-6 adapted from Knappett and Craig (2012). The points of failure are therefore assumed to occur along the locations of maximum tensile stress, denoted by the failure plane BD. The failure plane again separates the reinforced soil into an active and resistant zone, and the method considers stability of the active zone. The research shows plastic equilibrium develops in thin layers of soil along the path of fracture and, if assumed to be perfectly plastic, the failure plane becomes a logarithmic spiral with the exits at the bottom of the facing and at a point approximately 0.3 times the wall height behind the facing (Juran and Schlosser, 1978). The failure plane can further be simplified to the sizes shown below, with the earth pressure coefficient assumed to equal K_0 and linearly decreasing to K_a at a depth of six meters.

SABS (2011) further requires a minimum reinforcement length the greater of 7 m or 0.7*h* (where *h* is the total wall height) and requires a minimum embedment length, l_e, of *h*/20 for retaining walls. The embedment length is the section of reinforcement strip behind the failure surface in the resistant zone.

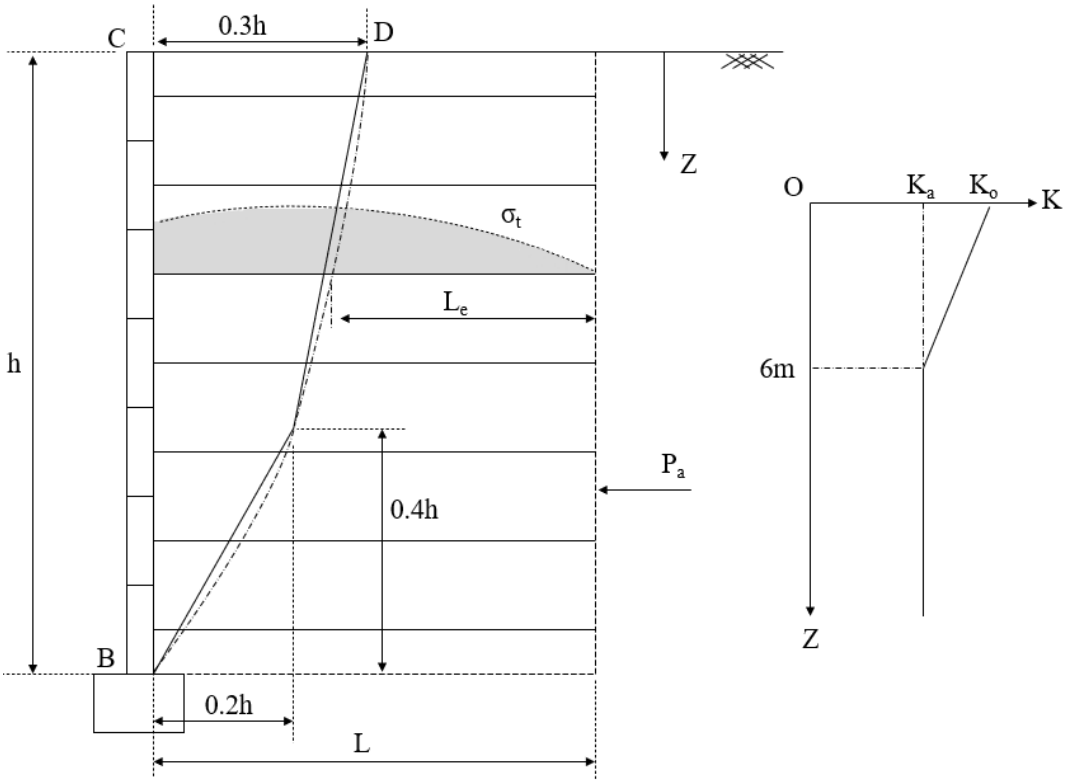

Figure 2-6. The coherent-gravity method after Knappett and Craig (2012).

2.5.2 Previous studies

Simply stated, to achieve external stability of the reinforced soil wall the overall surrounding ground must be stable and to achieve internal stability there must essentially be stability in the reinforced soil mass. Kikumoto *et al.* argued the length and spacing of geosynthetic reinforcement are critical to the stability of the soil wall. If the reinforcement is not sufficiently long, a shear band forms in the backfill and the wall becomes externally unstable. Too little reinforcement caused internal stability in the reinforced soil body as the load was too large and soil wall failure occurred (Kikumoto *et al.*, 2010).

In 2002, Holtz and Lee executed numerical and experimental work to improve the understanding of internal stress-strain distribution in wrapped geosynthetic reinforced retaining structures. A parametric study of more than 250 numerical models was performed to determine the effect of soil properties, reinforcement stiffness and reinforcement spacing on the

performance of the soil walls. Plane-strain soil properties, the effect of low confining pressure on the soil dilation angle, and low strain geosynthetic reinforcement properties were considered in the project. The researchers also recommended a new technique to predict wall face deformations and design recommendations for the internal stability of geosynthetic reinforced soil walls (Holtz and Lee, 2002).

Holtz and Lee (2002) argued the current design methods regarding wall face deformations "*do not provide useful performance information*" and the common tie-back wedge method is too conservative and leads to uneconomical designs. Furthermore, little reliable information pertaining to internal stress or strain distributions in geosynthetic soil walls existed and geosynthetic material and interface properties were not well understood.

The researchers concluded the following findings for wrapped geosynthetic soil walls (Holtz and Lee, 2002):

- A reinforcement length to wall height ratio of 0.8H (H was the height of the wall) was adequate for all the simulations. Models that contained poor backfill materials with friction angles less than 25°, and models with weak reinforcement tensile strength of 55 kN/m, exhibited localised failures at the wall face.
- Localised failure occurred at the wall face when the reinforcement spacings greater than 0.6 meters were simulated. This caused internal instability and outward rotation of the wall face.
- Correct plane-strain soil properties and low strain rate reinforcement stiffnesses are necessary to accurately simulate geosynthetic soil wall performance.
- Good quality backfills consisted of soils with 35° or higher friction angles. Poor backfill soils caused large wall face deformations, as well as large reinforcement tensions.
- Dilation angles as high as 40° were observed for granular soils at low confining pressures, whereas low dilation angles of 26° were observed under higher confining pressures.
- The stiffness of reinforcement had less effect on the deflection of the wall face than the quality of the backfill soil.
- The researchers plotted a normalised distribution of the reinforcement tension against the height of the walls. The maximum reinforcement tension occurred at 0.6H wall height.

Moraci and Recalcati (2006) performed over 40 pull-out tests on HDPE extruded geogrids with compacted granular soil to study the effect of reinforcement stiffness and length. Three

reinforcement lengths were used (L = 0.40, 0.90, 1.15 m) while the reinforcement widths were kept constant. The following conclusions were presented:

- The reinforcement embedded in the soil had similar tensile strength to those tested in air. Hence, the influence of the granular soil confinement regarding tensile strength was negligible.
- The pull-out behaviour was strongly influenced by the applied confining stress and by the embedded reinforcement length. The longer reinforcement lengths (L = 0.90 and 1.15 m) at confining pressures higher than 25 kPa exhibited strain-hardening behaviour as the pull-out resistance increased progressively with an increase in displacement. In contrast, the short reinforcement and long reinforcement under low confining pressures exhibited strain-softening behaviour as the pull-out resistance progressively decreased after the peak resistance was reached.
- The long reinforcement under high confining pressures induced a progressive mobilisation of the interaction mechanisms, whereas the short reinforcement showed lower longitudinal strains, causing the interaction mechanisms to develop almost immediately.
- The reinforcement stiffnesses had no correlation to the interaction coefficient of friction. The shape and geometry of the geogrids, however, did influence the coefficient of friction but not as much as the effect of dilation.
- Low confinement stress and the short reinforcement (L = 0.4 m) caused low reinforcement strains and low peak pull-out resistance.
- The actual locations of maximum reinforcement tensions occurred at heights between 0.2H and 0.5H, instead of at the bottom of the walls, as predicted by the tie-back wedge method.

Bathurst *et al*. (2006) constructed full-scale walls to demonstrate the effect of the wall facing on internal stability by using two types of facing, namely stiff modular block wall face and flexible geosynthetic wrapped facing. The researchers kept the type of reinforcement material constant and used geosynthetic grids in the experiment. The results showed that the loads exerted on the reinforcement were significantly reduced when the soil wall was constructed with the stiff facing. Strain gauges were installed on the reinforcement to record reinforcement strains. Further findings of the research were as follows:

- The peak reinforcement loads were three and a half times greater in the flexible wall than the stiff-face wall at the end of construction and about two times greater at the end of surcharging.

- The largest facing displacements occurred 3 m above the toe of the 11 m walls for both types of facing.
- At a surcharge of 80 kPa, the wrapped-face wall displacement was three times greater than the stiff-face wall.
- Reinforcement strain magnitude for stiff-faces were less than 1%, whereas the wrapped-face soil wall showed reinforcement strains up to 4%.

Bathurst *et al*. (2010) further summarised the horizontal displacement of wall facings constructed with hard and soft facings and reinforced with different types of geosynthetics. The wall heights, reinforcement lengths and reinforcement vertical spacing also varied. Figure 2-7 below presents the normalised horizontal facing displacement for soil walls constructed with hard facings as a function of reinforcement length. It is interesting to note the design guidelines (FHWA, 2008 and AASHTO, 2009) predict larger deformations than almost all the combinations of soil walls tested. Most of the soil walls tested were constructed with 0.7 L/H reinforcement lengths and the normalised facing displacements ranged from 0.1% to 1.2%. Facing displacements with reinforcement lengths less than 0.6 L/H start to increase exponentially at 0.3 L/H.

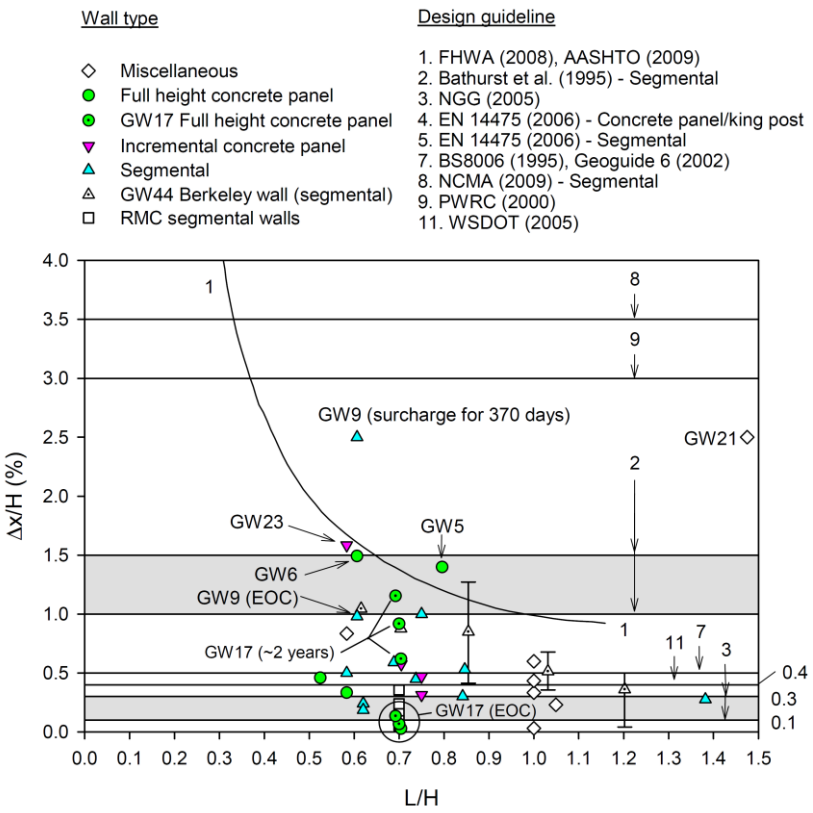

Figure 2-7. Normalised horizontal displacement of hard-faced walls reinforced with geosynthetics. Adapted from Bathurst *et al.* (2010).

Bathurst *et al*. (2010) also plotted the normalised horizontal displacement results of soft-faced walls. The results are shown in Figure 2-8. The soft-faced walls were reinforced with reinforcement of greater length, mostly averaging between 0.8 and 1.0 L/H. Even with longer reinforcement, most of the soft-faced walls showed displacements that exceeded the FHWA (2008) and AASHTO (2009) guideline. Furthermore, the soft-faced walls deformed significantly more than the walls constructed with hard facings, ranging up to an order of magnitude larger.

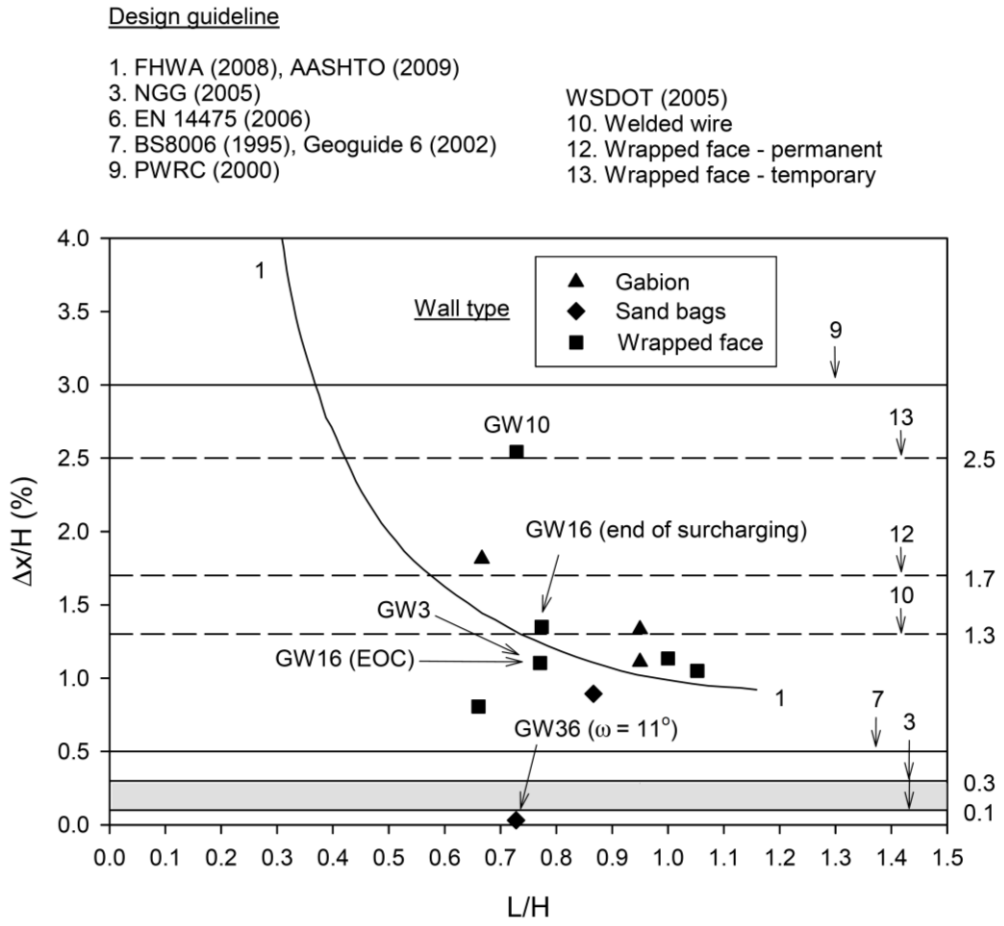

Figure 2-8. Normalised horizontal displacement of soft-faced walls reinforced with geosynthetics. Adapted from Bathurst *et al.* (2010).

Bourgeois *et al*. (2011) carried out full-scale tests on a soil wall reinforced with steel strips for local loads associated with rail traffic. Galvanised steel strips were used, 45 mm wide and 5 mm thick, with an elastic modulus of 210 GPa. Static loads were applied in the experiment and the results were used to indicate the accuracy of deformation predictions made by numerical modelling tools and the evolution of tensile forces in the reinforcing strips during construction

and loading. Linear variable differential transformers were fastened to the soil wall facing and measured the horizontal displacement.

The experimental set-up is shown in Figure 2-9 and the facing displacement results are shown in Figure 2-10 for loading at 90 kN and 850 kN. It was shown the facing deformed the most around the middle section of the wall. The least deformation was observed at the top of the wall. Strain gauges were installed on the reinforcement strips near the facing at the theoretical maximum tensile loads, and at the end of the reinforcement strips. The results depicted in Figure 2-11 show the tensile forces in the reinforcement peaked at just below 1.5 m from the facing and reduced to zero at the end of the reinforcement strips.

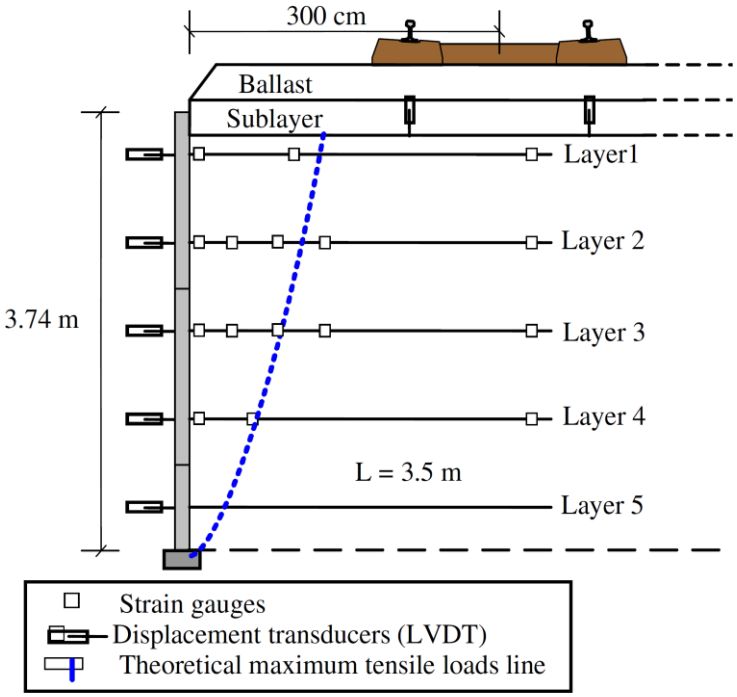

Figure 2-9. Instrumentation of the soil wall adapted from Bourgeois *et al*. (2011).

The experiment results showed maximum horizontal deformation of the facing at mid-height or layer 3. Two load conditions were applied to the soil wall, 90 kN and 850 kN, and the results are plotted in Figure 2-10 from Bourgeois *et al.* (2011).

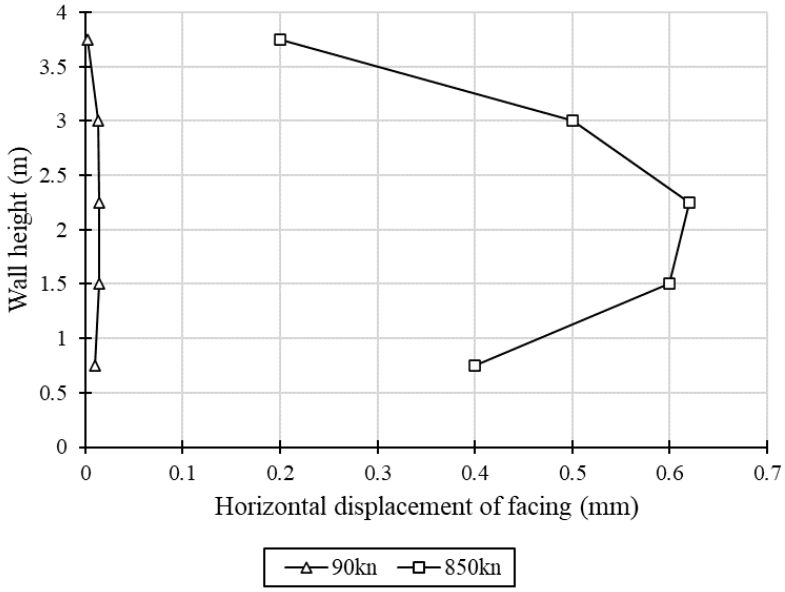

Figure 2-10. Wall facing displacement results by Bourgeois *et al*. (2011).

The tensile force measured along the steel strip at layer 3 was presented and is shown in Figure 2-11 adapted from Bourgeois *et al.* (2011) for the two load cases: 90 kN load and 850 kN load. The largest force was identified at just below 1.5 m from the facing.

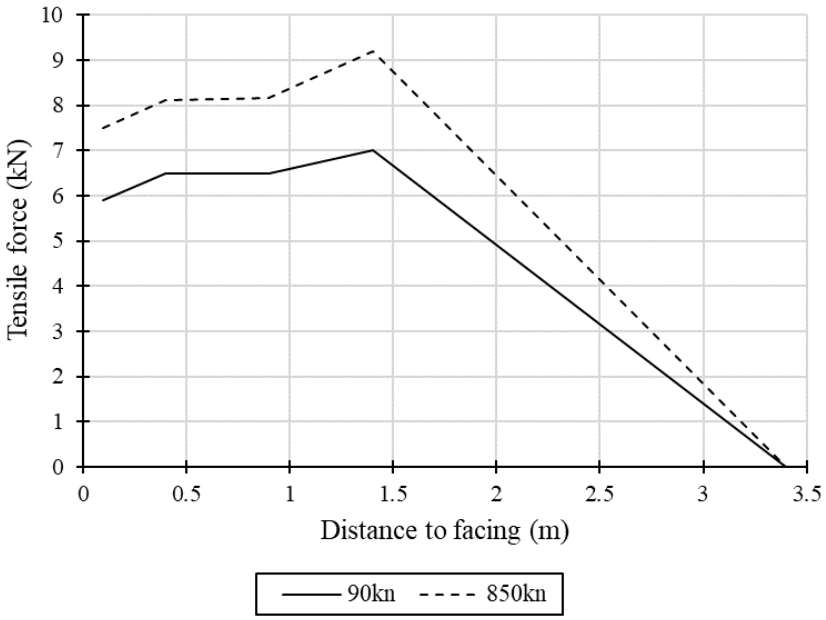

Figure 2-11. Reinforcement tensile force results by Bourgeois *et al*. (2011).

There exists in the research one study done by Bonaparte and Schmertmann 1988 that made a direct comparison of inextensible and extensible reinforcement in soil walls by conducting a parametric study. The researchers analysed the relationships and trade-offs between different design methods and construction performance results by comparing soil walls reinforced with steel strips and geosynthetic material. The following was concluded (Bonaparte and Schmertmann, 1988):

- The tensile stiffness of the steel reinforcement was sufficient to prevent full mobilization of the shear strength of the soil and thereby are best associated with an at-rest (K_0) state of stress.
- The lower tensile stiffness of the geosynthetic reinforcement meant equilibrium would not be reached in the soil wall until sufficient strain occurred to fully mobilise the shear strength of the soil. Therefore, an active (K_a) plastic state of stress was concluded to develop in the geosynthetic-reinforced soil walls.
- Classic limit state analysis methods are appropriate and conservative for analysis and design of reinforced soil walls and the selected method had little influence on the calculated tensile forces.
- Reinforcement stiffness was inversely proportional to reinforcement strains and elongations.
- An increase in wall height and decrease in soil strength increased reinforcement strains significantly.

Additional researchers have shown that the ability of reinforcement to elongate allowed plastic mechanisms to form and improved soil wall performance by preventing reinforcement slip (Gaudio, 2018; Masini *et al*., 2015; Watanabe *et al*., 2003). The interaction between the soil and the reinforcement is the key component to transferring the vertical stress in the soil mass to tensile forces in the reinforcement. In the case of extensible reinforcement, it has been shown the ability to slowly deform allows the soil wall to withstand larger vertical loads (Jayashree *et al*., 2017).

The three most common failure modes in reinforced soil walls are directly related to the type of reinforcement used and include (Juran and Christopher, 1989):

1. Excessive facing displacement
2. Sliding of reinforcement
3. Reinforcement breakage

Due to the high extensibility of geosynthetics, large soil wall facing displacements were observed in laboratory experiments (Juran and Christopher, 1989). Soil friction failure is

another major soil wall failure and breakage of the geosynthetic elements themselves were observed. Extensible reinforcement elongate under increased tensile stresses and reach peak tensile strength and can fail before pull out occurs. Inextensible reinforcement, on the other hand, do not elongate and may lead to increased reinforcement slippage as the friction bond between the soil and reinforcement is broken before failure of the reinforcement occurs (Juran and Christopher, 1989).

2.6 FIBRE OPTIC STRAIN INSTRUMENTATION

2.6.1 Introduction

Fibre optic technology was used in this study to measure the reinforcement strains in the soil walls. The use of fibre optic technology in reduced-scale physical models is relatively uncommon and so a brief overview of fibre optics and their use in physical models is presented.

A fibre Bragg grating (FBG) is a variation in the refractive index of a fibre core that causes a reflection of a certain known Bragg wavelength, λ_B. It is named a Bragg wavelength after Sir William Lawrence Bragg who discovered the Bragg law of X-ray diffraction in 1912. Bragg's law defines the interference of a crystalline lattice separated by a distance *d*:

$$2dsin\theta = n\lambda \qquad \text{(Equation 2-7)}$$

Where:

d = distance between interference peaks

θ = incident angle

n = integer

λ = wavelength

The diffraction of light intensity is measured as a function of the angle θ, depicted in Figure 2-12, and the strong intensity of scattered wavelengths is known as the Bragg peak, represented as λB and shown in Figure 2-13.

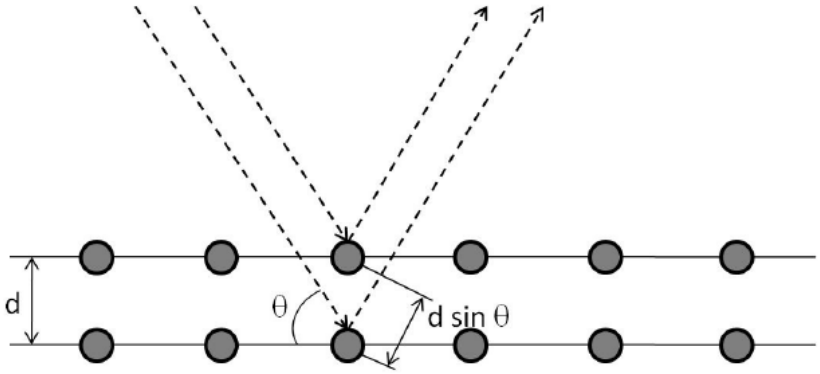

Figure 2-12. The Bragg law demonstrating radiation reflected by a crystal lattice structure from Werneck *et al*. (2013).

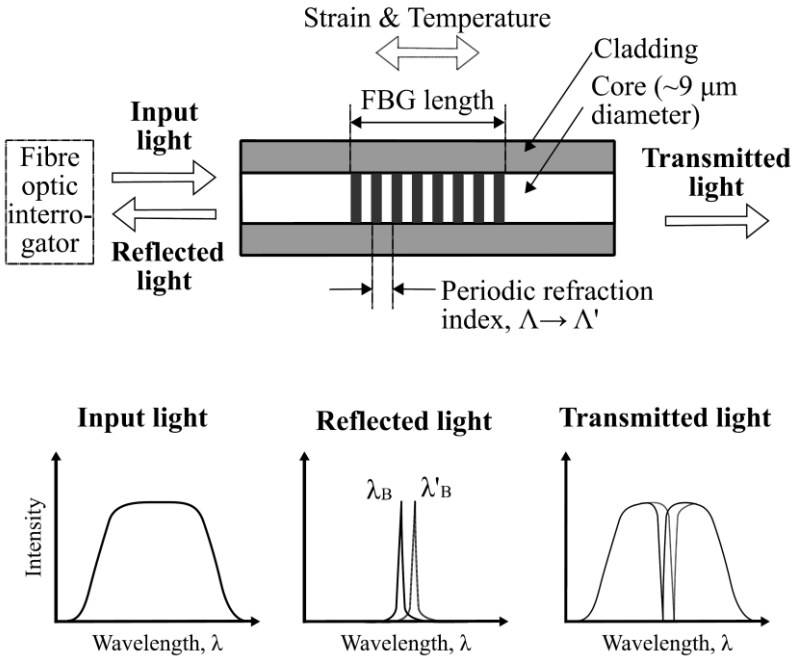

Figure 2-13. A schematic diagram of the Fibre Bragg Grating operation after da Silva *et al*. (2016).

Since the light is transmitted perpendicular to the bragg grating in the fibre core θ = 90°, and *d* is the distance between the peaks of interference caused by the bragg gratings, Equation 2-7 can be re-arranged to determine the Bragg wavelength, λ_B:

$$\lambda_B = 2n_{eff}\Lambda \qquad \text{(Equation 2-8)}$$

Where:

n_{eff} = fibre effective refractive index

Λ = grating periodicity

The sensitivity of the Bragg wavelength with regards to strain and temperature is calculated by taking derivatives of Equation 2-8 according to temperature and displacement respectively. This leads to the accurate measurement and determination of strains with the following formula:

$$\frac{\Delta\lambda_B}{\lambda_B} = K_\varepsilon \varepsilon + K_T T \quad \text{(Equation 2-9)}$$

Where:

K_ε = strain coefficient

K_T = temperature coefficient.

2.6.2 The use of fibre optic instrumentation in geotechnical centrifuges

There has been use of fibre optic instrumentation in geotechnical centrifuges however there exists limited literature on the topic (da Silva *et al*., 2016). Lienhart *et al*. (2015) and Voet *et al*. (2005) measured geotextile strain by attaching the fibre to a single strand of a geogrid or woven into the geotextile structure. Villard and Briancon (2008) argued that the use of small, flexible fibres reduces the total conformance errors that are experienced by conventional instrumentation such as strain gauges that are glued onto the surface and may record more accurate strain measurement. Da Silva (2017) used fibre optic instrumentation to measure the strains of geosynthetic material that spanned a void in a centrifuge model. Fibre was chosen as opposed to strain gauges to eliminate local stiffening of the geosynthetic reinforcement over the void. Kapogianni *et al*. (2010) made use of fibre optics to measure geotextile strains in reinforced soil wall physical models that were tested in the centrifuge. The 20 mm long FBGs were glued onto the geotextile reinforcement and the interrogator was placed near the centre of the centrifuge to minimise effects of acceleration on the interrogator.

2.7 SUMMARY OF LITERATURE

It has been shown there exists a variety of reinforced soil walls due to the type and combination of soil wall components chosen to construct cost-effective reinforced soil walls suitable for all kinds of applications. The three components of a soil wall, the wall facing, the soil backfill, and the reinforcement, all significantly influence the behaviour and performance of the soil wall and allow for numerous variations of soil wall designs. The possible types of soil walls range from flexible walls with large deformations and strains to stiff walls with very limited movement, and combinations of flexible and stiff walls in between. The most flexible walls consist of flexible geosynthetic facings and reinforcement with loose backfill, whereas the stiff walls are made of stiff modular block facings and steel reinforcement with well-compacted backfill. The optimum soil backfill for soil walls consists of non-cohesive, granular, well-graded, well-compacted backfill. Cohesive soil is unfavourable for soil walls due to the low permeability and the generation of large excess pore pressures that dissipate over long periods of time.

A stiff facing acts as a structural element and provides additional stability to the soil wall. It is highly resistant to deformation and does not settle together with the reinforced soil body, inducing large stresses at the reinforcement joints. A more flexible facing on the other hand deforms together with the reinforced soil body acting as a unit and relies more on the reinforcement to provide the stability required. Larger wall facing displacement is expected when a flexible facing is used.

The development of the failure plane and soil wall behaviour has been shown to be sensitive to the type of reinforcement selected, particularly regarding the extensibility of the reinforcement. The conventional tie-back wedge method based on Coulomb's method best describes the behaviour of a soil wall with extensible reinforcement. The entire soil body is in an active state as the shear strength of the entire soil body is mobilised, and the failure plane is expected to develop at an inclined angle equal to $45° + Ø'/2$ to the horizontal. A soil wall reinforced with inextensible reinforcement is better analysed with the coherent gravity method where the failure plane progresses along the points of maximum reinforcement tension and the earth pressure coefficient is either active or at-rest depending on the depth.

Reinforcement pull-out is a common failure mechanism in soil walls dependant solely on the surface interaction between the reinforcement material and the soil particles. Increasing the friction coefficient of the reinforcement surface has been shown to be significant in the improved performance of the reinforcement.

The literature review shows the strain gauge to be the choice instrument used to measure the strains that develop along the reinforcement strips and linear variable differential transformers to measure the horizontal movement of the wall facing. An introduction to the relatively new fibre optic technology was presented and can be used to measure the reinforcement strains with possible reduction in conformance errors.

The main objective in this study was to investigate the change in soil wall behaviour related to the change in reinforcement extensibility. Geosynthetic reinforcement and steel reinforcement are commonly used in industry and are often compared to one another to identify which option is best. The work carried out in this study sought to directly compare soil walls reinforced with extensible reinforcement and soil walls reinforced with inextensible reinforcement. This was done by isolating as many variables as possible and was guided by the existing literature.

3 EXPERIMENTAL METHODOLOGY

3.1 INTRODUCTION

Four reduced-scale physical models were constructed to investigate the effect of reinforcement extensibility in vertical soil walls. The soil wall models were accelerated in the geotechnical centrifuge to simulate the equivalent soil stresses and strains expected in life-sized soil walls. Experimenting with small-scale models allowed for a cost-effective way to test the behaviour of four soil walls under loading in a relatively short amount of time. Testing small-scale models also allowed for simple control of soil wall properties, constant boundary conditions and detailed recorded measurements for each test.

The soil wall models were constructed in a strongbox with a side window which allowed for side-view photographic images to be captured of the soil walls during test flight. A loading actuator and four linear variable differential transformers (LVDTs) were fixed to the strongbox. Remote-controlled vertical loads were applied on the surface of the backfill with the actuator and the LVDTs recorded the displacement of the wall face. Further testing was conducted where the LVDTs were removed from the test set-up and reinforcement strain instrumentation in the form of fibre optic Braggs and strain gauges were included. The fibre optic Braggs and strain gauges were fastened to the reinforcement strips and captured the tensile strains that developed along the reinforcement strips.

In this chapter centrifuge modelling principles are discussed, followed by a description of the experimental methodology employed to construct, test, and record the performance of the soil walls with extensible and inextensible reinforcement elements. The properties and preparatory work of the soil wall components are presented, as well as the use of fibre optic instrumentation.

3.2 CENTRIFUGE MODEL

3.2.1 Overview

Four individual soil wall models were constructed in the centrifuge strongbox and tested in the geotechnical centrifuge. Two types of experiments were conducted, namely a load-displacement analysis and a stress-strain analysis. Soil wall models 1 and 2 were constructed for the load-displacement tests and models 3 and 4 were constructed for the stress-strain tests. An overview summary of the soil wall models and components used in the four centrifuge tests is shown in Table 3-1.

Table 3-1. Centrifuge soil wall models and components.

Experiment	**Load-Displacement**		**Stress-Strain**	
Centrifuge model	**1**	**2**	**3**	**4**
Reinforcement material	PVC, extensible	Brass, inextensible	PVC, extensible	Brass, inextensible
Instrumentation	LVDTs		Strain Gauges	Fibre Braggs
Model size (mm)	300 x 150 x 333 (high)			
Wall facing	Flexible, U-shaped brass panels			
Backfill soil density (kg/m^3)	1482	1461	1507	1515
Foundation soil density (kg/m^3)	2140	2152		
Load block area (mm^2)	16 240		33 785	

All four soil walls were constructed to the same size: 300 x 150 x 333 (high) mm and were tested at an acceleration of 30 G. At a scale factor of $n = 30$, the models converted to a prototype soil wall size of 9 m in length, 4.5 m in width, and 10 m in height. Plane-strain behaviour was assumed for all the soil wall models and a sketch of the centrifuge models constructed for the load-displacement tests is shown in Figure 3-1, and a centrifuge model sketch for the stress-strain tests is shown in Figure 3-2. The sketches are not drawn-to-scale and all the dimensions are in millimetres. The load actuator and, in the case of the load-displacement tests, the LVDT instruments were fixed to the frame of the strongbox. All the soil wall components mentioned in Table 3-1 are discussed in greater detail in the sections to follow.

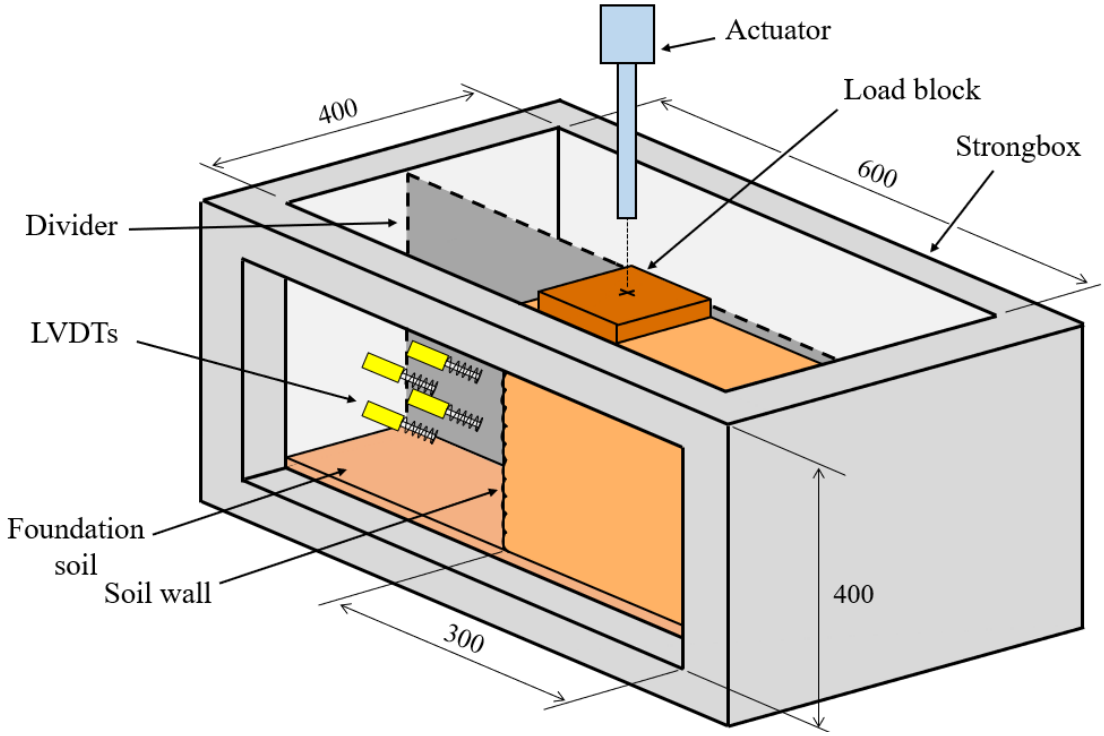

Figure 3-1. An isometric sketch of the centrifuge model used in the load-displacement tests. Not drawn-to-scale and all dimensions are in millimetres.

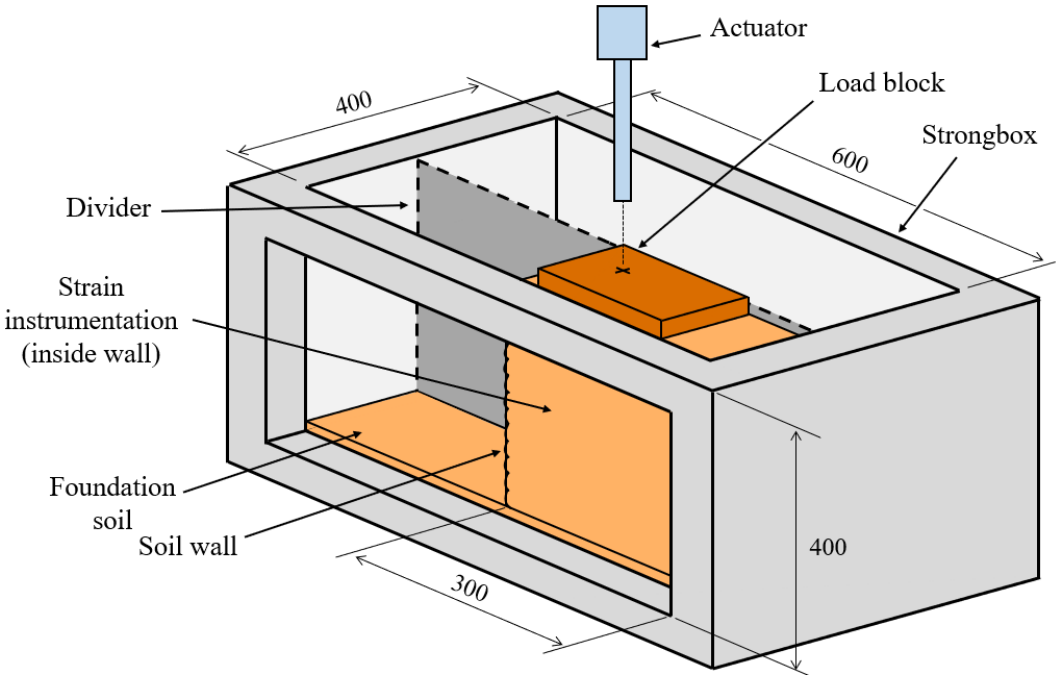

Figure 3-2. An isometric sketch of the centrifuge model used in the stress-strain tests. Not drawn-to-scale and all dimensions are in millimetres.

3.2.2 Soil wall models

The four reinforced soil wall models constructed for the load-displacement and stress-strain experiments consisted of three main components: the wall facing, the reinforcement elements, and the backfill. The soil wall facing was constructed out of brass U-shaped panels that were aligned together with flexible hypodermic needles. The facing was erected by fixing the hypodermic needles into holes that were drilled into an aluminium strip foundation.

The aim of the load-displacement and stress-strain experiments was to present the effect of reinforcement extensibility on soil wall behaviour. Therefore, two types of materials were used to construct the reinforcement elements, namely PVC (extensible) and brass (inextensible). The reinforcement strip lengths were constructed to seventy percent of the soil wall height, in this case, 233 mm in the model. The reinforcement strips were laid horizontally in the soil and placed in 33 mm vertically spaced layers resulting in ten layers in total.

The soil wall models were backfilled with fine silica sand from a commercial source near Cullinan, located approximately 40 km east of Pretoria, South Africa. In the load-displacement tests, the backfill consisted of loose dry sand and was placed on top of a 40 mm foundation layer of dense sand. The backfill and the foundation layer in the stress-strain models consisted of slightly compacted dry sand. The sand was placed in a controlled manner with a sandhopper and is discussed further in chapter 3. A cross-section of the load-displacement soil wall model is shown in Figure 3-3 and in Figure 3-4 a cross-section sketch of the stress-strain model is presented. The sketches are not drawn-to-scale and all dimensions are in millimetres.

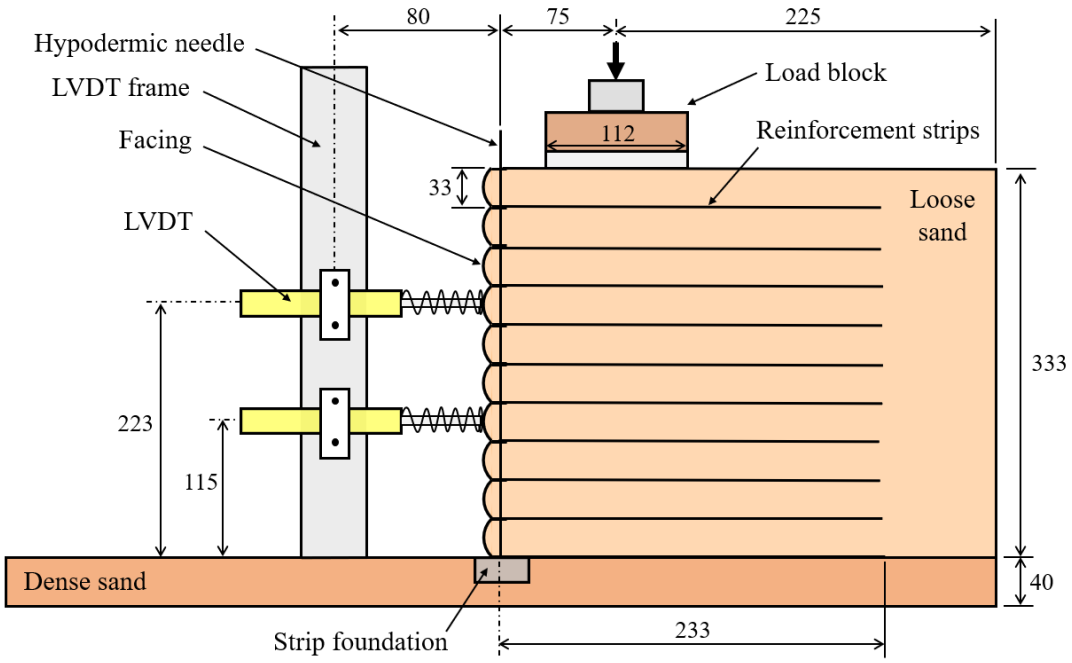

Figure 3-3. A cross-section of the load-displacement soil wall models. Not drawn-to-scale and all dimensions are in millimetres.

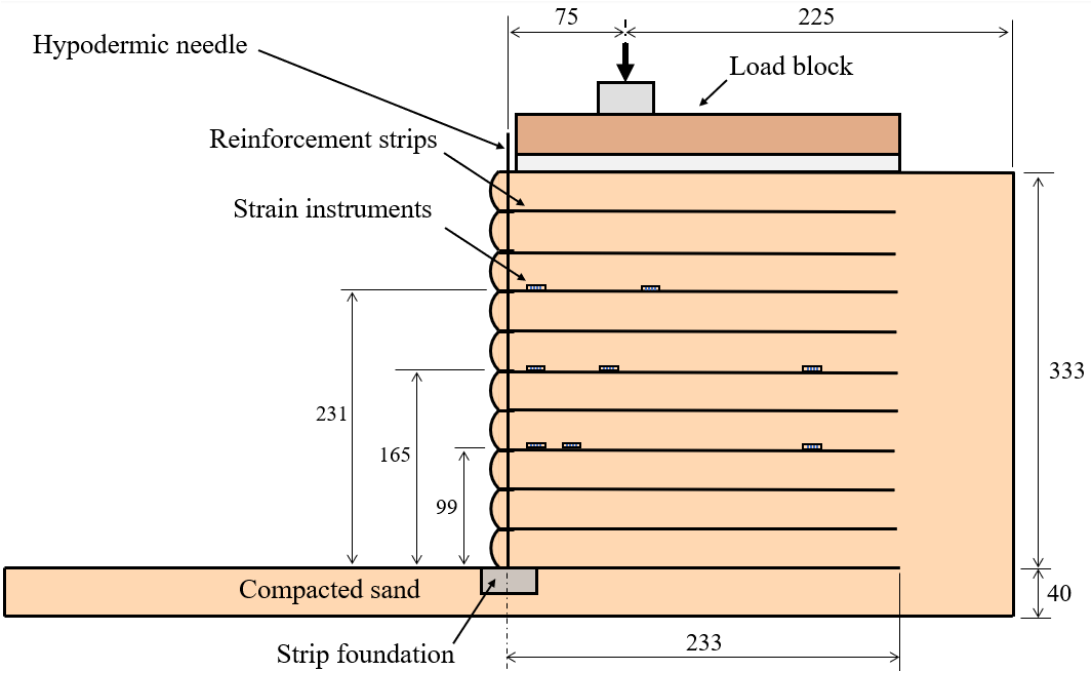

Figure 3-4. A cross-section of the stress-strain soil wall models. Not drawn-to-scale and all dimensions are in millimetres.

3.2.3 Strongbox

The soil wall models were constructed in an aluminium strongbox with internal dimensions 600 x 400 x 400 mm high. The strongbox contained a glass window for side-viewing of the soil wall and an aluminium divider was inserted to limit the soil wall width to 150 mm. The divider was fixed securely into position with an extension brace and is shown in Figure 3-5. Mild steel bar with tapered holes were fixed to the top of the strongbox unto which the actuator frame was fastened. Once the model set-up was complete, the strongbox was fitted onto the geotechnical centrifuge swing and contained the soil walls during centrifuge flight.

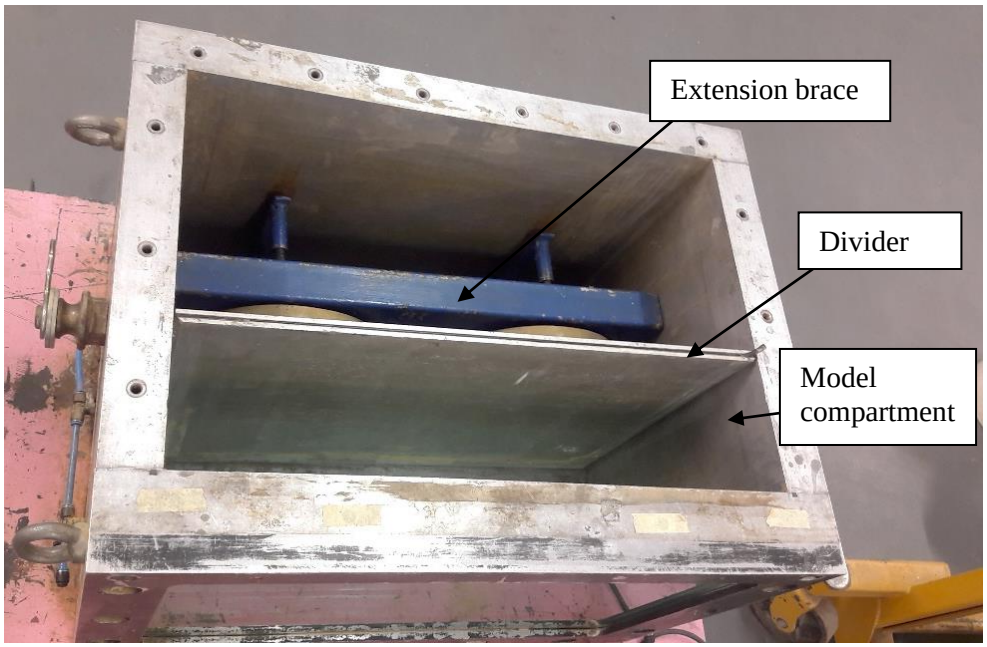

Figure 3-5. Top view of centrifuge strongbox with extension brace and divider.

3.2.4 Geotechnical centrifuge

The geotechnical centrifuge at the Department of Civil Engineering of the University of Pretoria was used to conduct the centrifuge modelling for this research (Jacobsz *et al.*, 2014). The centrifuge has a radius of 3 m from its centre to the model platform and is shown with the centrifuge model in Figure 3-6. Ten LED lights and a Canon digital single-lens reflex (DSLR) camera were installed in the centrifuge to capture any deformations in the soil wall models during flight. The DSLR camera was remote-controlled from the centrifuge control room. The centrifuge models were designed and constructed at a scale factor of n = 30 and accelerated in the centrifuge to 30 times that of Earth's gravity, or 30 G, to induce the appropriate stress distribution in the soil.

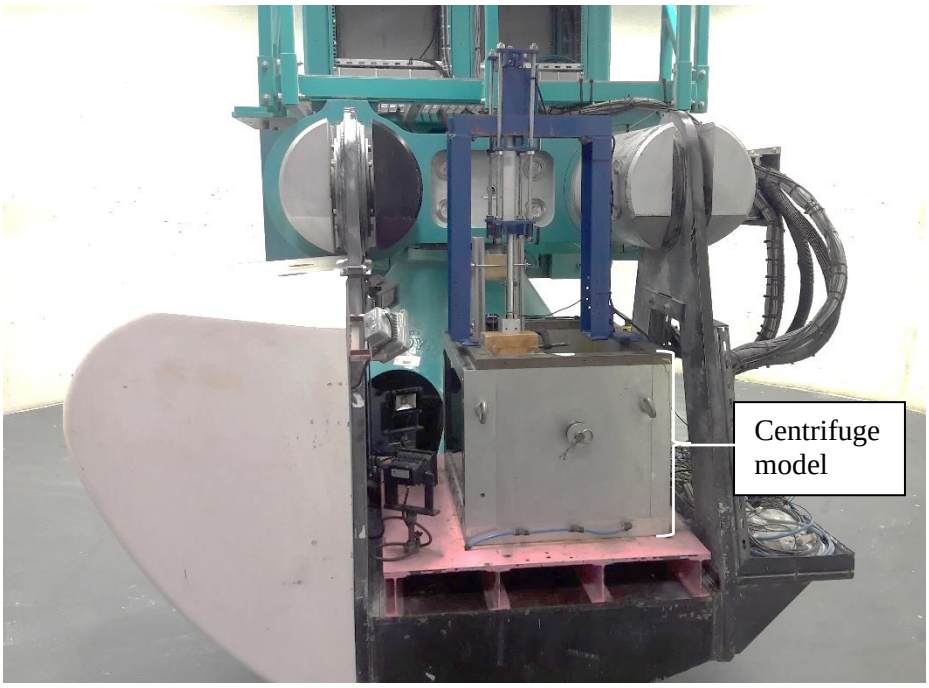

Figure 3-6. The centrifuge model in the geotechnical centrifuge at the University of Pretoria.

3.2.5 Instrumentation

1. Load control actuator

A 2 kN SFX actuator was used to apply vertical loads on the surface of the soil wall. The actuator was fixed inside the actuator frame which was attached to the mild steel plates on top of the strongbox. The load actuator was remotely controlled from the centrifuge control room during testing, and the completed set-up is shown in Figure 3-7.

A 0.5 kN load cell, shown in Figure 3-8, was attached to the end of the actuator to record the load applied. The load cell was positioned on the centre line of the soil surface, which was 75 mm from the inside of the strongbox and 75 mm from the wall facing. The load exerted by the actuator was transferred to the soil wall through the load block. The load block was constructed out of three materials of decreasing stiffnesses, aluminium, wood, and polystyrene, to transfer an evenly distributed surcharge pressure over the surface of the soil wall and to prevent the load block from punching through the soil.

The load block used in the load-displacement tests had dimensions 112 x 145 mm wide and a total surface area of 16 240 mm^2 to achieve 30 kPa of stress with an applied vertical load of 500 N. In the stress-strain tests, a larger load block was constructed with dimensions 233 x 145 mm wide to apply a distributed surcharge load across the full-length of the 233 mm reinforcement strips. The larger surcharge area was chosen for the stress-strain tests to ensure loading was applied to the full length of the reinforcement strips to record the reinforcement strain along the entire length of the reinforcement. The smaller load block used in the load-deformation tests ensured the loading was concentrated near the wall facing as the movement of the wall facing was observed during loading. A sketch of the smaller load block used in the load-displacement experiment is shown in Figure 3-9, and the length of the load block used in the stress-strain tests is given in parenthesis.

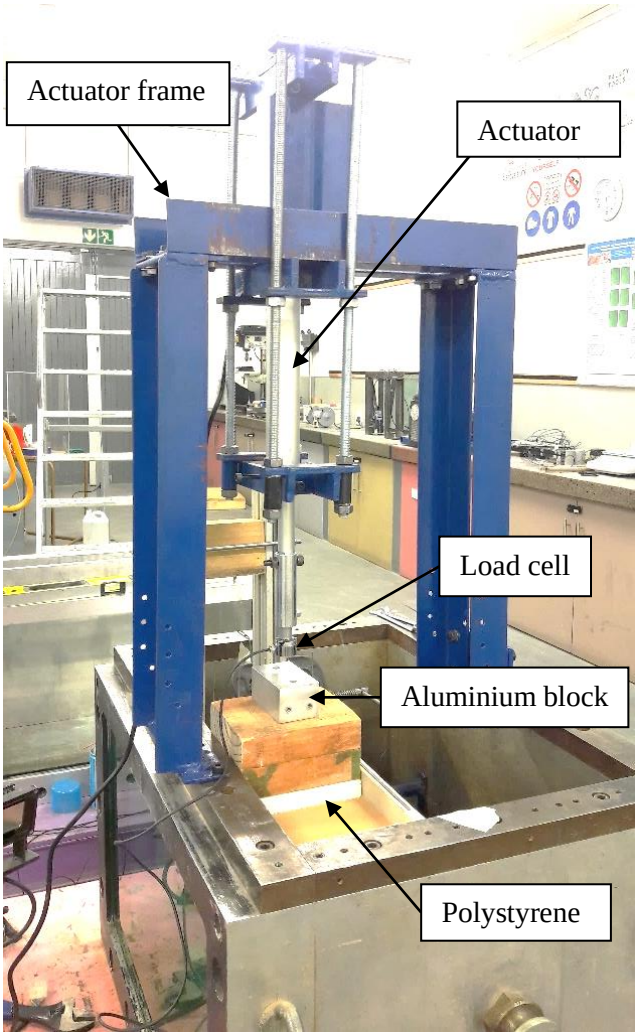

Figure 3-7. Actuator frame setup.

Figure 3-8. The actuator and load cell used in the experiment.

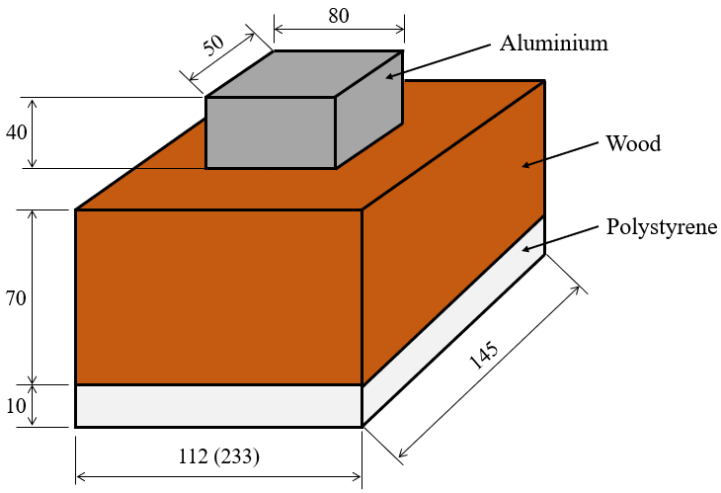

Figure 3-9. A 3D sketch of the load block used, not drawn-to-scale and all dimensions are in millimetres.

2. LVDTs

In the load-displacement experiment, four Solartron linear variable differential transformers (LVDTs) with 30 mm range were fixed inside the strongbox to measure the displacement of the soil wall facing under loading. The LVDTs were fastened to two aluminium frames that were clamped to the strongbox. The LVDTs were set in pairs to measure the displacement at 1/3 and 2/3 of the total soil wall height, in other words, at heights of 115 mm and 223 mm, respectively. The centres of the LVDTs were fixed 45 mm from the sides of the strongbox and the LVDT tips were extended to the surface of the soil wall facing. Small springs were coiled from 0.8 mm diameter piano wire and placed onto the extension rod of the LVDTs. The LVDT springs provided a small resistance to prevent the LVDT tips from sliding away from the soil wall facing during centrifugal spin-up and during testing. The completed LVDT set-up is shown in Figure 3-10.

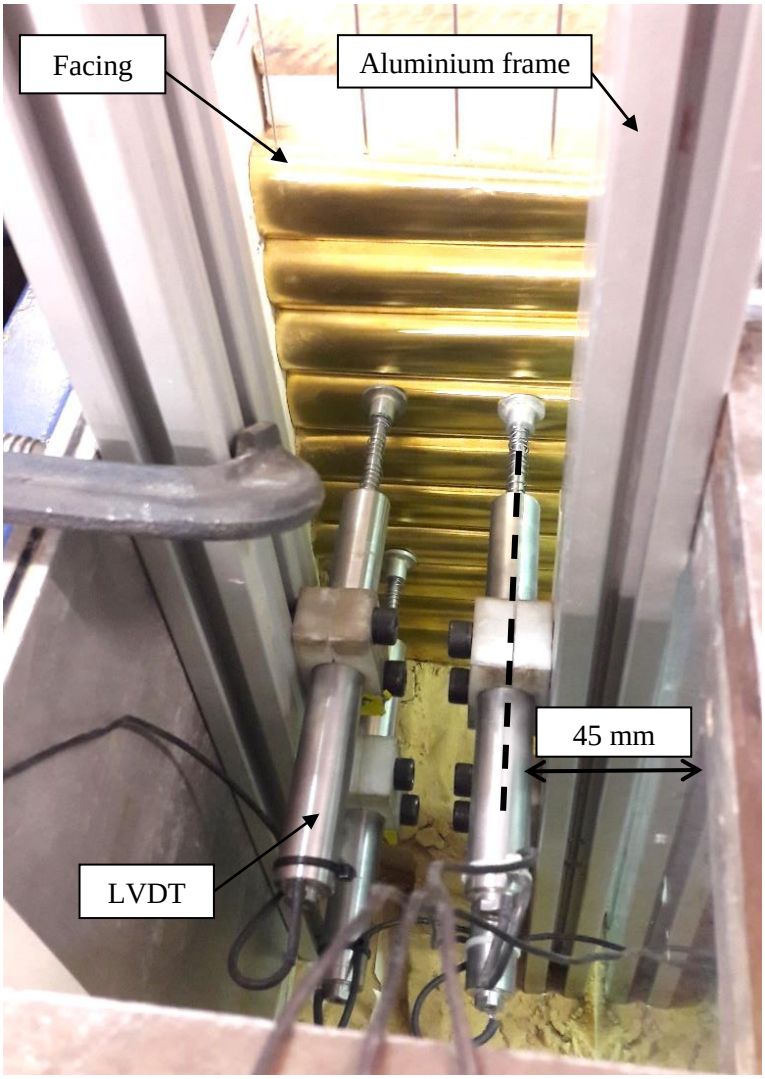

Figure 3-10. Four LVDTs fastened on the aluminium frame inside the strongbox.

3. Strain measurement

The inherent self-weight stresses of the soil wall, and any external applied stresses to the soil wall, are transferred to the reinforcement strips through friction. The soil wall stresses then cause strains along the reinforcement to develop as the reinforced soil wall resists shearing. The development of these reinforcement strains was measured in the stress-strain experiment by conducting two tests with reinforcement strain instrumentation.

The first stress-strain soil wall test consisted of extensible PVC reinforcement and was instrumented with conventional strain gauges. The second test was instrumented with Fibre Bragg gratings (FBGs) that measured the strains in the inextensible brass reinforcement strips. The FBGs were only used in the brass reinforced soil wall test as the PVC reinforcement strained beyond the FBGs strain limit.

The FBGs strain limit was determined as follows:

$$\frac{\Delta\lambda_B}{\lambda_B} = K_\varepsilon \varepsilon_{fibre} + K_T \Delta T \qquad \text{(Equation 3-1)}$$

Where:

$\Delta\lambda_B$ = change in Bragg wavelength (4 nm)

λ_B = Bragg wavelength (1 550 nm)

K_ε = strain coefficient (0.78)

ε_{fibre} = fibre optic strain

K_T = thermal coefficient

ΔT = temperature change (assumed 0 °C)

The tests were conducted at constant temperature in the geotechnical centrifuge and so temperature change was assumed negligible. The total allowable change in Bragg wavelength of 4 nm limited the strains of fibre cable to 0.3%:

$$\varepsilon_{fibre} = \frac{\Delta\lambda_B}{\lambda_B} \cdot \frac{1}{K_\varepsilon} \quad \text{(Equation 3-2)}$$

$$= \frac{4}{1\,550} \cdot \frac{1}{0.78}$$

$$= 0.003 = 0.3\%$$

The expected reinforcement axial strains in the soil walls were calculated for both reinforcement material types using Hooke's Law:

$$\varepsilon = \frac{\sigma}{E} = \frac{F}{EA} \quad \text{(Equation 3-3)}$$

Where:

F = axial force in reinforcement (N)

A = cross-sectional surface area of reinforcement (m^2)

E = Young's modulus (Pa)

Due to the self-weight of the soil, the theoretical axial force for each layer of reinforcement strips was determined using Coulomb's Law for a failure wedge occurring at $\theta = 45° + \phi'/2$.

$$T_i = \frac{i}{n(n+1)} K_a \gamma H^2 \quad \text{(Equation 3-4)}$$

Where:

T_i = reinforcement tensile force per layer (kN)

i = reinforcement layer

n = total number of layers (10)

K_a = active earth pressure coefficient (0.25)

γ = unit weight of soil (16 kN/m^3)

H = soil wall height (10 m)

The tensile forces expected at each reinforcement layer are tabulated in Table 3-2.The largest theoretical tensile force per metre length of wall occurs in the tenth layer, at the bottom of the soil wall.

Table 3-2. Theoretical tensile force at each reinforcement layer per metre length of wall.

Layer, i	T_i (kN)
1	3.6
2	7.3
3	10.9
4	14.5
5	18.2
6	21.8
7	25.5
8	29.1
9	32.7
10	36.4

With the maximum reinforcement tensile force assumed to be 36.4 kN, the strains expected for the PVC and brass reinforcement elements were calculated for the prototype after centrifugal scaling laws were applied to the model dimensions:

$$\varepsilon_{PVC} = \frac{F}{EA} = \frac{36\,400}{(2.5 \cdot 10^9)(0.72 \cdot 10^{-3})} = 2\% > 0.3\%$$

$$\varepsilon_{brass} = \frac{F}{EA} = \frac{36\,400}{(65 \cdot 10^9)(0.72 \cdot 10^{-3})} = 0.08\% < 0.3\%$$

The expected PVC reinforcement strains exceed the FBG allowable strains and, as a result, were not used to instrument the PVC strips. The expected brass reinforcement strains, however, were lower than the allowable FBG strains and were therefore instrumented with fibre optic strands.

Eight FBGs were attached to the brass reinforcement strips and eight linear 120 Ω strain gauges were attached to the PVC reinforcement strips. The FBGs and strain gauges were fixed at three soil wall heights: 3 m, 5 m, and 7 m prototype heights to capture the development of strains across the height of the soil wall. A cross-section of the placement of both FBG and strain

gauges in the soil wall is shown in Figure 3-11 with model dimensions in millimetres. Following the methodology employed by Bourgeois *et al*. (2011), three FBGs and strain gauges were fastened as close as practically possible to the wall facing (30 mm in the model) to measure the strains at the wall facing. Another three were fastened on the Coulomb failure plane, namely 50 mm, 73 mm, and 84 mm from the wall facing to capture the theoretical maximum strains (Coulomb, 1776). The final two sets of FBGs and strain gauges were placed at two-thirds of the total strip length, or 155 mm from the wall facing, to capture the strains near the end of the reinforcing strip lengths.

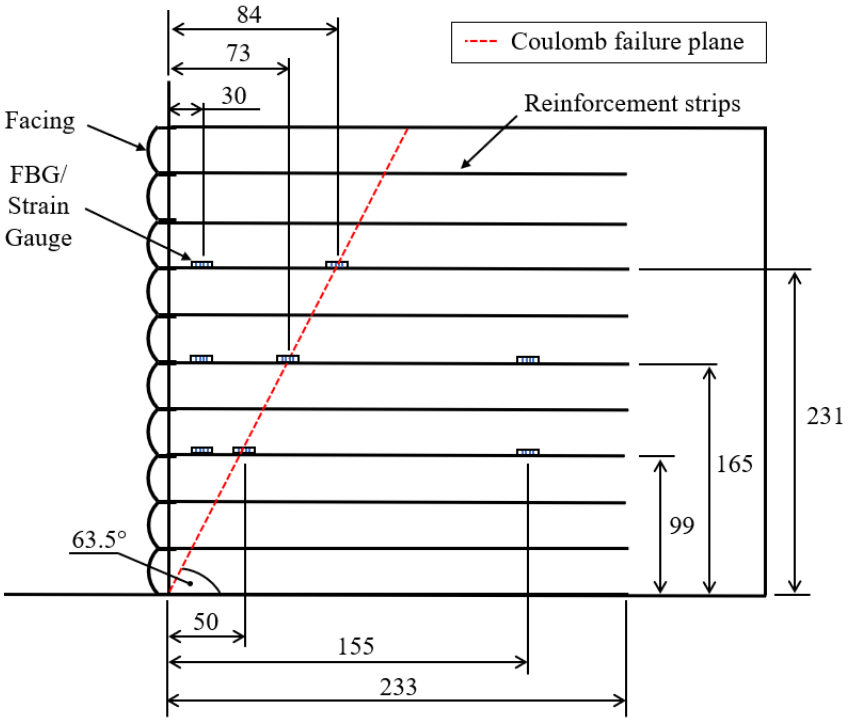

Figure 3-11. Fibre Bragg gratings and strain gauge locations in the soil wall, not drawn-to-scale and all dimensions are in millimetres.

The FBG fibre strands and the strain gauges were fastened to the centre reinforcement strip in the same manner. First, the reinforcement strip was lightly sanded by hand at the locations where the strain instruments were to be placed. The reinforcement strip was then cleaned with alcohol and the strain instruments were glued onto the strip with epoxy glue. A set of PVC reinforcement strips and a set of brass reinforcement strips instrumented with strain gauges and FBGs respectively are shown in Figure 3-12 and Figure 3-13.

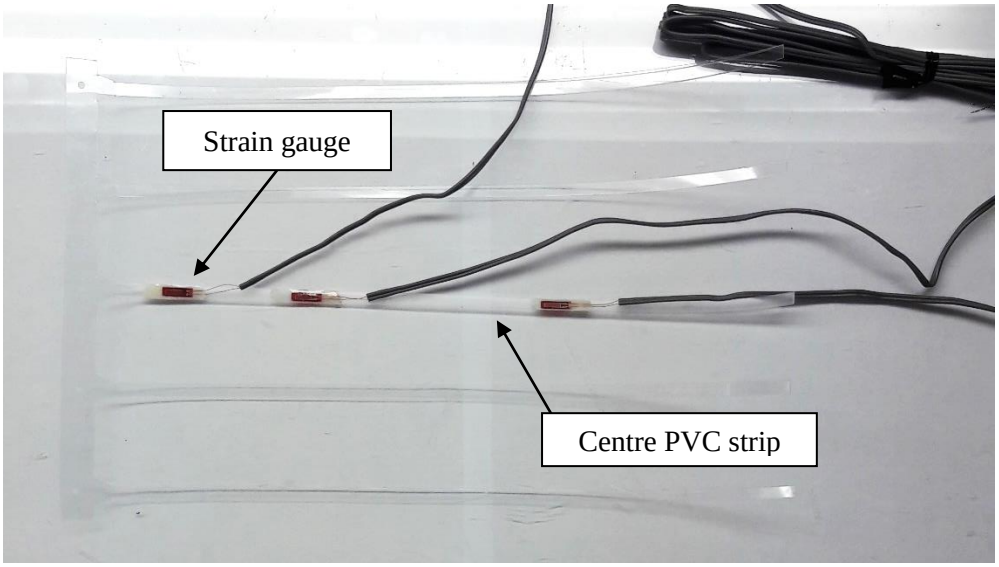

Figure 3-12. Strain gauges glued onto the centre PVC reinforcement strip.

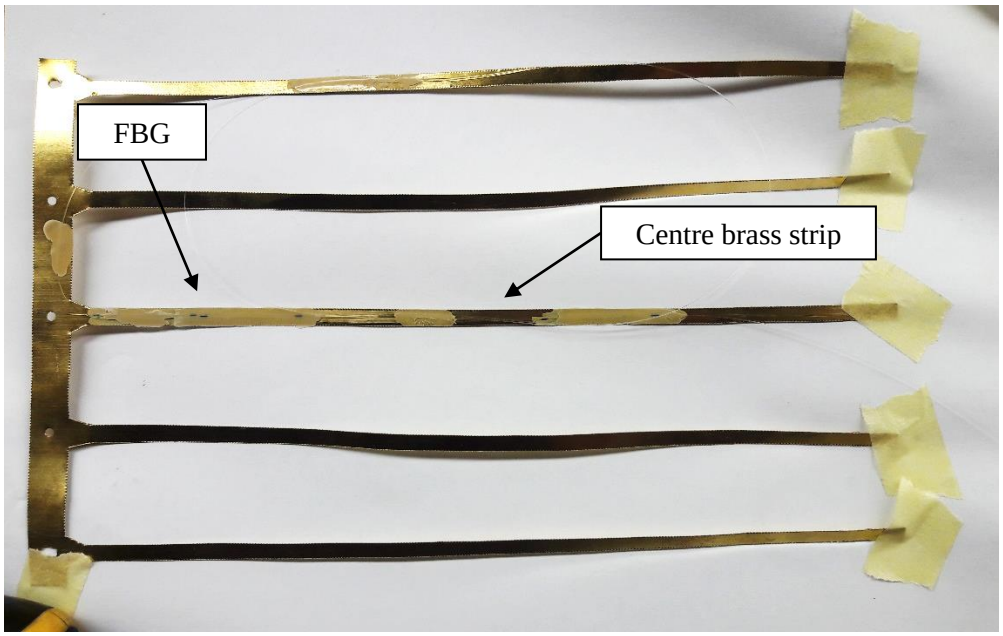

Figure 3-13. FBGs glued onto the centre brass reinforcement strip.

The strain instruments were connected to the following devices: The strain gauges were connected to a strain gauge transducer and converted with a quarter Wheatstone bridge. The three fibre optic strands containing the FBGs were connected to the HBM FS22 Industrial Optical Interrogator (Dynamic). The fibre optic interrogator was fastened as close as possible to the centre of the centrifuge on the centrifuge beam to minimise the centripetal acceleration experienced by the interrogator and is shown in Figure 3-14. The three reels of fibre strands were placed inside the strongbox and are shown in Figure 3-15.

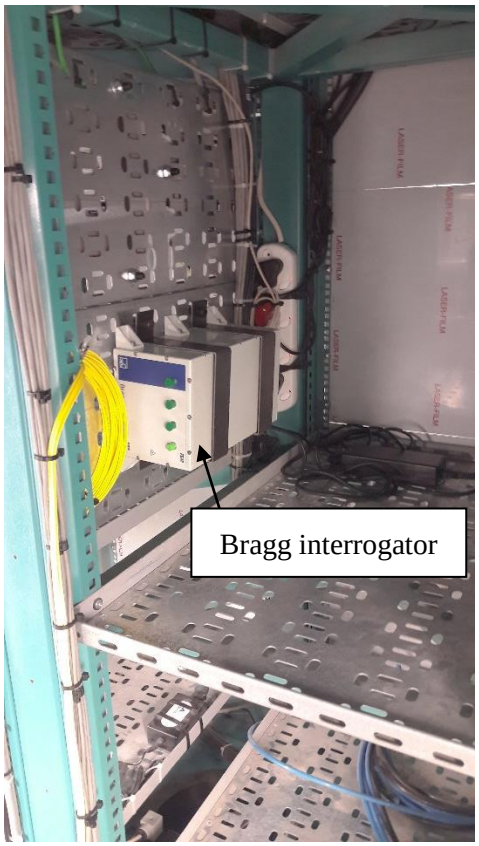

Figure 3-14. HBM fibre Bragg interrogator in the centrifuge.

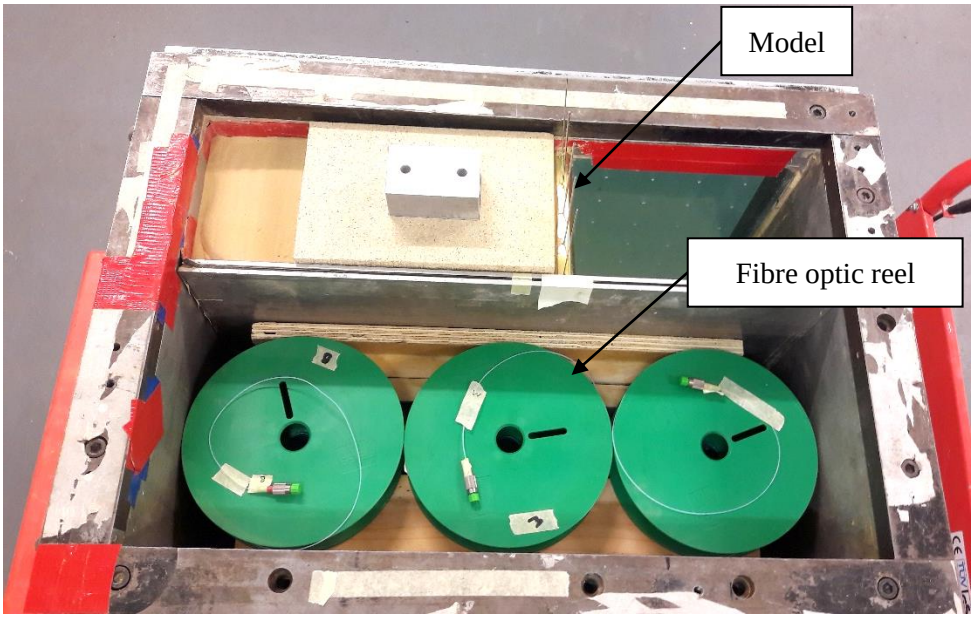

Figure 3-15. Constructed soil wall model with fibre optic reels inside the strongbox.

3.3 MODEL PREPARATION

3.3.1 Wall facing

A flexible metallic facing was formed out of U-shaped panels that were laid horizontally to replicate the conventional facings used in the first soil walls (Vidal, 1966). Due to the limitation of constructing the soil wall model at 1 G and then accelerating the completed model to 30 G in the centrifuge, large soil settlements were expected to take place. During the centrifugal acceleration, a rigid facing would not settle together with the backfill, placing large stresses on the facing and reinforcement joints. Therefore, the solution was to use flexible metallic material in the form of brass shim stock that would deform in unison with the reinforced backfill during centrifugal acceleration. The dimensions of the U-shaped panels are shown in Figure 3-16.

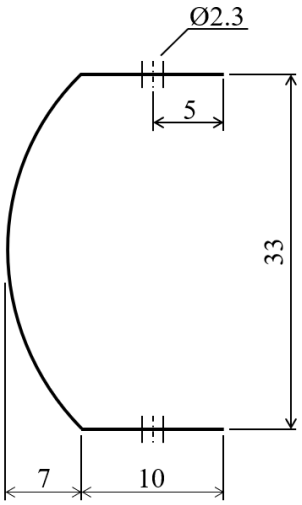

Figure 3-16. A cross-section sketch of the flexible U-shaped panel. Not drawn-to-scale and all dimensions are in millimetres.

The U-shaped panels were assembled and aligned vertically by sliding them through five hypodermic needles. The needles were 2.3 mm in diameter and acted as the facing joints unto which the reinforcement strips were connected. At the bottom of the facing, the needles were fixed into the 20 mm thick aluminium strip foundation. The facing and reinforcement strips were able to slide freely vertically to preserve unison of movement together with the backfill soil. The partly assembled wall facing is shown in Figure 3-17.

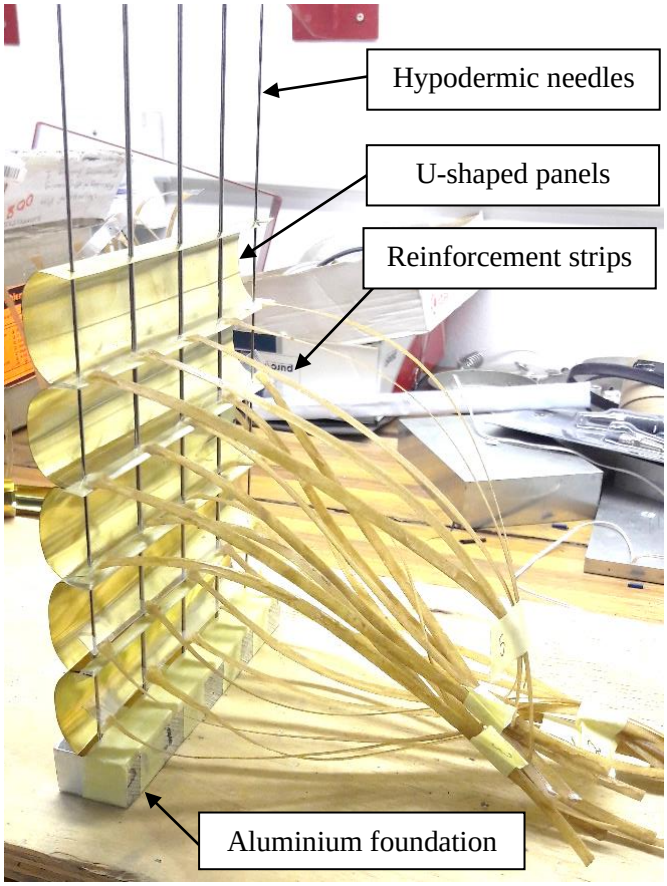

Figure 3-17. Partly assembled soil wall facing with reinforcement strips.

3.3.2. Reinforcement elements

1. Design

Brass shim stock and polyvinyl chloride (PVC) were the two types of materials used to replicate the steel (inextensible) reinforcement and geosynthetic (extensible) reinforcement respectively used in soil walls. The soil wall models were designed with the Coulomb tie-back wedge method and the minimum number of reinforcement strips was chosen per metre width of wall to ensure displacement of the soil wall, and possibly failure, under loading. The total force, T_w, required to resist self-weight failure in the prototype was calculated as follows:

$$T_w = W \times \tan(\beta) \qquad \text{(Equation 3-5)}$$

Where:

W = self-weight (kN): area of unit weight γ (16 kN/m^3)

β = internal angle: 90° - (45° + ϕ/2)

Therefore:

$$T_w = (0.5 \times 10 \times 5 \times 16) \times \tan(26.5)$$

= 199 kN/m per metre width.

The 199 kN/m force is distributed across the height of the soil wall with a maximum self-weight force of 36.4 kN in the tenth layer, as shown in Table 3-2. The tensile strength of geosynthetic strips range between 37.5-100 kN and medium tensile steel strips have 114 kN strength. One reinforcement strip was placed at one metre horizontal and vertical spacings to provide adequate self-weight stability and to allow for wall movement once a surcharge is applied to the models.

Each vertical layer of reinforcement elements in the soil wall models consisted of five strips with 33 mm horizontal spacings. The reinforcement strips were cut to 33 mm horizontal spacings to replicate the 1 m prototype horizontal spacings, as shown in Figure 3-18 and Figure 3-19. Each of the five strips were connected through the shoulder strip to prevent horizontal strip rotation and were cut at an angle to form a small “neck”. The neck improved the strength of the joint and prevented a weakened shear zone through the drilled hole. The 2.5 mm holes were drilled into the shoulder strips to slide the hypodermic needles through. The vertical spacing of the reinforcement strips corresponded to the 33 mm height of each U-shaped panel, equating to ten layers of reinforcement strips in the wall.

Initial design specifications for soil walls with flexible facing recommended conservative reinforcement lengths at eighty percent of the wall height, H (Jones, 1985). However, 0.7H reinforcement lengths can prove sufficient to resist bond failure. The ratio of 0.7H equates to 7 m prototype reinforcement strips lengths and 233 mm equivalent model strip lengths.

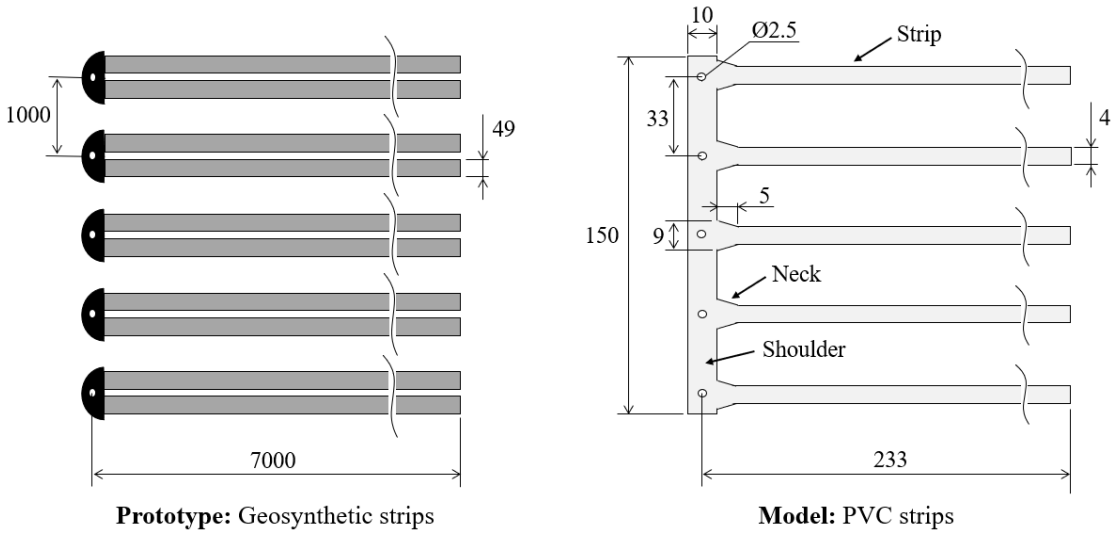

Figure 3-18. Plan view sketch of the extensible reinforcement used in the prototype and model. Sketch is not drawn-to-scale and all dimensions are in millimetres.

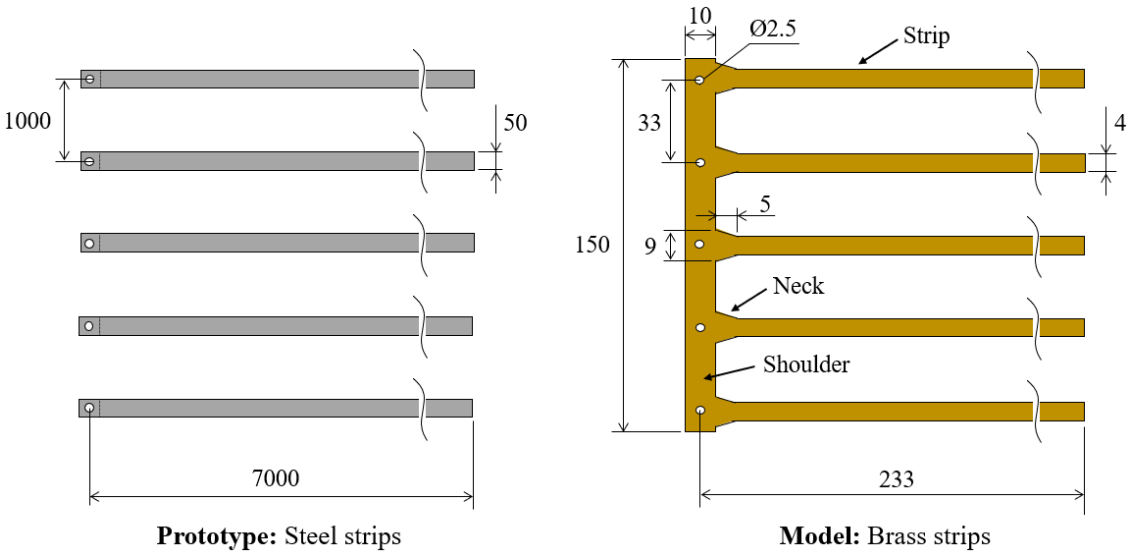

Figure 3-19. Plan view sketch of the inextensible reinforcement used in the prototype and model. Sketch is not drawn-to-scale and all dimensions are in millimetres.

To replicate the prototype reinforcement extensibility, the axial stiffnesses of the steel and geosynthetic materials must be known and scaled down to accurately construct the centrifuge model. The reinforcement axial stiffness (EA) is the product of the elastic modulus of the material (E) and the cross-sectional area of the reinforcement (A).

$$Axial\ stiffness, EA = E \times A$$

The axial stiffnesses of the steel and geosynthetic reinforcement in the prototype soil wall are known and were converted to the equivalent model axial stiffnesses with the applicable scaling law:

$$EA_{prototype} = n^2 \times EA_{model} \qquad \text{(Equation 3-6)}$$

Where n = 30.

The elastic modulus of the PVC and brass materials used in the models were determined by conducting a standard tensile test using a universal 50 kN tensile test machine. The PVC and brass materials were 0.2 mm thick, causing the width of reinforcement to be the only adjustable variable. The reinforcement strip dimensions, axial stiffnesses, and the equivalent prototype properties for both extensible and inextensible reinforcement elements are listed in Table 3-3.

Table 3-3. Prototype and model reinforcement strip dimensions and axial stiffnesses.

Parameter	Units	Extensible		Inextensible	
		Prototype (Geostrap)	**Model (PVC)**	**Prototype (Steel)**	**Model (Brass)**
Length, L	mm	7 000	233	7 000	233
Width, w	mm	98	4	50	4
Thickness, t	mm	5	0.2	4	0.2
Cross-sect. Area, A	mm^2	490	0.8	200	0.8
Elastic modulus, E	GPa	3	2.5	210	65
Axial stiffness, EA	kN	1 470	2	42 000	52
EA after scaled conversion	kN	N/A	1 800	N/A	46 800

2. Interface Friction

The final reinforcement property to consider is the interface friction, *f*, or the adhesiveness between the surface of the reinforcement and the soil particles. As the soil mass strains under stress, strains are mobilised in the reinforcement elements through the interface friction. The relationship is presented with the following equation:

$$\tau = f\sigma \qquad \text{(Equation 3-7)}$$

Where:

τ = shear stress in reinforcement

σ = normal stress in soil

A low coefficient of interface friction between the soil and reinforcement would allow only a small shear stress to develop in the reinforcement before slipping failure occurred in the soil wall. To prevent the reinforcement from slipping out of the soil walls prematurely, sand particles were glued to both sides of the reinforcement surfaces with an adhesive resin. The adhesive resin was applied to the reinforcement surfaces and the sand was poured over the strips by hand. This increased the interface friction coefficient equal to the friction between the soil particles:

$$f = \tan(\emptyset) = \frac{\tau}{\sigma}$$

$$f = \tan(37°) = 0.75$$

Surface preparation of the reinforcement strips is shown in Figure 3-20.

Figure 3-20. Surface preparation of the reinforcement strips.

3.3.3. Backfill

1. Soil grading

In centrifuge modelling, it is preferable to use uniformly graded soil to limit the extent of settlement during centrifugal acceleration. Uniformly sized particles largely maintain density during spin-up due to the absence of smaller sized particles that would settle into the voids. Hence, a uniformly graded cohesionless silica sand from the Cullinan mine (commercial source located 40 km east of Pretoria) was used as backfill in the soil wall.

The sand had a friction angle of 37° and was measured using a conventional shear box (Jacobsz, 2013). The soil was graded by Archer (2014) with a sieve analysis according to the British Standard BS1377-2:1990. The grading curve is shown in Figure 3-21 and indicates a uniformly graded fine sand. Archer also established the percentage fines in the sand by utilising a Malvern Mastersizer 2000 apparatus that makes use of laser diffraction.

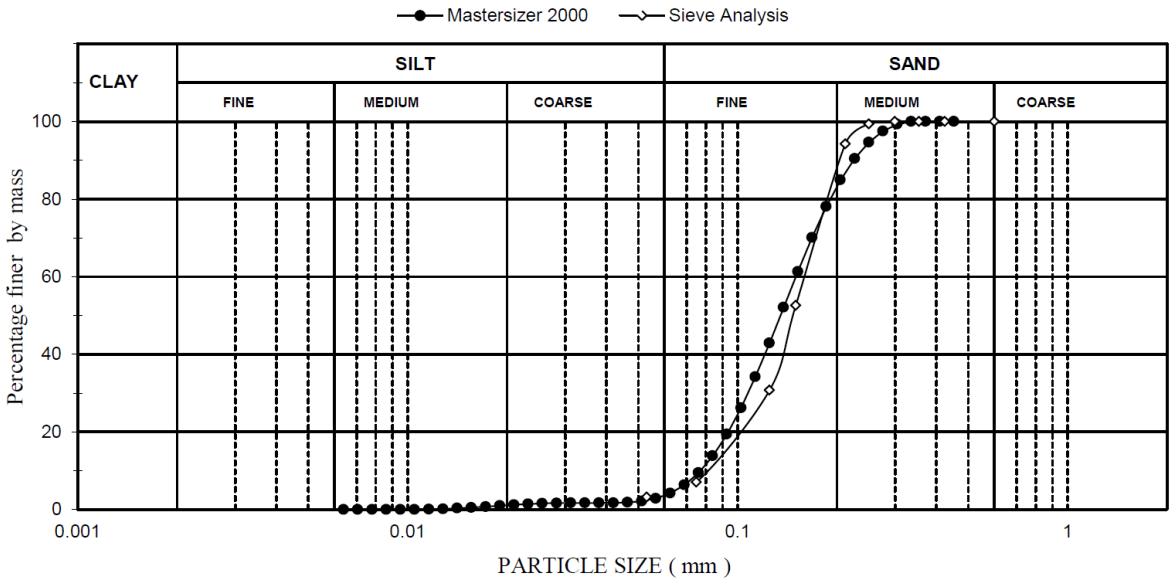

Figure 3-21. Particle size grading chart of the Cullinan sand after Archer (2014).

Based on the results presented in Figure 3-21, the soil is classified as a slightly silty sand, and according to the Unified Soil Classification System – USCS (ASTM Standard D2487. 2011), the soil is graded as a poorly graded sand (SP). Poorly graded sand is either uniformly graded or gap graded depending on the coefficient of uniformity, C_U:

$$C_U = \frac{D_{60}}{D_{10}} \qquad \text{(Equation 3-8)}$$

Where: D_{10} = the largest sieve size through which 10% of the soil particles pass

D_{60} = the largest sieve size through which 60% of the soil particles pass

According to Smith (2006), a poorly graded soil with $C_U < 4$ is considered uniformly graded and a soil with $C_U > 4$ indicates a gap graded soil. The C_U calculated in this study was 1.95, confirming a uniformly graded soil. Other soil particle properties included a maximum particle size of 300 μm and the mean particle size (D_{50}) of 135 μm (Archer, 2014).

3.3.3.2 Soil density

Finally, Archer (2014) conducted four tests to determine the maximum and minimum dry densities and void ratios of the sand according to the following two ASTM standards:

- D4254 - 00: Minimum Index Density and Unit Weight of Soils and Calculation of Relative Density.

- D4253 – 00: Maximum Index Density and Unit Weight of Soils using a Vibratory Table.

The test results are presented in Table 3-4 and indicate the average values for the minimum and maximum densities and corresponding void ratios.

Table 3-4. Cullinan sand minimum and maximum densities and void ratios (Archer, 2014).

Parameter	Units	Value
Maximum dry density	kg/m^3	1669
Minimum dry density	kg/m^3	1392
Maximum void ratio	e_{max}	0.92
Minimum void ratio	e_{min}	0.60

The density of the backfill was kept as constant as possible for each of the soil wall models by using a sandhopper to place the sand into the strongbox. In the load-displacement tests the dense foundation soil was placed with a five percent moisture content to increase the apparent cohesion and achieve greater compaction. The construction process is discussed in more detail in the next section.

Table 3-5 and Table 3-6 present the densities of the backfill and foundation soils, as well as the backfill void ratios, *e*, and relative densities, $I_{D,}$ of the four models. The void ratios and relative densities were determined from the measured densities of the dry soils as follows:

$$e = \frac{G_s}{\rho_d}\rho_w - 1 \qquad \text{(Equation 3-9)}$$

Where:

e = void ratio

G_s = specific gravity of soil particles (2.67)

ρ_d = measured dry soil density (kg/m^3)

ρ_w = density of water (1000 kg/m^3)

And:

$$I_D = \frac{e_{max} - e}{e_{max} - e_{min}} \quad \text{(Equation 3-10)}$$

Table 3-5. Backfill and foundation soil density in the load-displacement tests.

Soil Wall Model	Backfill			Foundation
	Density (kg/m^3)	Void Ratio, e	Relative Density, I_D	Density (kg/m^3)
1. PVC (Extensible)	1482	0.80	0.37	2140
2. Brass (Inextensible)	1461	0.83	0.29	2152

Table 3-6. Backfill and foundation soil density in the stress-strain tests.

Soil Wall Model	Backfill and Foundation Density (kg/m^3)	Void Ratio, e	Relative Density, I_D
3. PVC (Extensible)	1507	0.77	0.46
4. Brass (Inextensible)	1515	0.76	0.49

Berry and Byrne (2008) indicate the following consistencies for typical dry densities of quick draining, non-cohesive materials:

- Very loose < 1450 kg/m^3
- Loose 1450 – 1600 kg/m^3
- Medium dense 1600 – 1750 kg/m^3
- Dense 1750 – 1925 kg/m^3
- Very dense > 1925 kg/m^3

The consistency of the backfills and the foundations in each soil wall model were therefore considered loose and very dense respectively.

3.3.4 Soil wall construction

The procedure for constructing the soil wall models in the strongbox is described in three major steps:

1. Preparation of strongbox

The aluminium divider was marked to indicate the centre of the box where the hypodermic needles were placed and marked horizontally to indicate the height of each layer where the reinforcement strips were laid. The marked divider is shown in Figure 3-22 and was inserted into the strongbox and set into the correct position with the extension brace. The strongbox was thoroughly cleaned with (alcohol) before each test and the internal corners of the model were sealed with duct tape to prevent soil leakage.

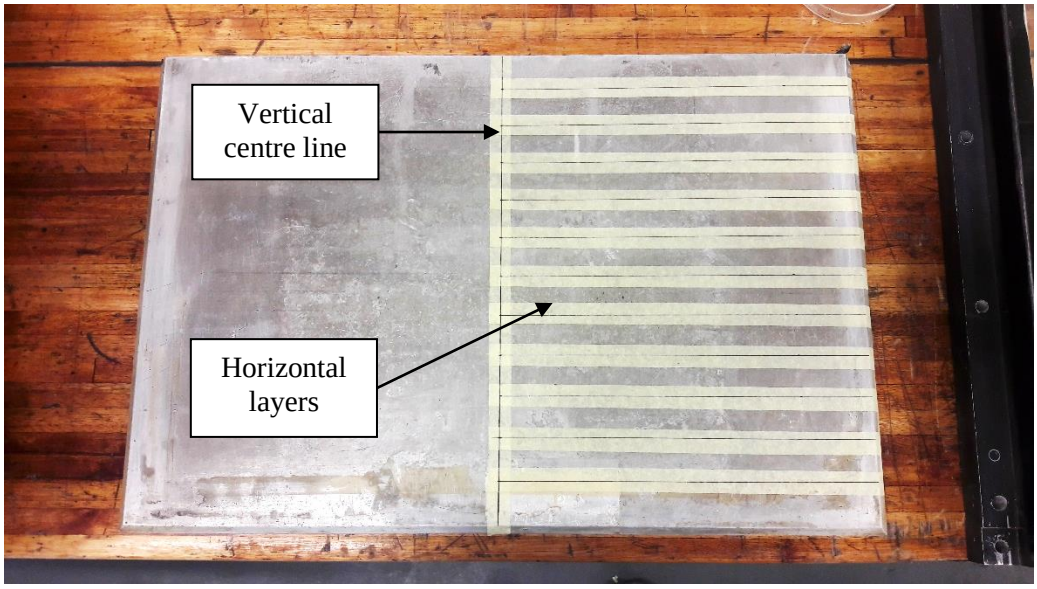

Figure 3-22. Centre line and horizontal layers markings on the aluminium divider.

2. Construction of foundation soil

For the load-deformation tests, a dense foundation was constructed. Five percent moisture content was added to the dry Cullinan sand to facilitate compaction and increase the apparent cohesion and resulted in a very dense foundation soil. The moist sand was manually compacted with a wooden block to a height of 40 mm. The foundations in the stress-strain tests were constructed with dry soil and compacted to achieve a relative density of approximately 0.5 by dropping a 2.3 kg mass from a 100 mm height above the soil. The foundation soil and backfill constructed in the stress-strain tests were made homogenous to allow all the soil to act in unison.

3. Construction of soil wall

The assembled wall facing together with the reinforcement strips were placed into the strongbox and the aluminium foundation strip was placed inside a trench prepared in the foundation soil. The gaps between each U-shaped panel were sealed with masking tape to prevent soil leakage. Furthermore, moist sand was pressed by hand to close the gaps on the sides of the U-shaped panels to prevent soil leaking out between the facing and the glass window, and between the facing and the divider.

The first layer of reinforcement strips was placed onto the foundation soil and the sand hopper, shown in Figure 3-23 was used to pour the dry sand evenly on top of the reinforcement at a constant drop height and speed. During pouring, the end of the pipe nozzle was kept 200 mm above the surface level of each layer of sand to maintain constant density throughout the height of the soil wall and in each of the four soil wall models. In the stress-strain tests, the soil was compacted by dropping a 2.3 kg mass from a height of 100 mm above the soil in 20 mm layers. The compaction procedure aimed to achieve a consistent relative density of approximately 0.5 between both tests.

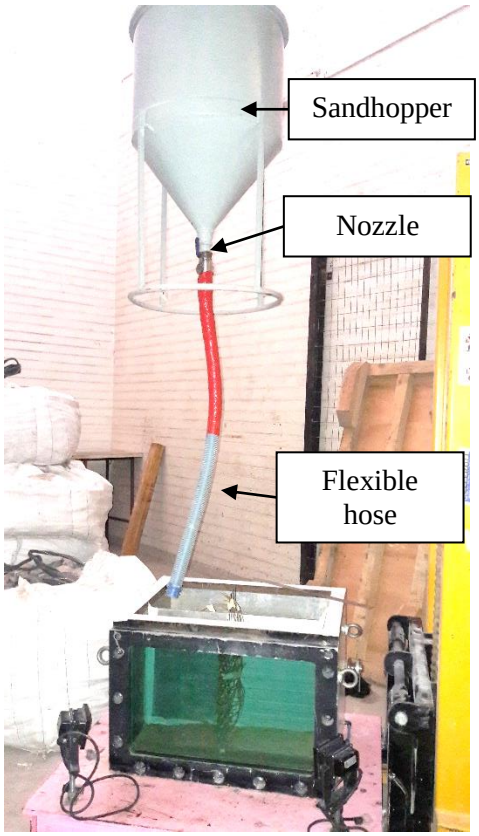

Figure 3-23. Sand was poured into the strongbox with the sandhopper.

Once the first 33 mm layer was filled with dry sand, the surface was slightly compacted to remove excessive air voids. The slight compaction minimised initial settlement during acceleration of the centrifuge and prepared an even surface for the second layer of reinforcement strips. This process was repeated for the consecutive layers of reinforcement strips to finally construct a 333 mm tall vertical soil wall (the tenth layer of sand at the top of the soil wall was constructed 36 mm thick to account for the 3 mm deficit due to the 0.3 mm remainder at each layer). Figure 3-24 presents the front view and side view of the completed soil wall.

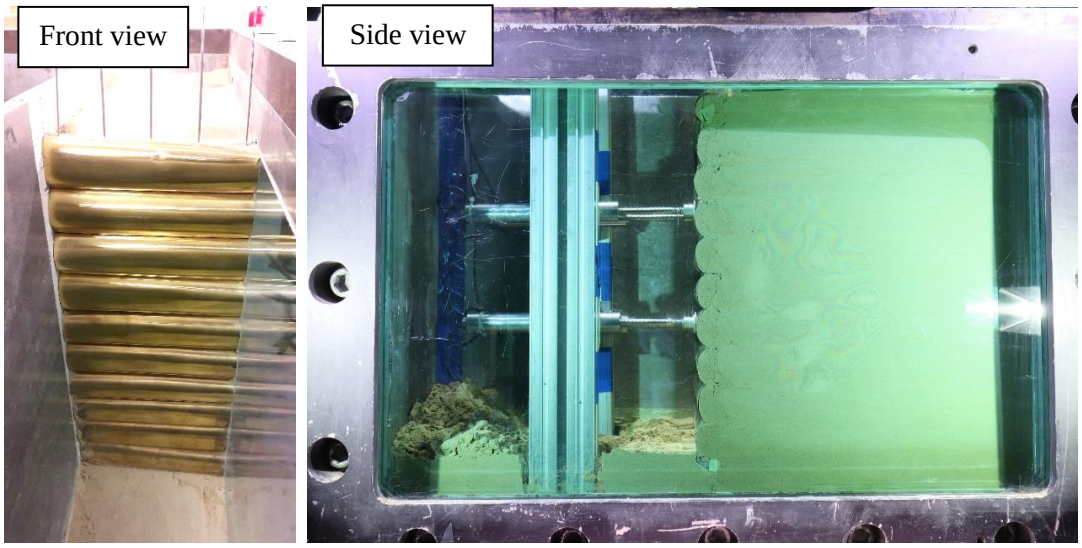

Figure 3-24. Front view and side view of the completed soil wall.

3.4 TEST PROCEDURE

The test procedure commenced once construction of the soil wall was completed. The strongbox housing the instrumented model was placed on the centrifuge platform. The four LVDTs were connected to the digital recording DigiDAQ system (Gaudin *et al.*, 2010) and were numbered starting from top left (purple) to bottom right (yellow), as is shown in Figure 3-25.

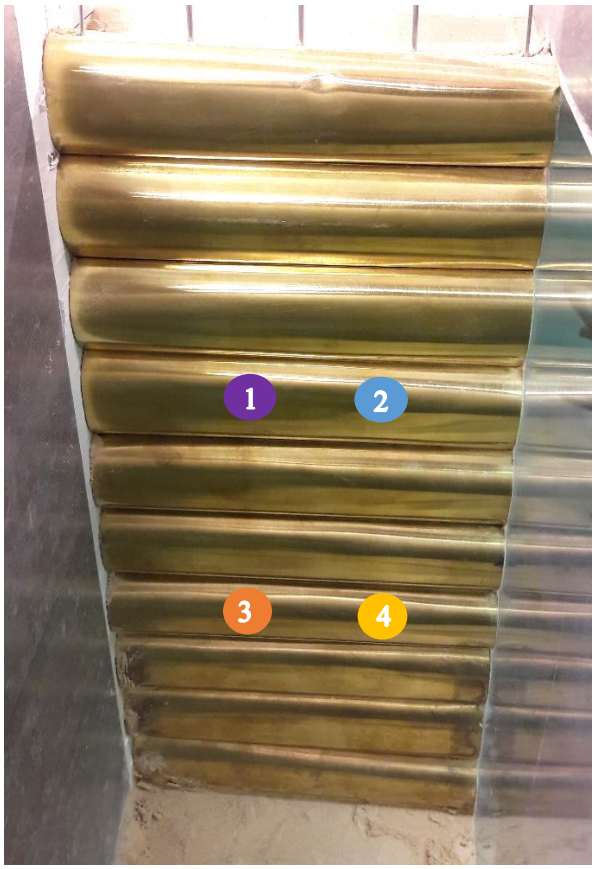

Figure 3-25. Numbering and colour-coding of the four LVDT positions.

The fibre optic cables were connected to the Bragg meter which was fastened on the centrifuge and the wavelength readings were monitored on the digital CATMAN software. The force recorded by the actuator load cell and the displacement of the actuator itself were also digitally monitored using the CATMAN software.

Once all systems were running, acceleration of the centrifuge began. The centrifuge software automatically counterbalanced the payload of the model and kept constant acceleration at 30 G. Once initial settlement and movement of the soil wall stabilised, the surcharge load was incrementally applied, not exceeding a force of 1 800 N, or equivalent surcharge pressure of

110 kPa, on the sand surface of the soil walls. The sequence of the four soil wall tests was as follows:

Class 1 (load-deformation tests):

1. Extensible reinforcement (PVC), without strain instrumentation.
2. Non-extensible reinforcement (brass), without strain instrumentation.

Class 2 (stress-strain tests):

3. Extensible reinforcement (PVC), with strain instrumentation.
4. Non-extensible reinforcement (brass), with strain instrumentation.

3.5 CHAPTER SUMMARY

Four physical soil wall models were prepared and tested in the geotechnical centrifuge. The models were constructed in the aluminium strongbox and tested at a centrifugal acceleration 30 G. An actuator was fixed to the strongbox and was used to apply surcharge loads to the surface of the soil walls. In the load-displacement tests, the displacement of the wall facing was recorded with four linear variable differential transformers (LVDTs) that were fixed inside the strongbox at two soil wall heights. In the stress-strain tests, strain instrumentation in the form of fibre optic Braggs and strain gauges were installed on the reinforcement strips at three heights in the soil wall. The fibre optic Braggs and strain gauges were fastened to the reinforcement strips and measured the tensile strains that developed along the reinforcement strips. The experimental methodology to prepare, construct, test, and record the performance of the soil walls was presented in this chapter, together with the properties of all the soil wall components including the soil wall facing, the backfill and the reinforcement elements.

4 LOAD-DISPLACEMENT RESPONSE OF REINFORCED SOIL WALL

4.1 INTRODUCTION

The load-displacement behaviour of two soil walls was investigated by applying surcharge loads to the soil behind the walls and measuring the response in movement of the wall facing. Two types of soil walls were tested in the geotechnical centrifuge: one was reinforced with extensible reinforcement in the form of PVC strips, and the other with inextensible reinforcement in the form of brass strips. The difference in load-displacement performance of the two types of soil walls is presented in this chapter and comparisons are made to understand the differences in behaviour.

The two load-displacement tests consisted of measuring the displacement of the soil wall facing induced by a surface surcharge load. Two reduced-scale soil walls were constructed, and four linear variable differential transformers (LVDTs) were set against the soil wall facing that measured the displacement. Two LVDTs were fixed at two-thirds height of the soil wall (223 mm), and the second pair were set at one-third height of the soil wall (115 mm) as shown in Figure 4-1. The loading of the surcharge on the soil wall surface and the corresponding LVDT displacement results are presented for the model tests and the results were scaled to the equivalent prototype soil wall.

PIV analysis was performed on the photographic images captured during the experiment. The displacement of the soil wall facings was analysed in terms of horizontal strains and the possible effects of setting the LVDTs against the wall facing were discussed. Finally, a summary of the load-displacement experiment is presented.

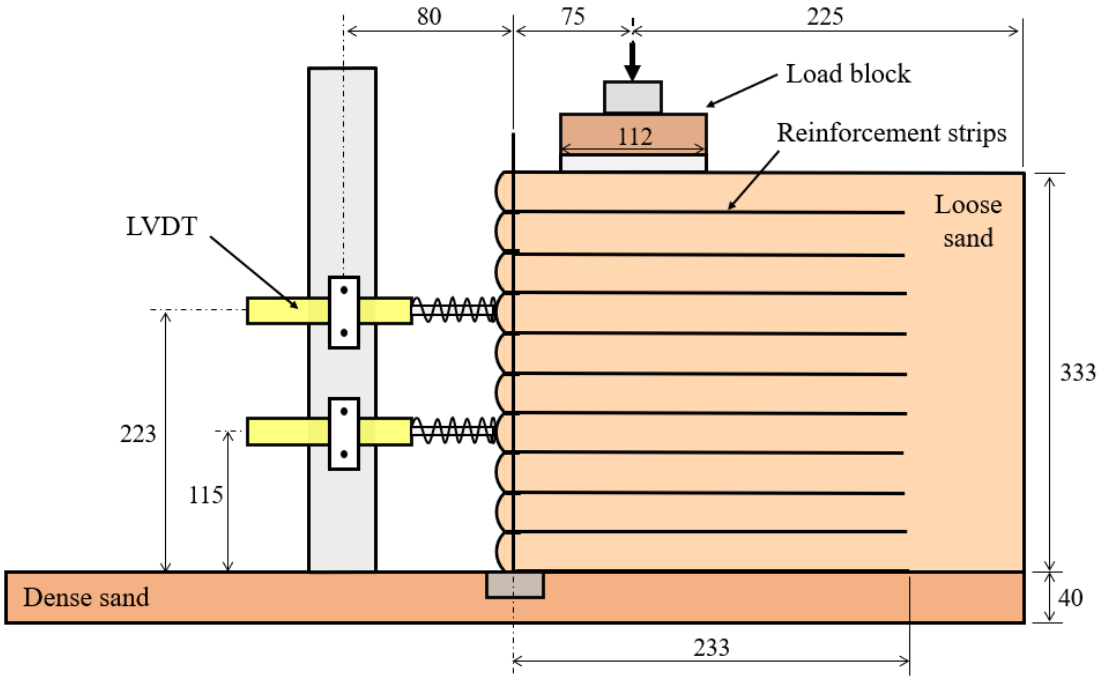

Figure 4-1. A cross-section of the load-displacement soil wall models. Not drawn-to-scale and all dimensions are in millimetres.

4.2 LOAD-DISPLACEMENT BEHAVIOUR

4.2.1 Load applied

Surcharge loads were applied directly to the top surface of the soil walls by exerting downward vertical forces with the overhead load actuator. The loads were applied after the centrifuge reached stability at 30 G acceleration. The actuator pressed directly onto the load block that was placed 75 mm behind the facing and covered a width of 112 mm. The load was increased manually in incremental steps to 100 kPa in both tests as it was not possible to apply constant loads. The forces exerted by the actuator were monitored with the 0.5 kN load cell attached to the tip of the actuator. The maximum load applied in both tests is presented in Table 4-1, and the incremental loading for both tests is shown in Figure 4-2. The force in newtons was converted to surcharge stress in kilopascals by dividing the applied force by the area of the load block, which was 16 240 mm^2.

Table 4-1. Maximum loads applied in load-displacement tests.

Test	Max Force (N)	Max Load (kPa)
Extensible (PVC)	1 780	102.8
Inextensible (Brass)	1 670	109.6

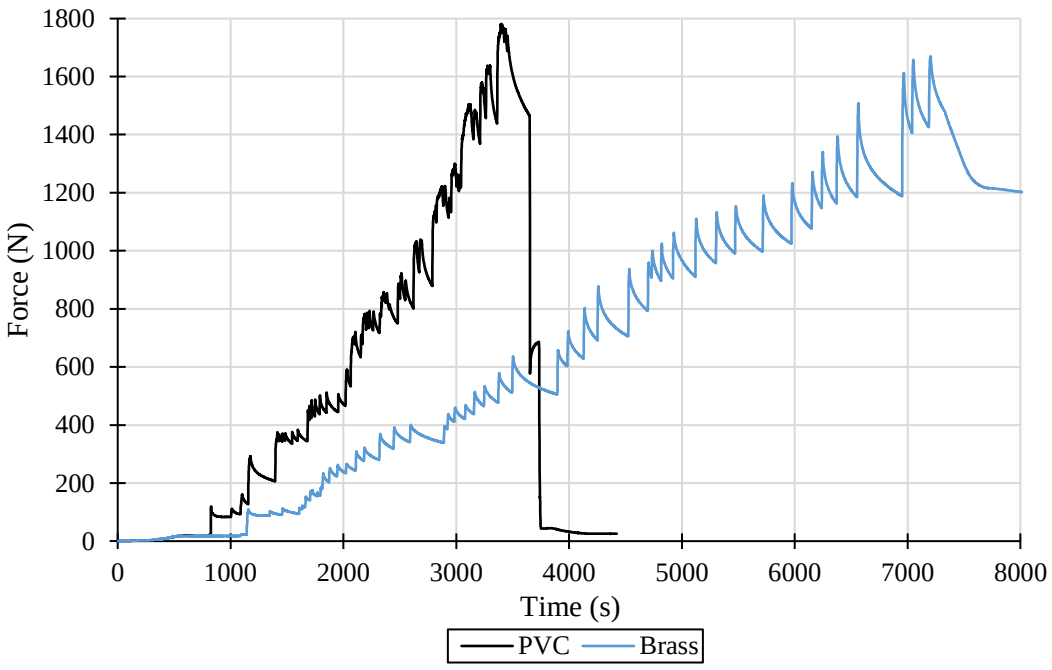

Figure 4-2. Surcharge loads applied in load-displacement tests.

4.2.2 Extensible reinforcement

1. Model

The surcharge load applied to the PVC reinforced soil wall transferred through the soil wall and caused displacement of the soil wall facing. The displacement was recorded by the four LVDTs during the experiment and is shown in Figure 4-3. LVDT 1 corresponds to the top left-hand position on the front of the soil wall facing, LVDT 2 to the top right, LVDT 3 to the bottom left, and LVDT 4 corresponds to the bottom right-hand side of the facing.

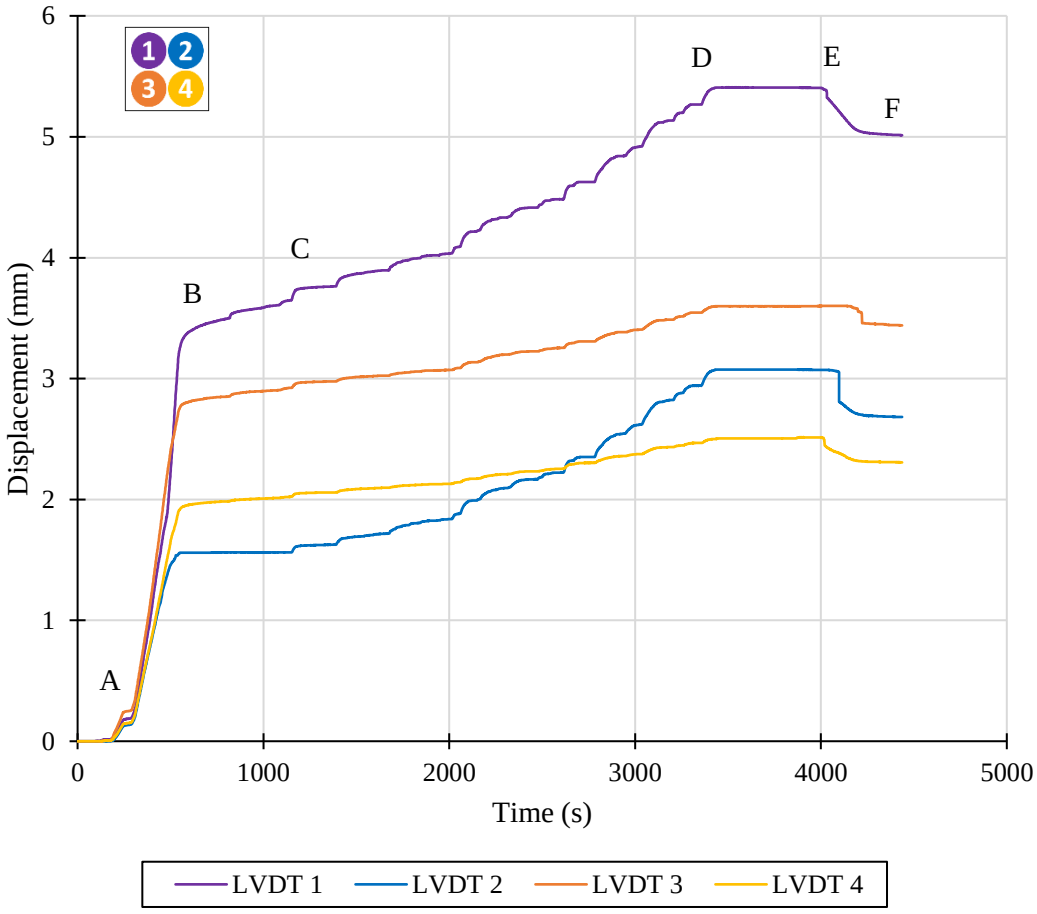

Figure 4-3. LVDT response in extensible (PVC) reinforced soil wall test.

The LVDTs in the PVC test recorded displacements in the range of 1.5 mm to 3.55 mm during centrifugal acceleration to 30 G, indicated from A to B in Figure 4-3. After the soil wall displacement stabilised, loading of the soil wall commenced and all four LVDTs responded with increased movement on the soil wall facing (C to D). LVDT 1 recorded the largest total displacement of 5.4 mm. Soil wall loading stopped at point D and the load actuator was removed from the load block. The total soil wall displacement under loading is therefore calculated between points C and D. The centrifuge was decelerated at E and small deformations were recovered as the centrifuge slowed back to 1G (E to F). The summary of displacements observed in the PVC reinforced soil wall is tabulated in Table 4-2.

Table 4-2. Summary of displacements for PVC reinforced soil test.

LVDT	Displacement (mm)		
	At 30 G	Maximum	Due to Loading
1	3.31	5.41	2.09
2	1.56	3.08	1.51
3	2.80	3.60	0.80
4	1.93	2.51	0.58

The LVDTs on the left side of the soil wall facing, i.e., LVDTs 1 and 3, recorded higher displacements than the LVDTs on the right-hand side at the same respective heights. The difference in behaviour is attributed to the strongbox wall that bordered the soil wall facing on the left-hand side as opposed to the strongbox window that bordered the facing on the right-hand side. It is concluded that the strongbox window resisted soil wall movement to a larger degree than the strongbox wall and identified the importance of installing two LVDTs at the same height to account for any possible differences in results.

The surcharge load applied to the soil wall surface was plotted together with the displacement response recorded by the four LVDTs in the PVC soil wall test and is shown in Figure 4-4. Each increase in applied load corresponded to an increase in recorded displacement. The top two LVDTs (LVDTs 1 and 2) recorded the largest displacement.

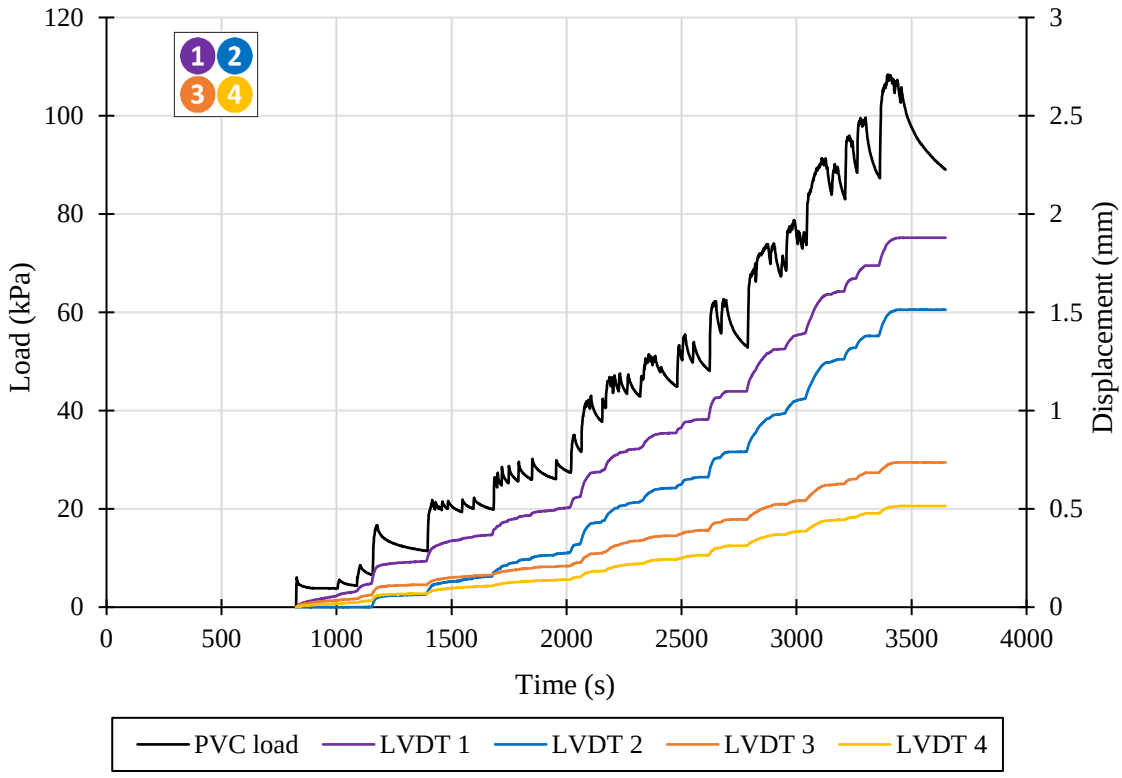

Figure 4-4. Load and LVDT response in extensible (PVC) reinforced soil wall test.

The displacement results were plotted as displacement of the soil wall facing in millimetres against the surcharge load applied on the soil wall surface in Figure 4-5. The displacements at all four LVDTs increased linearly with increased loading. The displacement at the top two LVDTs (LVDTs 1 and 2) increased at the same rate and the same observation is made for the bottom two LVDTs (LVDTs 3 and 4). This indicates consistent LVDT response to increased loading at the two soil wall heights. The displacement of the soil wall is presented in Figure 4-6 in surcharge load increments of 10 kPa for further clarity.

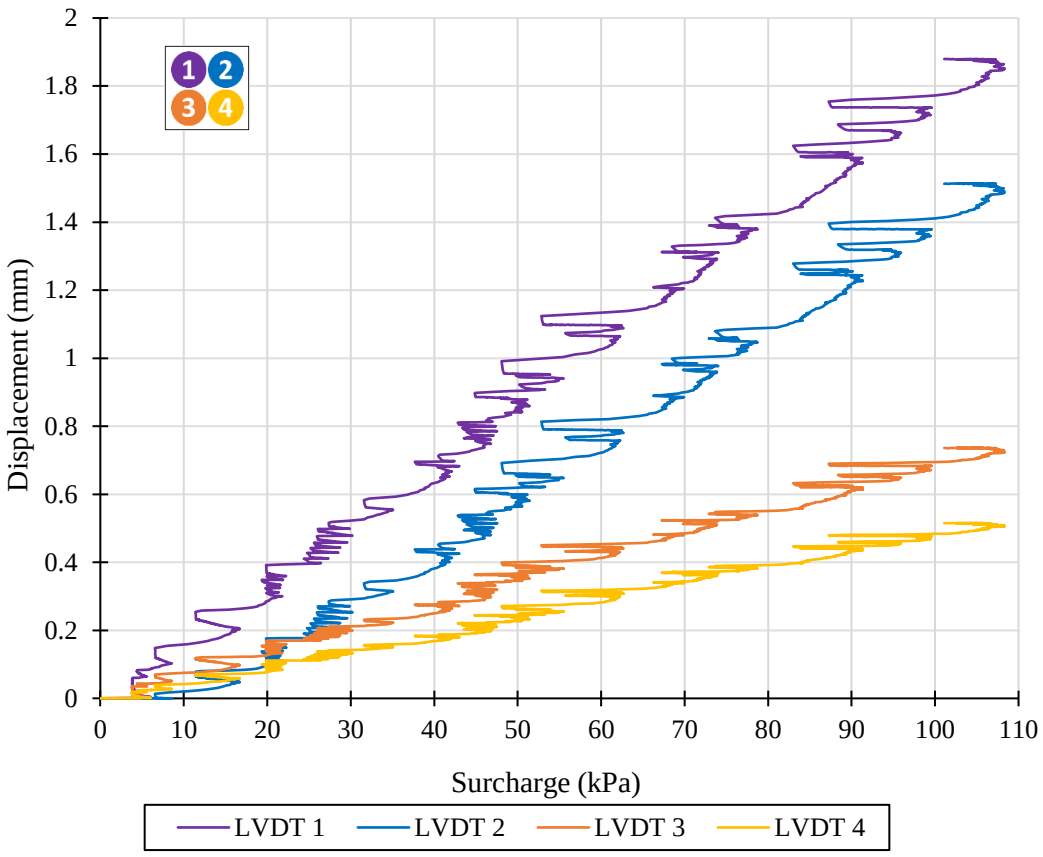

Figure 4-5. Displacement of extensible (PVC) reinforced soil wall test.

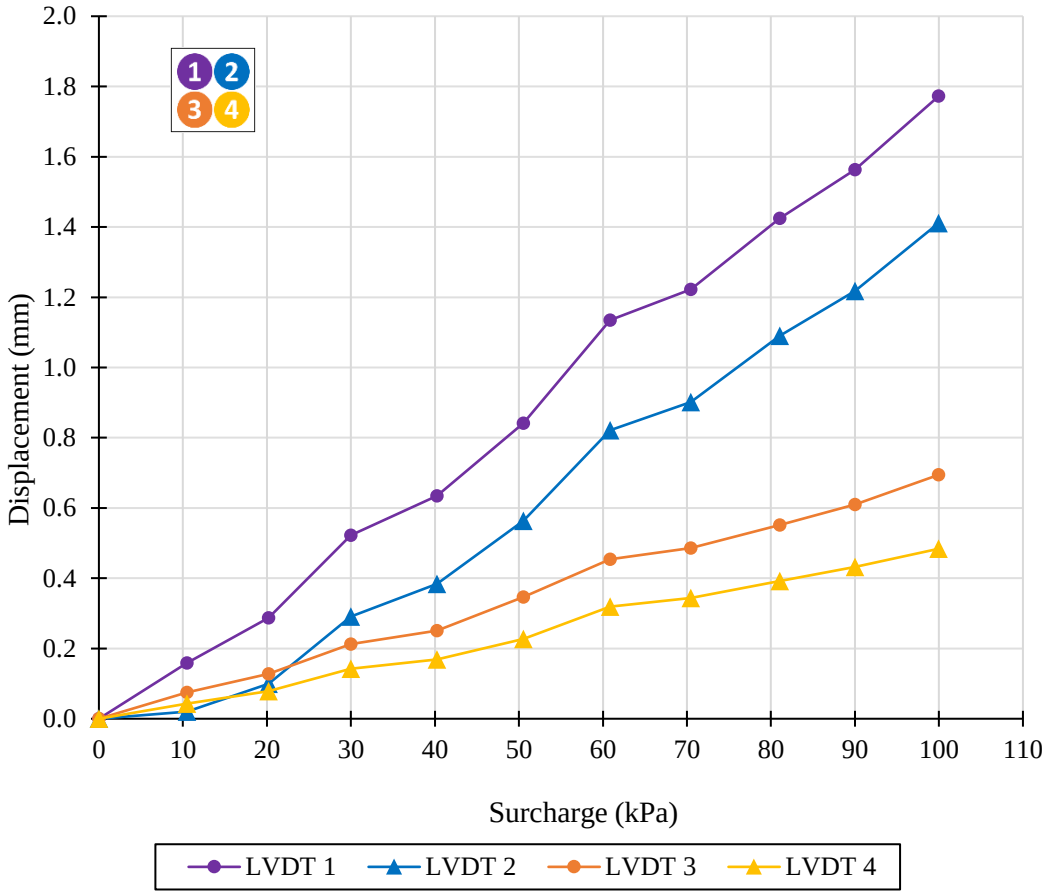

Figure 4-6. Displacement of extensible (PVC) reinforced soil wall test in 10 kPa load increments.

2. Prototype

The amount of displacement that occurred in the model was converted to the equivalent displacement expected for the prototype soil wall by applying the scaling factor of n = 30 for the one-dimensional displacement parameter. The equivalent prototype displacement in surcharge load increments of 10 kPa is presented in Figure 4-7 for the two equivalent heights of the four LVDTs, namely 6.7 m (LVDTs 1 and 2) and 3.5 m (LVDTs 3 and 4). It is shown the prototype soil wall at the height of 6.7 m would bulge 15.7 mm at 30 kPa and 53.2 mm at 100 kPa surcharge load when reinforced with extensible reinforcement. At one-third height of the wall, 6.4 mm and 20.8 mm displacement is expected at 30 kPa and 100 kPa respectively.

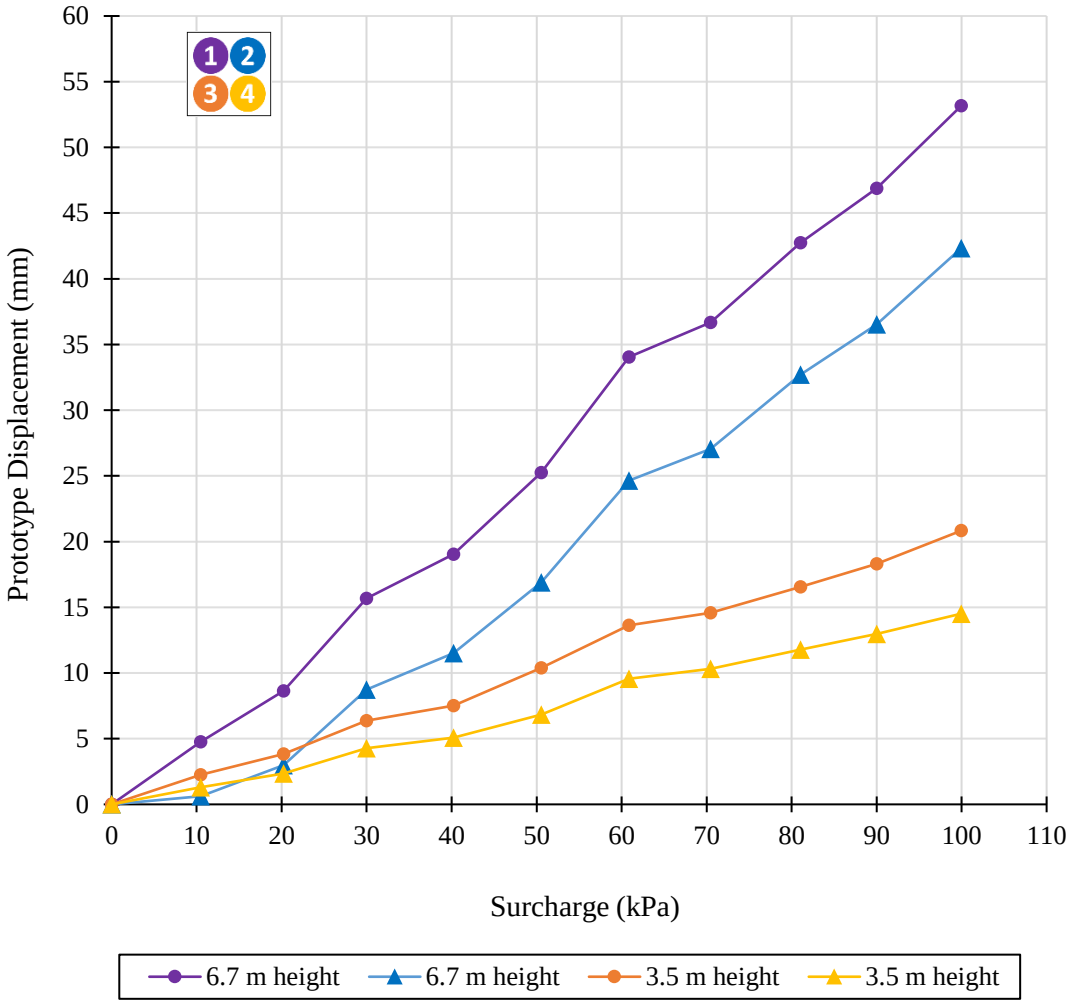

Figure 4-7. Displacement of extensible (PVC) reinforced prototype soil wall test in 10 kPa load increments.

The displacement of the prototype soil wall at the two soil wall heights of 3.5 m and 6.7 m is shown in Figure 4-8 together with the maximum deflected wall shape indicated with the dashed lines. Each marker corresponds to the 10 kPa surcharge load increments ending at 100 kPa and the amount of displacement is set on the horizontal axis.

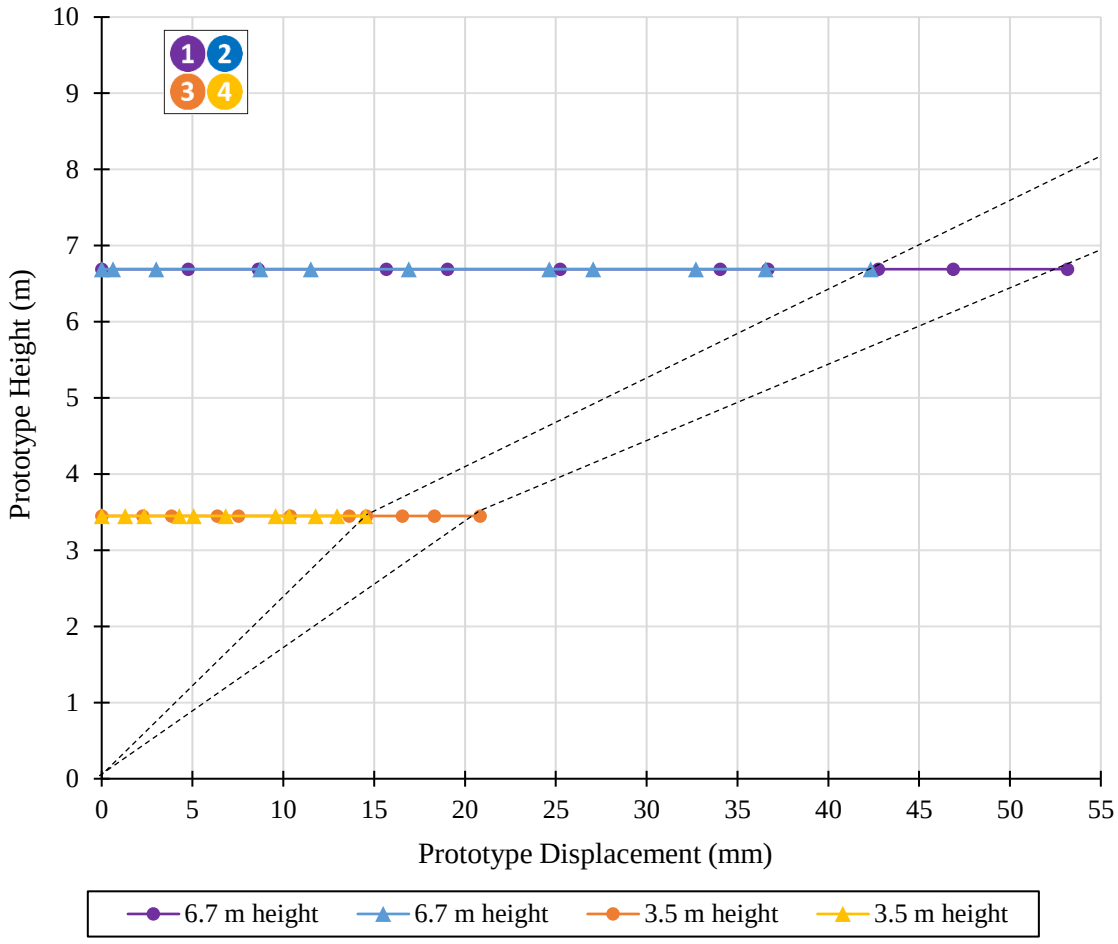

Figure 4-8. Displacement of extensible (PVC) reinforced prototype soil wall test at 3.5 m and 6.7 m heights.

4.2.3 Inextensible reinforcement displacement

1. Model

The LVDT displacements recorded in the brass reinforced soil wall test are presented in Figure 4-9. A similar procedure was followed in the brass test: centrifugal acceleration from A to B, loading commenced at C and loading ceased at D. Irregular displacement response took place between points D and E however, causing faulty displacements to be recorded. The test was subsequently terminated, and the measurement data between points D and E were excluded for analysis. The soil wall displacement during centrifugal deceleration was therefore not recorded in the brass reinforced soil wall test. Sufficient loading was achieved, however, and the test was a success.

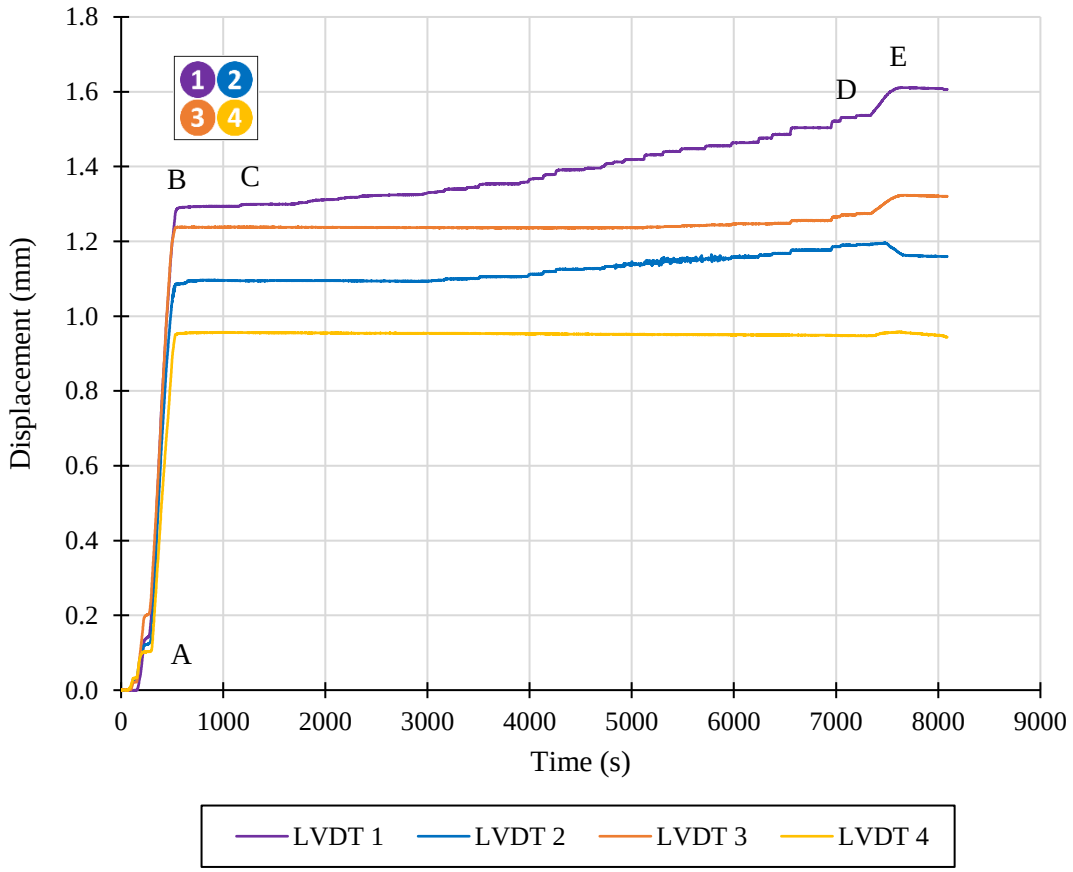

Figure 4-9. LVDT response in inextensible (brass) reinforced soil wall test.

The displacement results observed in the brass test are tabulated in Table 4-3. The inextensible reinforcement restricted the soil wall displacements to a maximum of 1.54 mm, three times less than the displacement that was observed in the PVC soil wall test. The displacement under loading was also considerably less – six and a half times less than observed in the PVC test. Similar to the results observed in the PVC test, the LVDTs on the window side of the facing (LVDTs 2 and 4) recorded lower displacements than the LVDTs on the partition side of the facing (LVDTs 1 and 3).

Table 4-3. Summary of displacements for brass reinforced soil test.

LVDT	Displacement (mm)		
	At 30 G	Maximum	Due to Loading
1	1.29	1.54	0.24
2	1.09	1.19	0.10
3	1.24	1.28	0.04
4	0.96	0.96	0.00

The load applied and displacement response with time that occurred in the inextensible brass reinforced test is plotted in Figure 4-10. Each increase in applied load corresponded to an equivalent increase in displacement. Similar to the PVC test, the first and second LVDTs had the greatest displacement response to the loading that was applied on the surface of the soil wall. The third LVDT however, measured minimal displacement (less than 0.05 mm) and the fourth LVDT did not record any increase in displacement. This indicated a greater resistance to soil wall displacement under loading when inextensible reinforcement was installed. Some noise was detected in the LVDT 3 measurement results in the 5000 – 6000 s period.

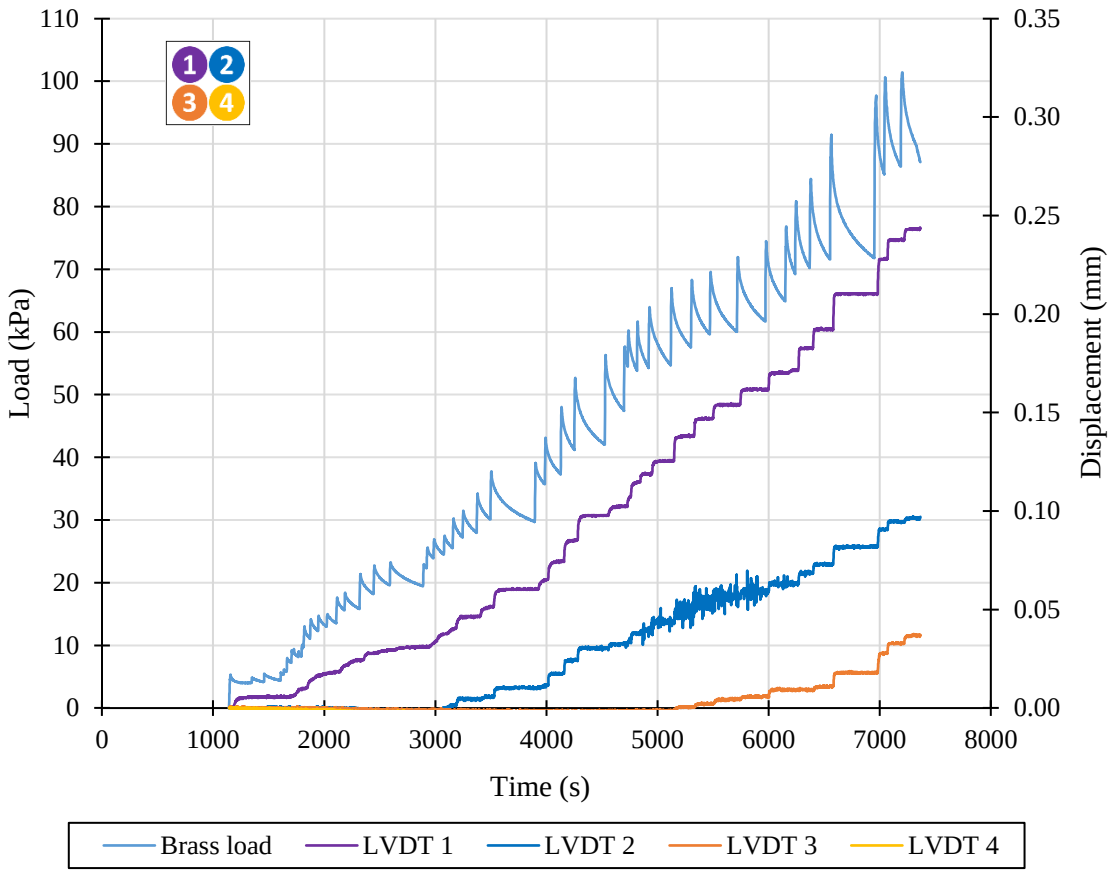

Figure 4-10. Load and LVDT response in inextensible (brass) reinforced soil wall test.

The displacement results were used to plot displacement of the soil wall facing against the surcharge load applied on the soil wall surface in Figure 4-11. The displacements increased linearly with increasing surcharge load and an increased rate of displacement is noted from approximately 55 kPa. Noise in the LVDT 2 response was reflected between 55 and 70 kPa. LVDT 4 measured a slightly negative displacement response of -0.01 mm. The result is deemed negligible due to the very low displacement recorded and assumed the soil wall facing did not bulge at the position of LVDT 4. A cleaned-up displacement record of the soil wall is presented in Figure 4-12 in surcharge load increments of 10 kPa for further clarity.

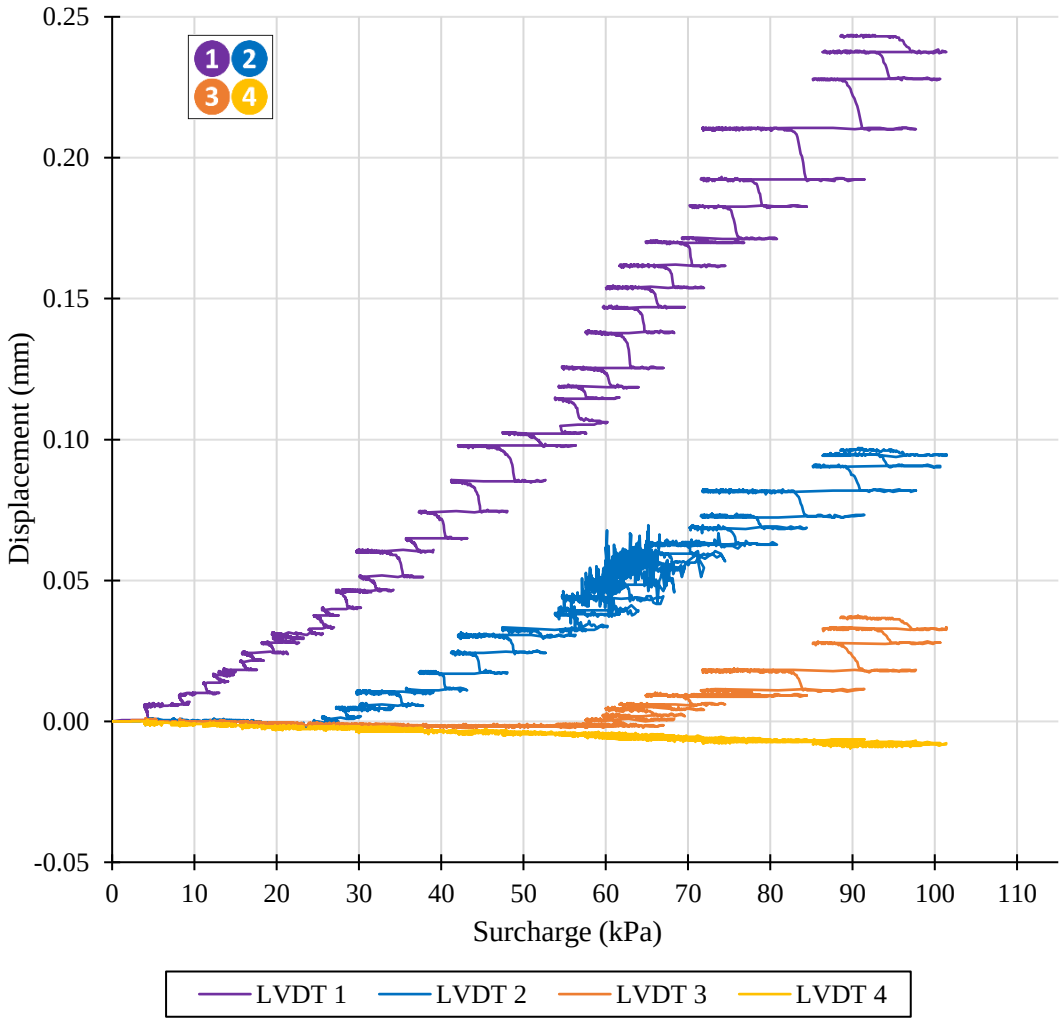

Figure 4-11. Displacement of inextensible (brass) reinforced soil wall test.

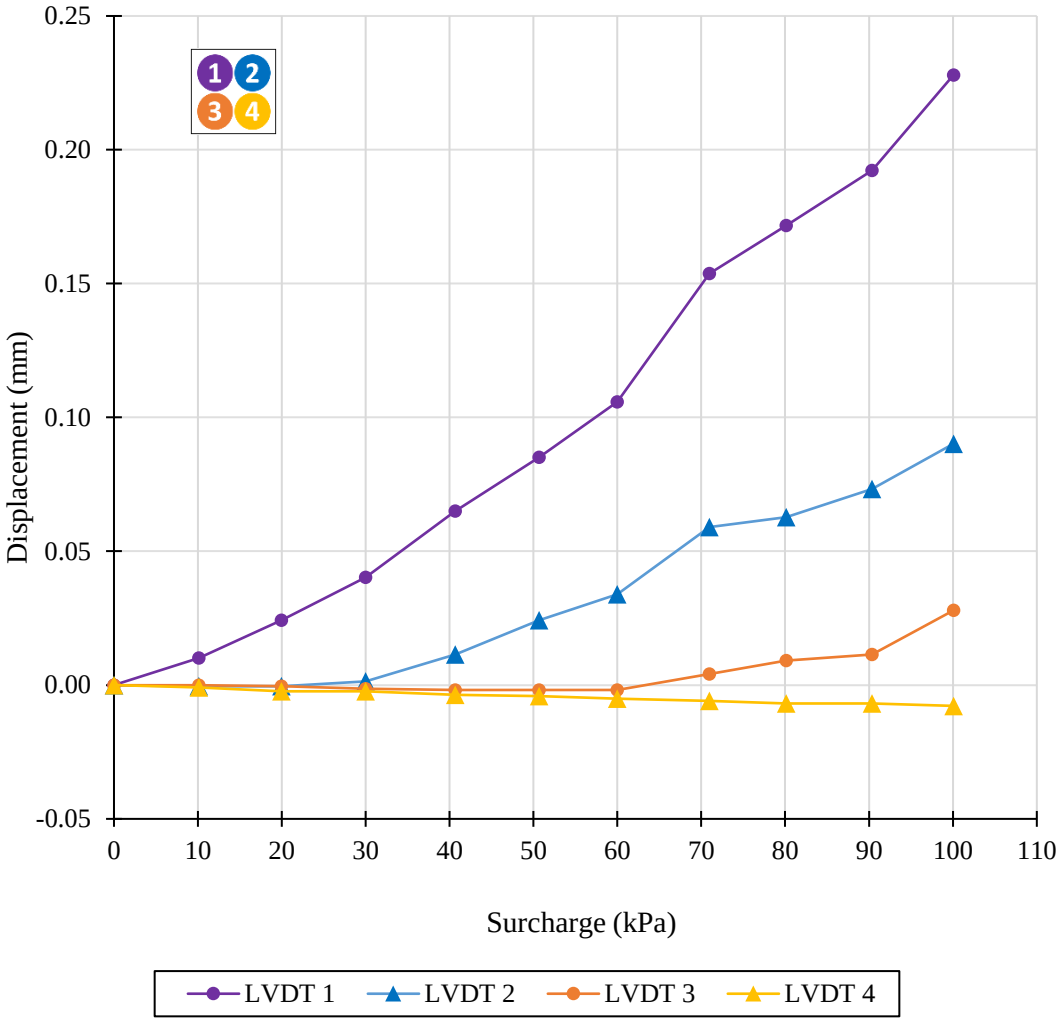

Figure 4-12. Displacement of inextensible (brass) reinforced soil wall test in 10 kPa load increments.

2. Prototype

The amount of displacement that occurred in the model was converted to the equivalent displacement expected for the prototype soil wall by applying the scaling factor of n = 30 for the one-dimensional displacement parameter. The equivalent prototype displacement in surcharge load increments of 10 kPa is presented in Figure 4-13 for the two equivalent heights of the four LVDTs, namely 6.7 m (LVDTs 1 and 2) and 3.5 m (LVDTs 3 and 4). It is shown the prototype soil wall at the height of 6.7 m would bulge 1.2 mm at 30 kPa and 6.8 mm at 100 kPa surcharge load when reinforced with inextensible reinforcement. At one-third height of the wall, 0 mm and 0.8 mm displacement is expected at 30 kPa and 100 kPa.

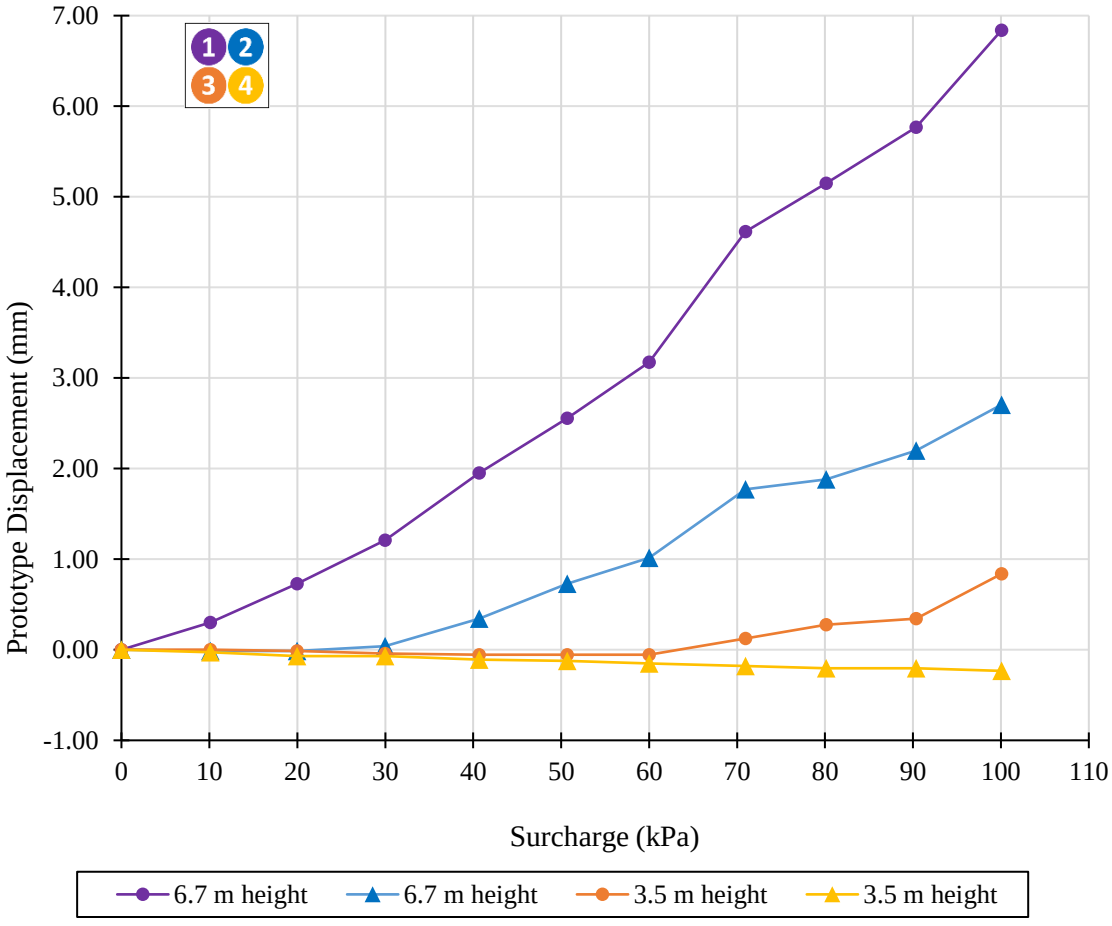

Figure 4-13. Displacement of inextensible (brass) reinforced prototype soil wall test in 10 kPa load increments.

The displacement of the prototype soil wall at the two soil wall heights of 3.5 m and 6.7 m is shown in Figure 4-14 together with the maximum deflected wall shape indicated with the dashed lines. Each marker corresponds to the 10 kPa surcharge load increments ending at 100 kPa and the amount of displacement is set on the horizontal axis.

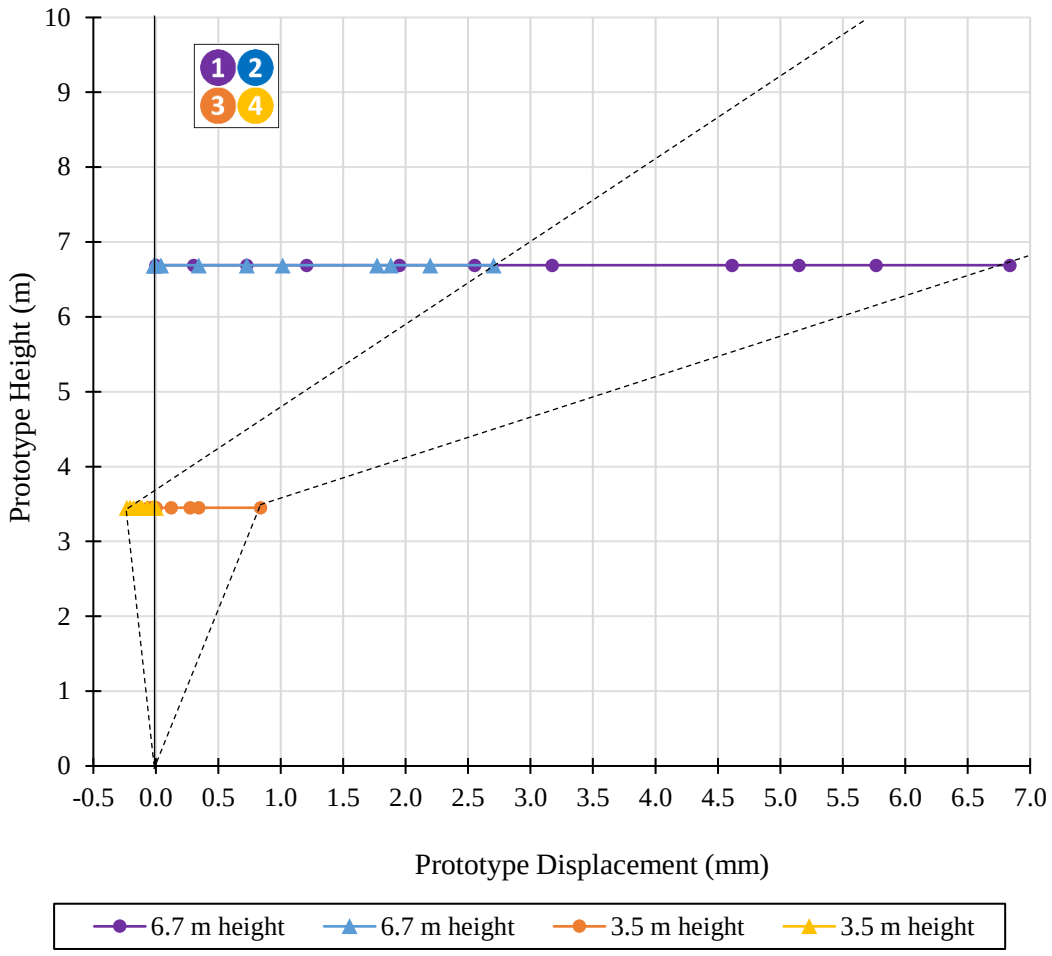

Figure 4-14. Displacement of inextensible (brass) reinforced prototype soil wall test at 3.5 m and 6.7 m heights.

4.2.4 Extensible and inextensible reinforcement comparison

The load-displacement response of the two tests is shown together on a single plot in Figure 4-15 with displacement of the soil wall facing in millimetres as the dependant variable, and the surcharge applied on the soil wall surface in kilopascals as the independent variable. The PVC results are plotted with dashed lines and the brass results are plotted with solid lines to distinguish between the two tests. The large difference in displacement of the soil wall facing observed in the two types of reinforcement material is noticeable in the plot. The soil wall facing reinforced with the extensible PVC reinforcement strips displaced nearly eight times as much as the soil wall reinforced with the inextensible brass reinforcement.

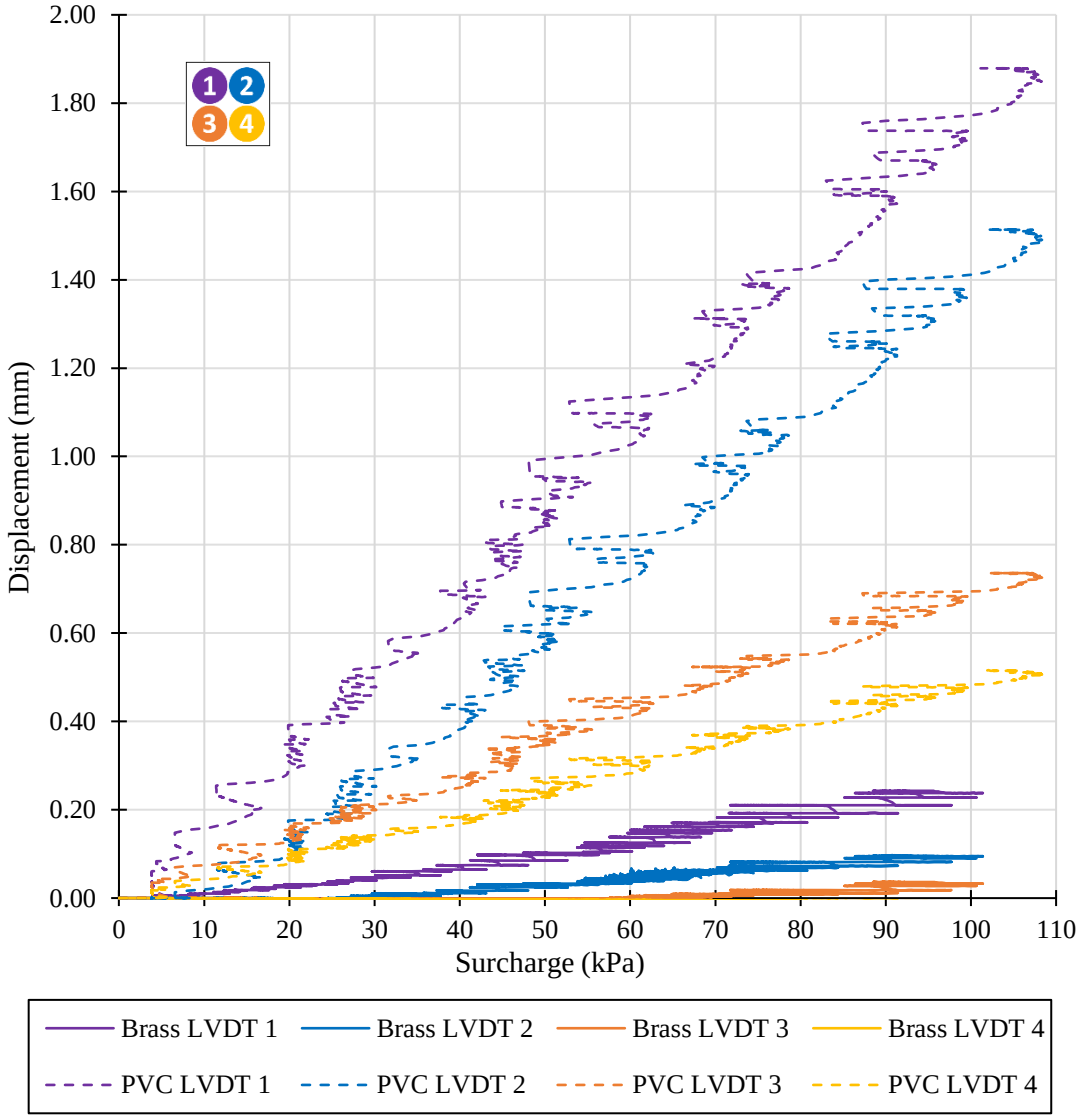

Figure 4-15. Displacement comparison of PVC and brass reinforced soil wall tests.

The top two LVDTs (LVDTs 1 and 2) recorded greater displacement compared to the bottom two LVDTs (LVDTs 3 and 4) for both material types. In the PVC test, the top two LVDTs followed a similar rate of displacement under loading, and LVDT 3 and LVDT 4 followed a similar bulge rate. Lower displacement rates were observed in the brass test compared to the PVC test. LVDT 4 did not respond to any loading exerted on the soil wall and the three LVDTs that recorded displacement under loading displaced at dissimilar rates. The rates of displacement for both tests are presented in Table 4-4.

Table 4-4. Displacement rates for PVC and brass tests.

	Displacement Rate (mm/kPa)	
LVDT	**PVC Test**	**Brass Test**
1	17.4×10^{-3}	2.41×10^{-3}
2	14.0×10^{-3}	0.957×10^{-3}
3	6.80×10^{-3}	0.370×10^{-3}
4	4.76×10^{-3}	0

A stiffness comparison was made by dividing the load applied on the soil wall by the amount of displacement of the soil wall facing. The two LVDTs near the top of the soil wall facing (LVDT1 and LVDT 2) were averaged together for both tests to determine the stiffness of the top part of the facing. Similarly, the results for the bottom two LVDTs (LVDT 3 and LVDT 4) were combined to determine the stiffness of the bottom of the facing. The wall stiffnesses at four discrete load stages (25 kPa – 100 kPa) for both the PVC and brass tests are shown in Figure 4-16.

Overall, the soil wall reinforced with inextensible reinforcing achieved at least four times the wall stiffness of that produced by the soil wall with extensible reinforcing. Both types of soil walls showed greater wall stiffness at the bottom of soil wall (LVDT 3 and LVDT 4) compared to the top (LVDT 1 and LVDT 2).

There were no wall stiffness results applicable at the bottom of the soil wall facing for the brass reinforced soil wall due to the near zero displacement results. A significant decrease in wall stiffness occurred in the brass reinforced soil wall test at both the top and bottom of the facing for loads greater than 50 kPa. The sudden decrease in wall stiffness indicated a tendency toward brittle behaviour under increased load. At this point the inextensible reinforcement strips may have lost some friction with the backfill soil and reinforcement slip may have occurred. The

extensible PVC reinforced soil wall stiffness, however, remained relatively constant under increased surcharge load, indicating a linear increase in deformation with increased loading.

The ratio of the reinforcement axial stiffness from Table 3-3 was 29, i.e., the brass reinforcement axial stiffness was 29 times stiffer than the PVC reinforcement strips. This translated to the large difference in average wall stiffnesses observed between the two types of soil walls. The average wall stiffness in the brass reinforced soil walls was at least 10 times greater than the soil wall reinforced with the PVC strips.

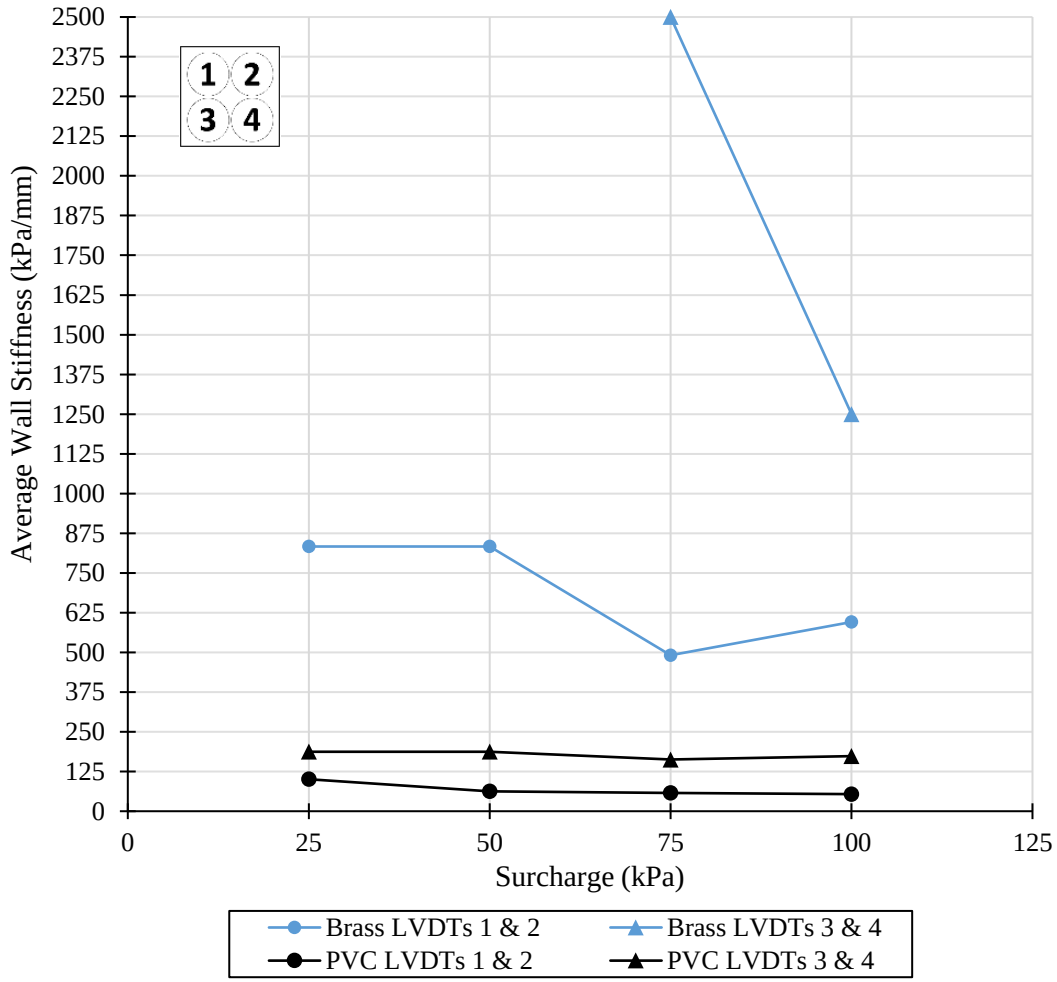

Figure 4-16. Wall stiffnesses at four load stages for both PVC and brass reinforced soil walls.

4.3 HORIZONTAL SOIL STRAINS USING PIV

Particle Image Velocimetry (PIV) was used to track the horizontal displacement of the soil wall facing in terms of strain. Photographic images of the soil wall were taken at 5 second time intervals during testing. Images taken during the PVC test and the brass test are shown in Figure 4-17 and Figure 4-18 respectively together with the meshes used in the PIV analysis. The photographs taken in the PVC test captured only the top portion of the soil wall whereas in the brass test the full height of the soil wall was photographed.

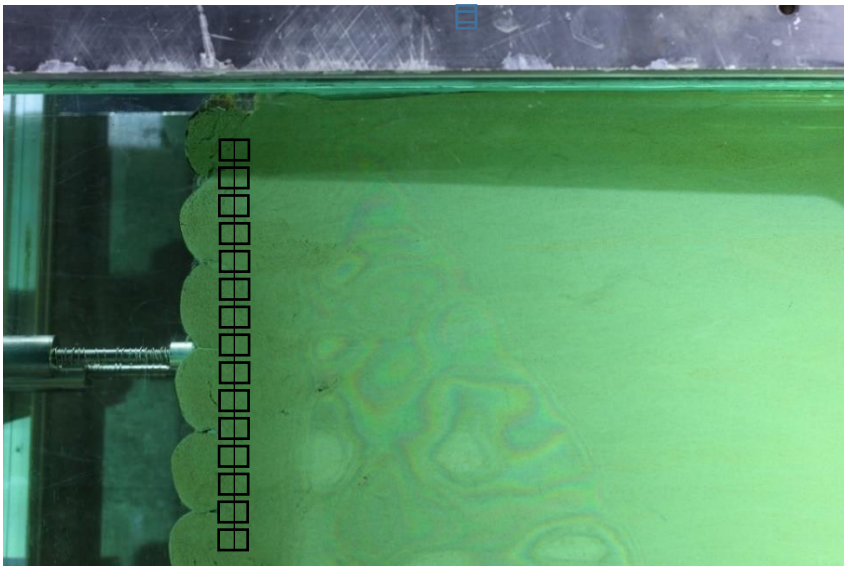

Figure 4-17. Photographic image taken during the PVC soil wall test with PIV mesh.

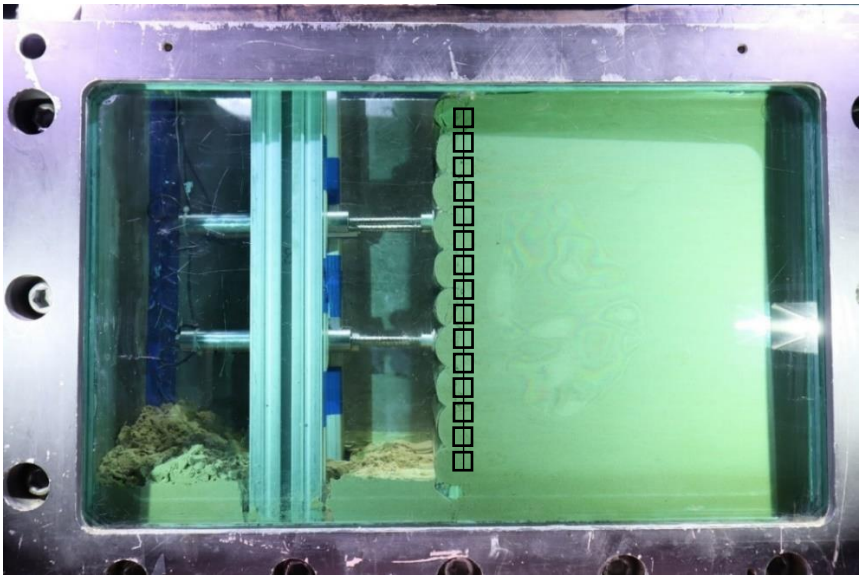

Figure 4-18. Photographic image taken during the brass soil wall test with PIV mesh.

The test time was used to correlate the time the images were taken with the loading stage of the soil wall. Images starting at the loading stage of 0 kPa and ending at 100 kPa were analysed for horizontal soil strain at 10 kPa load increments. The strain analysis was done on the soil just behind the wall facing for both the PVC and brass reinforced tests and the results are presented in Figure 4-19 and Figure 4-20 respectively. Only the data from 4.5 m soil wall height was captured during the PVC reinforced test. The locations of the top LVDTs (LVDTs 1 and 2) and bottom LVDTs (LVDTs 3 and 4) are indicated in the figures. The prototype wall height of 10 m was used to plot the results and the soil strains were plotted from right to left to mirror the direction of movement in the images.

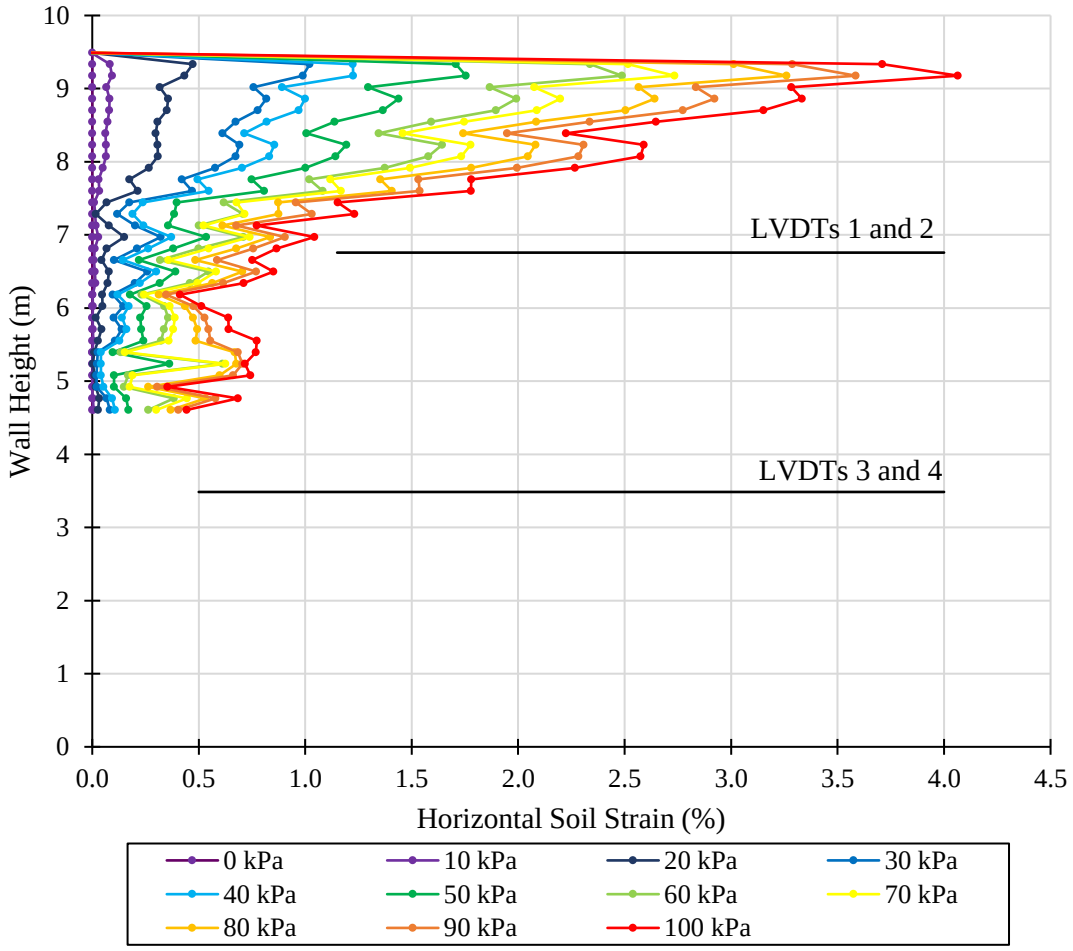

Figure 4-19. Horizontal soil strain percentage of PVC reinforced soil wall.

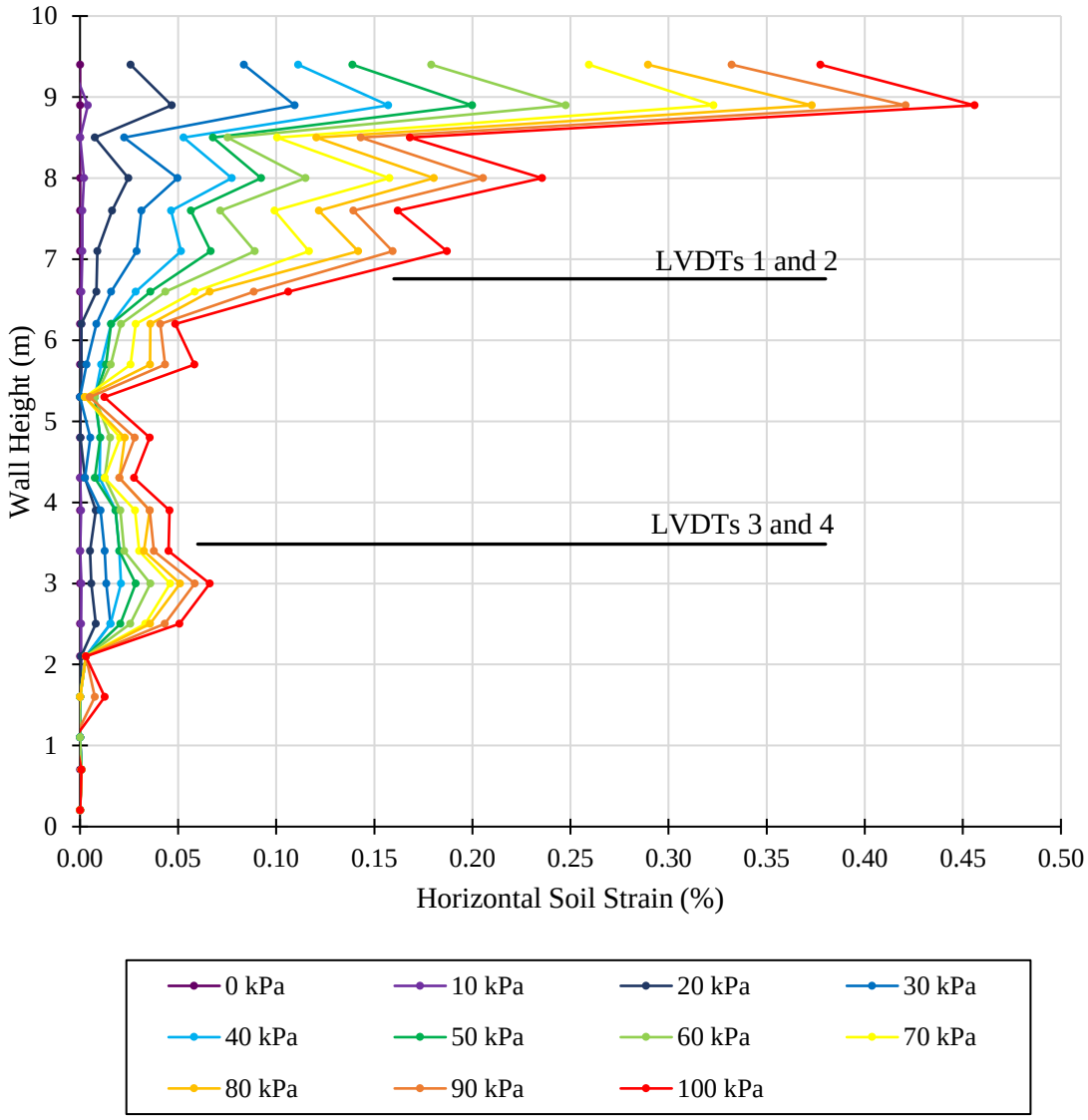

Figure 4-20. Horizontal soil strain percentage of brass reinforced soil wall.

The following observations were made from the PIV analysis for the PVC and brass tests:

- The results shown in Figure 4-19 and Figure 4-20 show there may have been a reduction in horizontal strains at the location of the LVDTs compared to the rest of the wall. This may suggest the LVDTs resisted movement of the soil wall facing. However, since the LVDTs were kept constant and were present in both tests, the same error occurs in both sets of results, allowing for direct comparisons to be made. In the next chapter, the LVDTs were removed from the experiment and allowed for a conclusion to be presented.
- The maximum horizontal strain occurred at 100 kPa and at 9 m soil wall height for both tests and is presented together with the strains measured at the heights of the LVDTs in Table 4-5. The normalised strains correspond well with those presented in the literature from Bathurst *et al* (2010) and fall well within the FHWA (2008) and AASHTO (2009) design guidelines, as well as for the *SANS 207:2011* guideline for a safe maximum of 2% for semi-elliptical steel face walls.

Table 4-5. Horizontal strains measured for both PVC and brass reinforced soil walls at 100 kPa.

Test	Max Strain (%)	Strain at LVDTs 1 & 2 (%)	Strain at LVDTs 3 & 4 (%)	Normalised Strain (Δx/H)
1. PVC at 100 kPa	4.07	1.04	-	0.4
2. Brass at 100 kPa	0.456	0.140	0.0452	0.05

- The deflected wall shapes for both types of soil wall at 50 kPa and 100 kPa are shown in Figure 4-21 in terms of horizontal strain. The large difference in soil behaviour is clearly observed in the figure. The soil wall reinforced with the PVC reinforcement strips deflected to slightly over 4% horizontal strain, whereas the soil wall reinforced with brass strips deflected to just under 0.5% strain at 100 kPa load.

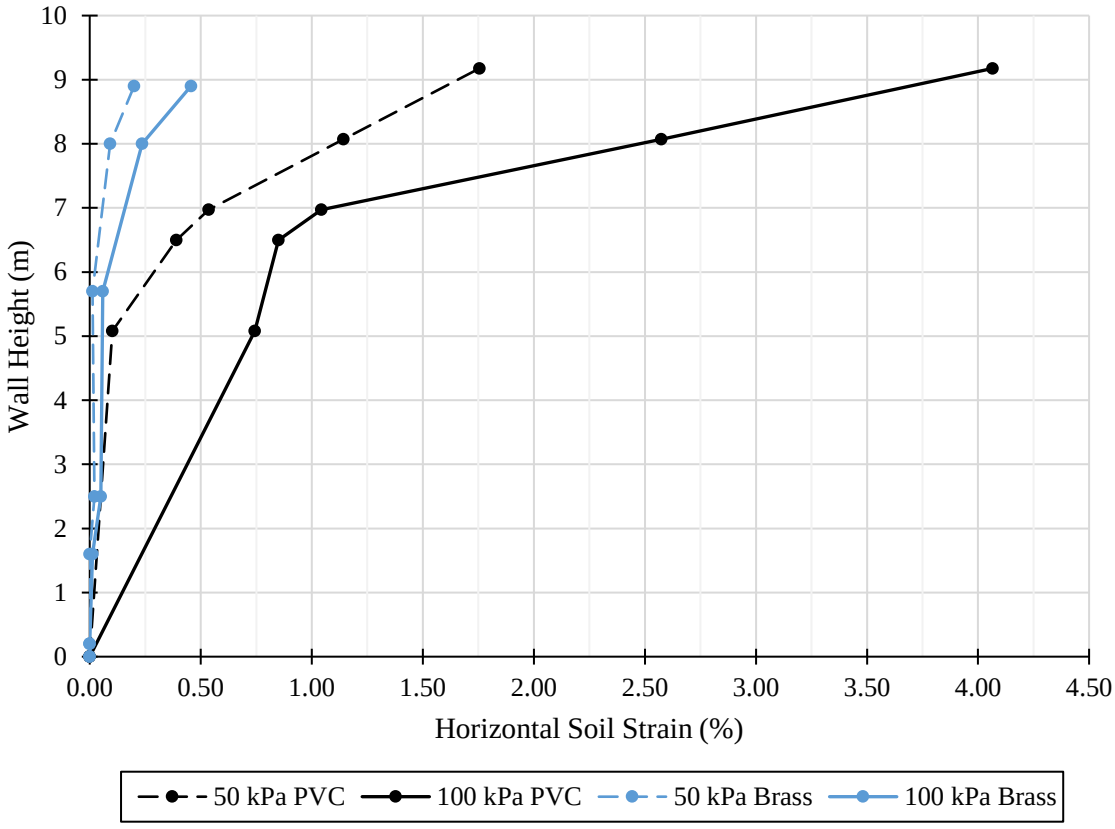

Figure 4-21. Comparison of horizontal soil strain between PVC and brass soil walls.

- The brass test result shows maximum strains at the top of the soil wall and close-to-zero strains mid-height of the wall, with a slight increase in strains again at 3 m height. The shape of the strains across the full height indicates either a tendency of the wall to kink at mid-height, the shape is purely due the resistance of the LVDTs, or the shape is a combination of both factors. In the following chapter, the stress-strain tests are conducted without LVDTs, and the PIV results are compared.
- The soil wall reinforced with the extensible PVC strips displaced one order of magnitude more than the brass reinforced soil wall. The brass reinforcement strips provided far greater stiffness to the soil wall and resisted movement almost entirely. This corresponds well with the difference in axial reinforcement stiffness between the brass and PVC strips. The axial reinforcement stiffness was 29 times greater for the brass strips.
- The order of magnitude difference in strains observed in the PIV analysis corresponded well with the difference in displacements measured by the LVDTs. The average wall stiffness in the brass reinforced soil walls determined from the LVDT response was at least one order of magnitude greater than the soil wall reinforced with the PVC strips.

- The horizontal soil strains increased overall with increasing soil wall height.
- The horizontal soil strains converged to near zero at mid-height of the soil wall in the brass test. This may be due to the resistance of the LVDTs.

The behaviour of the soil wall reinforced with PVC strips was classified as flexible and extensible, whereas the behaviour of the soil wall reinforced with brass strips was classified as rigid and inextensible.

4.4 CHAPTER SUMMARY

Two vertical soil wall load-displacement tests were conducted in the geotechnical centrifuge at an acceleration of 30 G. The load was applied to the top surface of the soil wall and the corresponding displacement of the soil wall facing was measured by four LVDTs: two near the top, and two near the bottom of the soil wall. The first soil wall was constructed with extensible reinforcement in the form of PVC strips and the second soil wall was reinforced with inextensible reinforcement, namely brass strips.

The soil walls were subjected to 100 kPa surcharge loads and the largest displacements were recorded by the soil wall reinforced with the extensible PVC reinforcement strips. The results show the PVC reinforced soil wall deformed almost an order of magnitude more than the brass reinforced soil wall. Displacement increased linearly with increasing load for both soil walls and the largest displacements were measured at the top left LVDT (LVDT 1) for both tests. Bourgeois *et al*. (2011) observed the largest wall deformation occurred at mid-height of their soil walls, and the least at the top of the wall. The researchers however constructed the walls with stiff facings, indicating changes in design correspond to different soil wall behaviour and performance. The normalised strains result for both types of reinforced soil walls corresponded well with those presented in the literature from Bathurst *et al* (2010) and fall within the FHWA (2008) and AASHTO (2009) guidelines, as well as for the *SANS 207:2011* guideline for a safe maximum of 2% for semi-elliptical steel face walls used in industry.

5 STRESS-STRAIN RESPONSE OF REINFORCED SOIL WALL

5.1 INTRODUCTION

The reinforcing elements within a soil wall provide the necessary strength to resist movement and failure within a soil wall. All inherent and external loads on the soil wall transfer through the soil skeleton and exert stresses on the reinforcement. As a result, reinforcement strains develop. It is this connection between stresses on the soil wall and the corresponding reinforcement strains that are investigated in this chapter.

The experiment consisted of conducting two stress-strain soil wall tests in the geotechnical centrifuge at 30 G centripetal acceleration. The first test consisted of a soil wall reinforced with extensible reinforcement in the form of PVC strips, and the second test consisted of a soil wall reinforced with inextensible reinforcement in the form of brass strips. The strains that developed in response to surcharge loading were measured at three different heights in the soil walls (model heights of 99 mm, 165 mm, and 231 mm) by installing strain instrumentation as shown in Figure 5-1. The PVC soil wall was instrumented with eight conventional strain gauges and the brass soil wall was instrumented with eight fibre Bragg gratings (FBGs).

The stress-strain results and the differences in soil wall behaviour between the two tests are presented in this chapter. An overview of the testing procedure is also included and finally a summary of the results is presented.

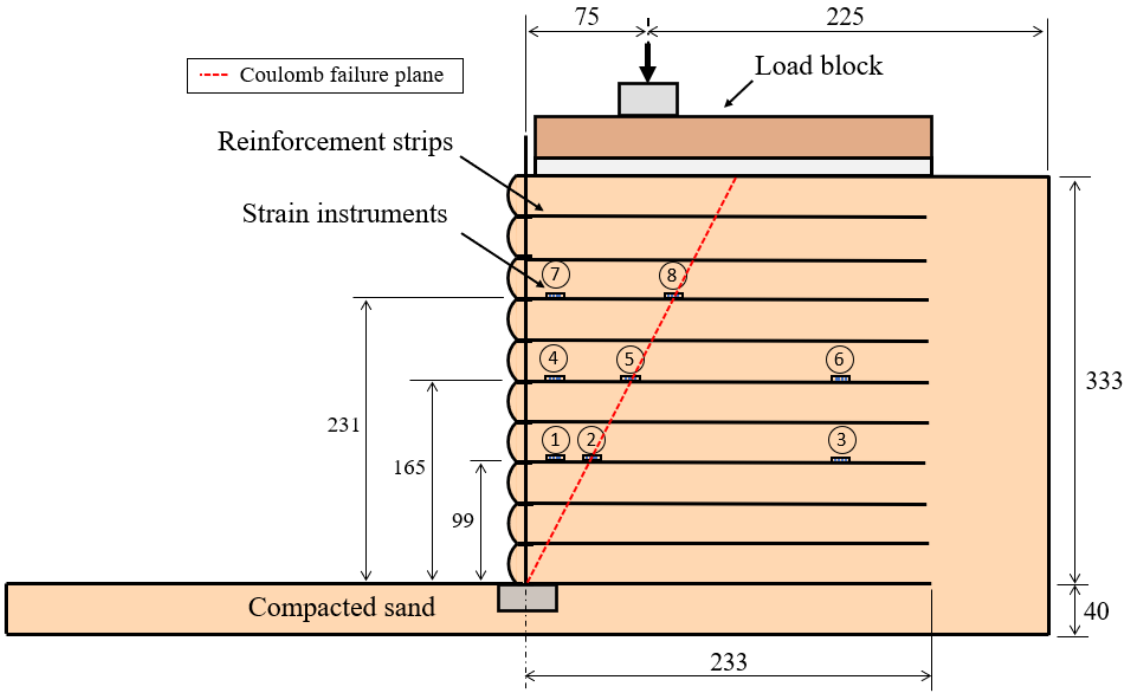

Figure 5-1. A cross-section of the stress-strain soil wall models. Not drawn-to-scale and all dimensions are in millimetres.

5.2 OVERVIEW

5.2.1 Load applied

Similar to the load-deformation tests discussed in Chapter 4, a vertical force was applied to the surface of the soil wall through pressing the actuator onto the load block at 30 G centripetal acceleration. The maximum forces applied in the two tests and the corresponding stress magnitudes are presented in Table 5-1. The force in newtons was converted to surcharge stress in kilopascals by dividing the force over the load block area of 33 785 mm^2 for further analysis. The load was not applied to the centre of the load block due to the configuration of the actuator frame on the strongbox. The surcharge applied was therefore not uniformly spread over the area. The applied forces for both tests are presented against time in Figure 5-2. The brass reinforced soil wall was loaded to double the force compared to the PVC soil wall due to a simple conversion error made during the experiment. The manual loading of the soil walls was meant to cease at 1 000 N due to the limited capacity of the 500 N load cell. The high loads indicate the load cell had a large safety factor. The brass reinforced soil wall test was reloaded to just over 1 500 N to observe how the reinforcement strains respond upon reloading.

Table 5-1. Maximum loads applied in stress-strain tests.

Test	Max Force (N)	Max Load (kPa)
1. Extensible (PVC)	1 099	32.5
2. Inextensible (Brass)	2 192	64.9

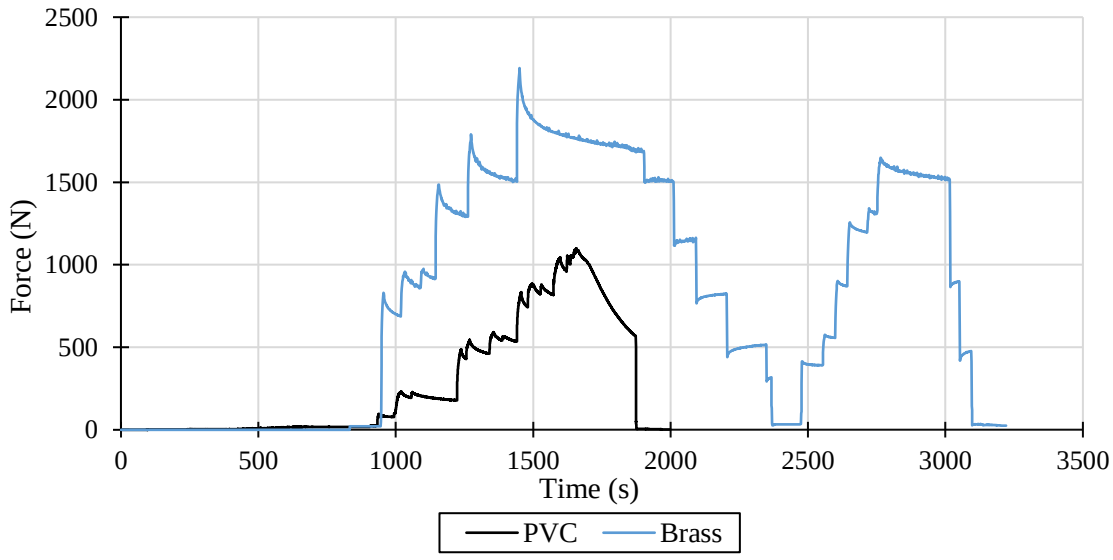

Figure 5-2. Surcharge loads applied in stress-strain tests.

5.2.2 Extensible reinforcement strains

Eight conventional strain gauges were fastened to the extensible PVC reinforcement strips at three different soil wall heights: 3 m, 5 m, 7 m – indicated with the colours orange (bottom), green (middle) and purple (top) respectively. The strain gauge responses are presented in Figure 5-3 and centrifugal acceleration to 30 G is shown from A to B, surcharge loading on the soil wall surface (C to D), unloading of surcharge load (E), and deceleration of the centrifuge to 1 G (F).

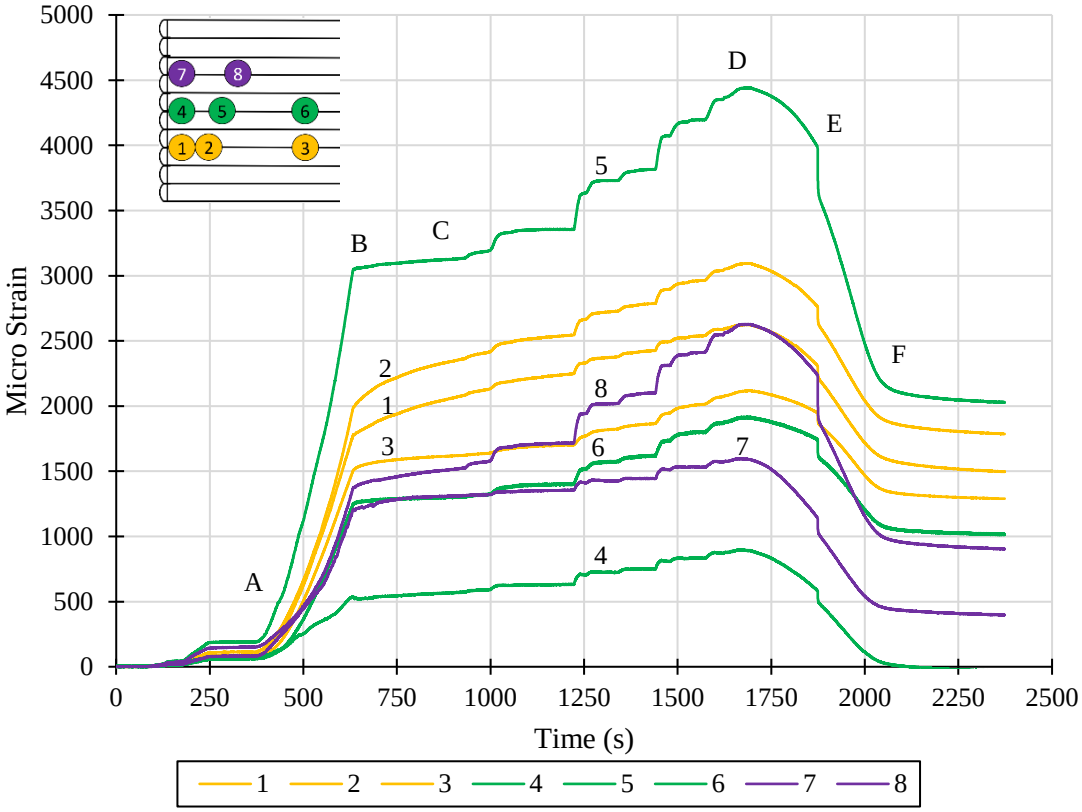

Figure 5-3. Strain gauge response in extensible (PVC) reinforced soil wall test.

In the bottom row, at the 3 m prototype height, strain gauges 1, 2 and 3 were placed at three horizontal zones along the length of the reinforcement strip: near the facing, at the maximum expected tension curve along the Coulomb failure plane, and towards the end of the reinforcement strip respectively (for strain gauge locations refer to Figure 5-1). The same horizontal zones were used for the middle strain gauges (4, 5 and 6) at a prototype height of 5 m. At the prototype height of 7 m, strain gauge 7 was placed near the facing and strain gauge 8 was placed at the Coulomb failure plane. The strain gauge readings were plotted according to the three horizontal zones, namely:

1. Near the facing (strain gauges 1, 4, 7), shown in Figure 5-4;
2. At the Coulomb failure plane (strain gauges 2, 5, 8), shown in Figure 5-5; and
3. Towards the end of the reinforcement strip (strain gauges 3, 6), shown in Figure 5-6.

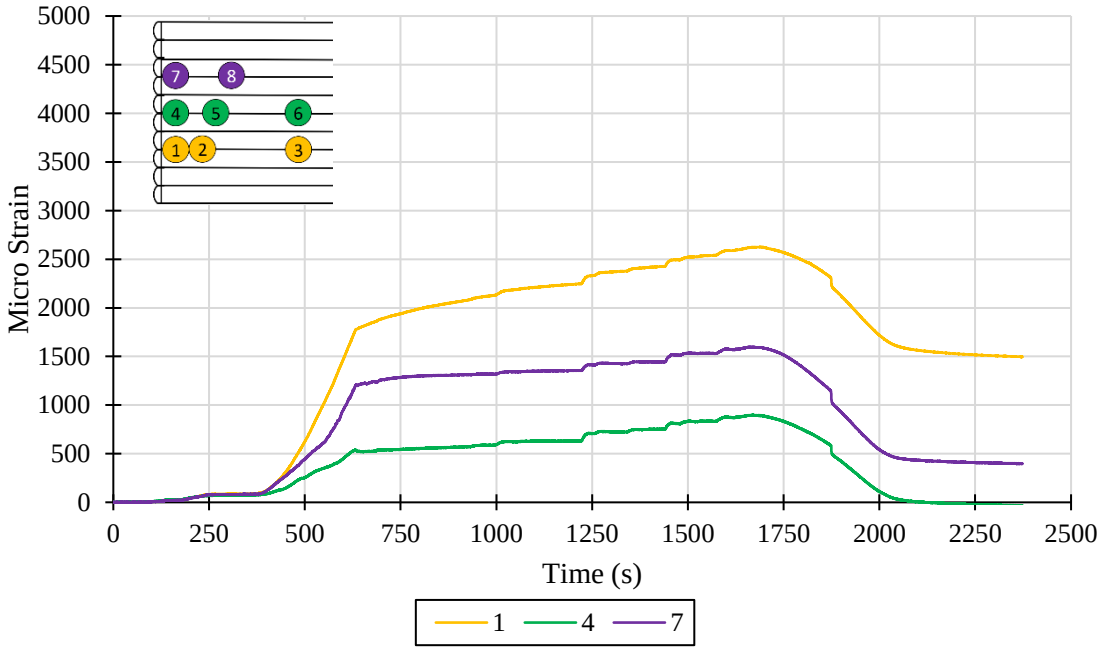

Figure 5-4. Strain gauge response near the facing in extensible (PVC) reinforced soil wall test.

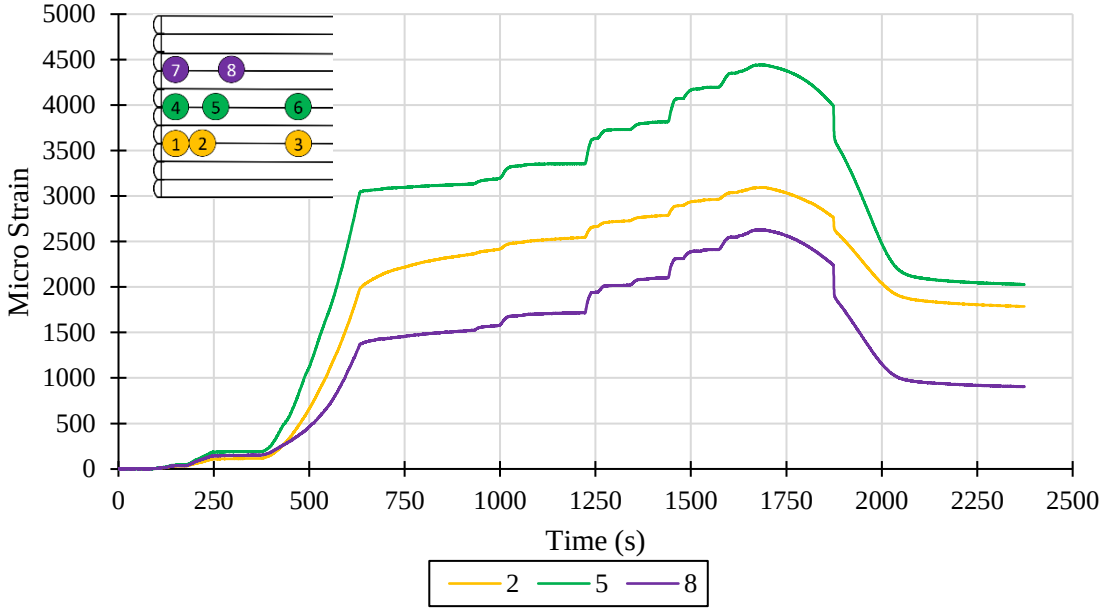

Figure 5-5. Strain gauge response at the Coulomb failure plane in extensible (PVC) reinforced soil wall test.

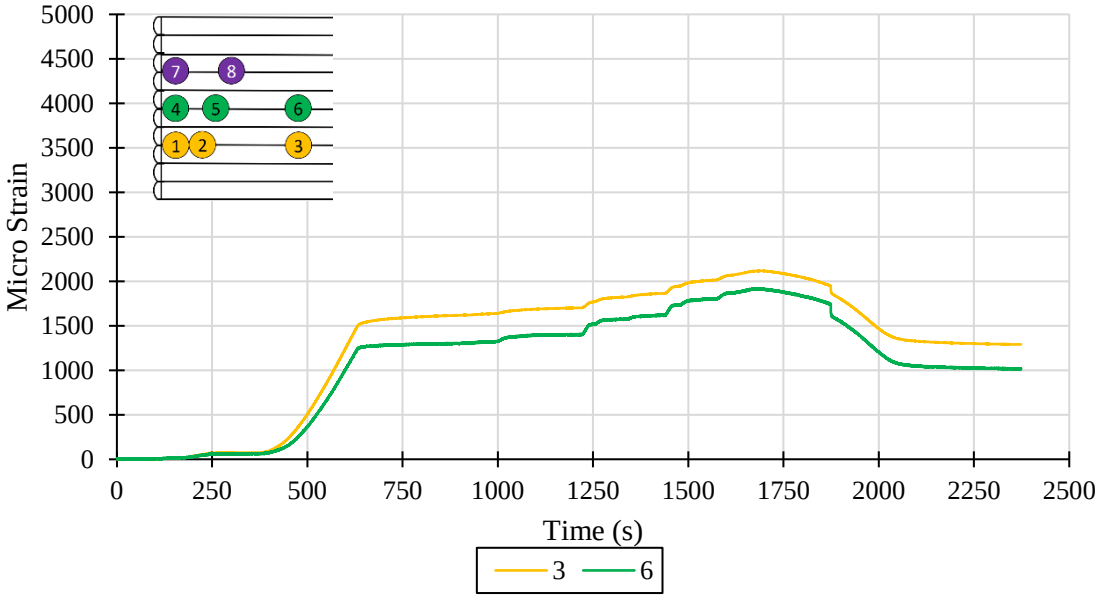

Figure 5-6. Strain gauge response towards the end of the reinforcement strip in extensible (PVC) reinforced soil wall test.

The largest strains occurred at the strain gauges placed at the Coulomb failure plane (strain gauges 2, 5, and 8), followed by the strain gauges placed near the wall facing (strain gauges 1, 4 and 7), and the lowest strains were observed near the end of the reinforcement strips (strain gauges 3 and 6).

5.2.3 Inextensible reinforcement strains

Eight fibre Bragg gratings (FBGs) were fastened to the inextensible brass reinforcement strips at the same locations as in the extensible PVC test, namely at soil wall heights: 3 m, 5 m, 7 m – colour-coded purple (bottom), green (middle) and orange (top) respectively. The FBG strain responses are presented in Figure 5-7 and show centrifugal acceleration to 30 G (A to B), surcharge loading on the soil wall surface (C to D), unloading of surcharge load (D to E), a second phase of loading and unloading the soil wall (F and G), and deceleration of the centrifuge to 1G (H).

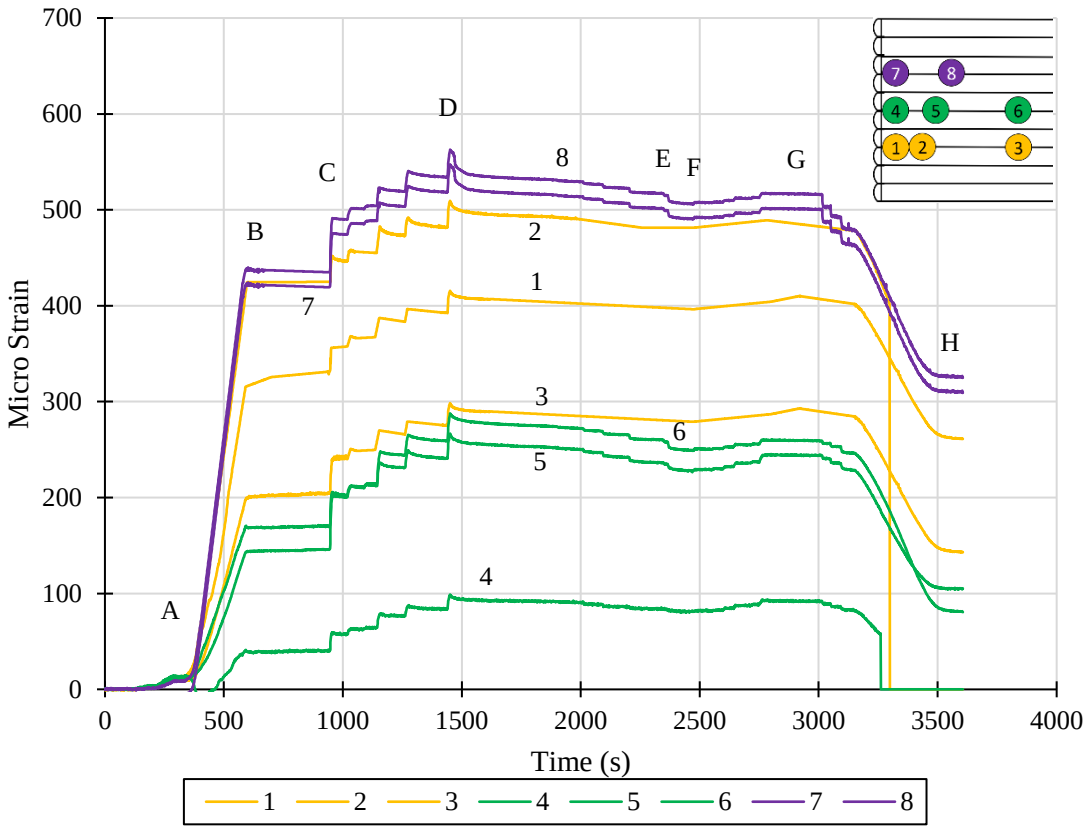

Figure 5-7. Strain gauge response in inextensible (brass) reinforced soil wall test.

The strain responses recorded by the FBGs were separated according to the same horizontal zones along the reinforcement length as the extensible reinforced soil wall test:

1. Near the facing (FBGs 1, 4 and 7), shown in Figure 5-8;
2. At the Coulomb failure plane (FBGs 2, 5, and 8), shown in Figure 5-9,
3. and near the reinforcement end (FBGs 3 and 6), shown in Figure 5-10.

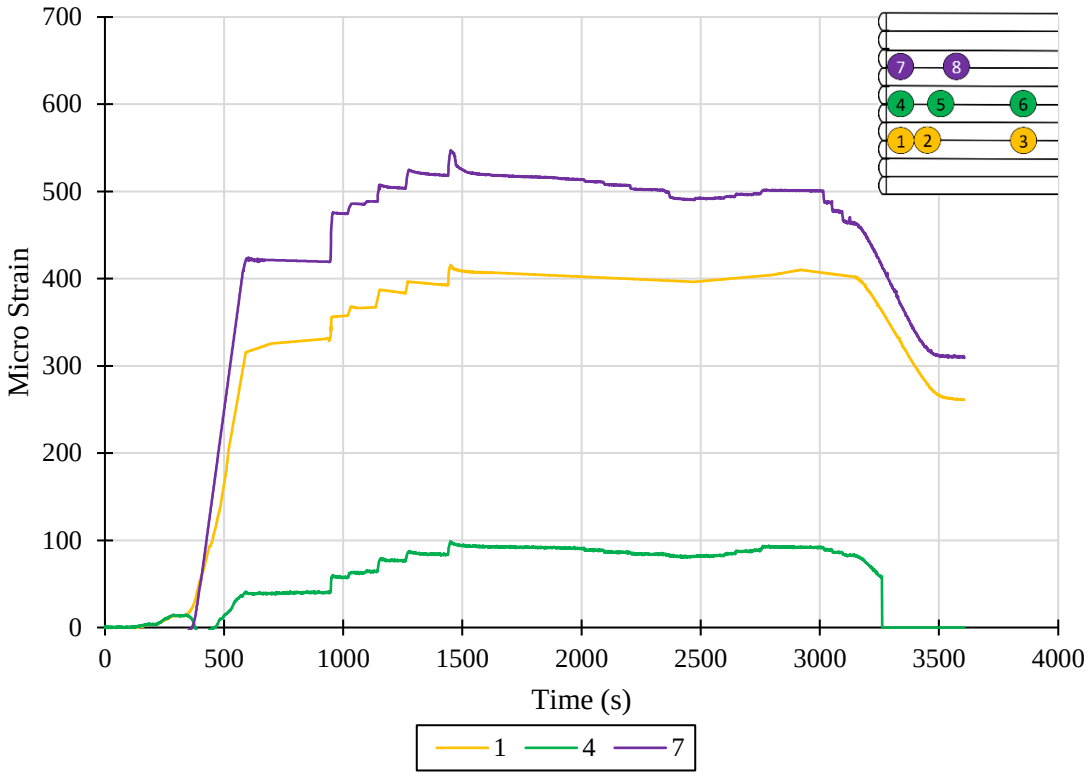

Figure 5-8. Strain gauge response near the facing in inextensible (brass) reinforced soil wall test.

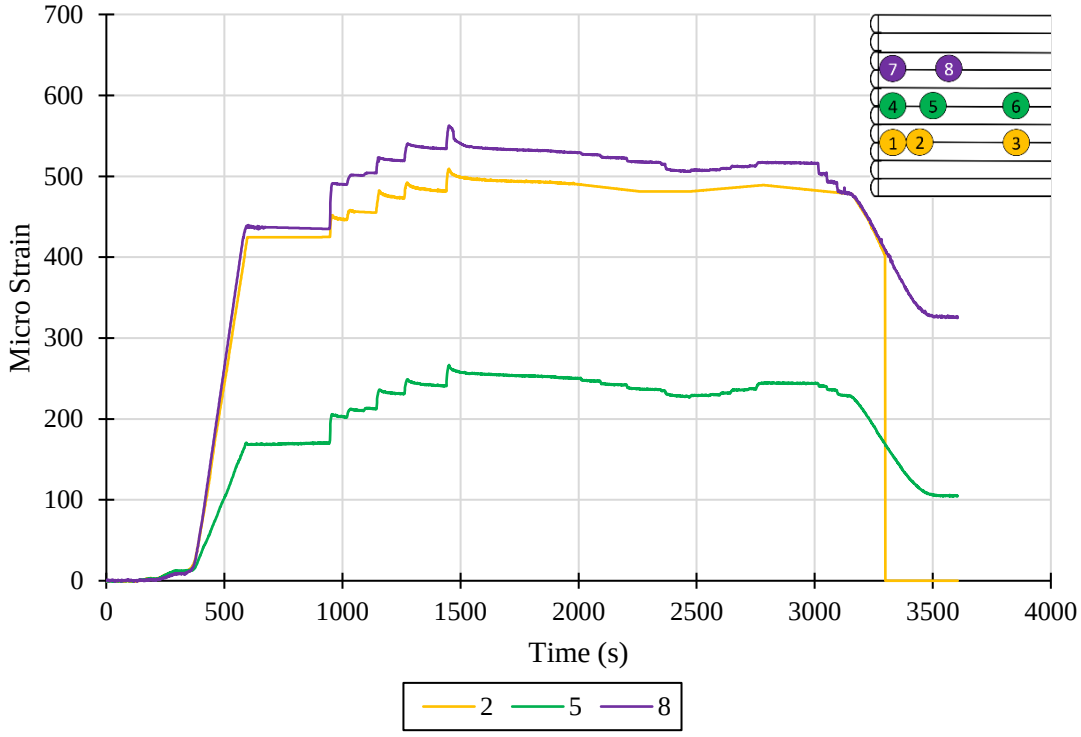

Figure 5-9. Strain gauge response at the Coulomb failure plane in inextensible (brass) reinforced soil wall test.

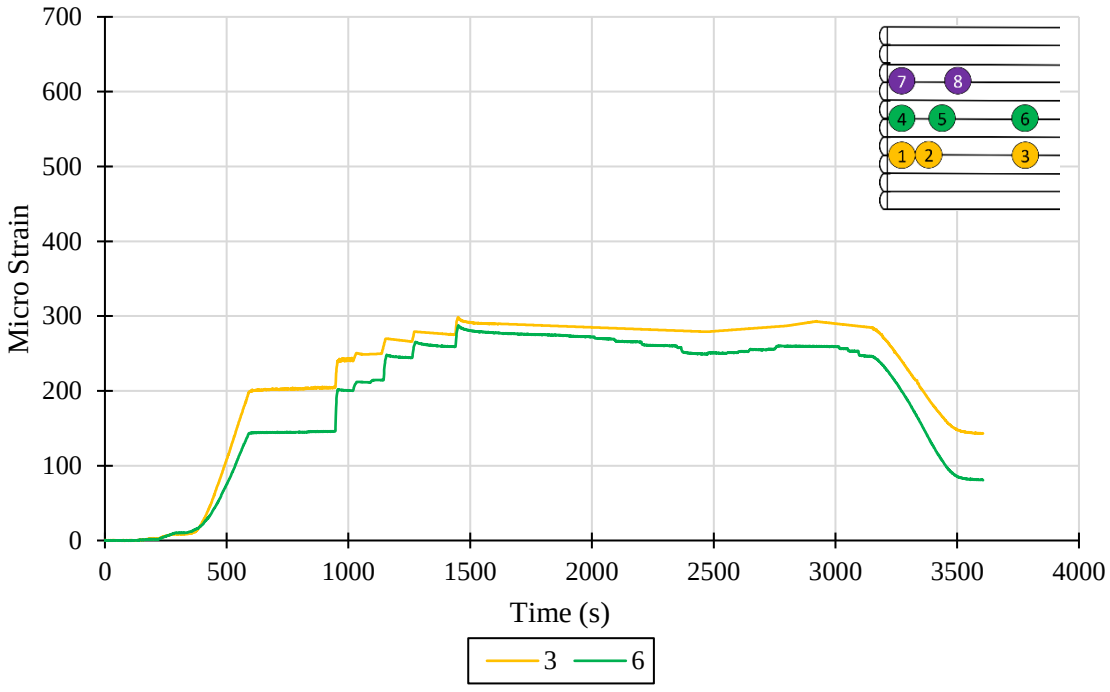

Figure 5-10. Strain gauge response towards the end of the reinforcement strip in inextensible (brass) reinforced soil wall test.

The largest strains occurred at the strain gauges placed at the Coulomb failure plane (strain gauges 2, 5, and 8), followed by the strain gauges placed near the wall facing (strain gauges 1, 4 and 7), and the lowest strains were observed near the end of the reinforcement strips (strain gauges 3 and 6).

5.3 STRESS-STRAIN BEHAVIOUR

5.3.1 Extensible reinforcement

The surcharge load applied to the soil wall surface was converted to stress in kilopascals and was plotted with the strain response measured by the eight strain gauges in the extensible (PVC) reinforcement test. The stress-strain results are presented in Figure 5-11. The micro strain response was zeroed at 30 G in the figure. An increase in applied stress corresponded to an increase in reinforcement strain in the reinforcement strips.

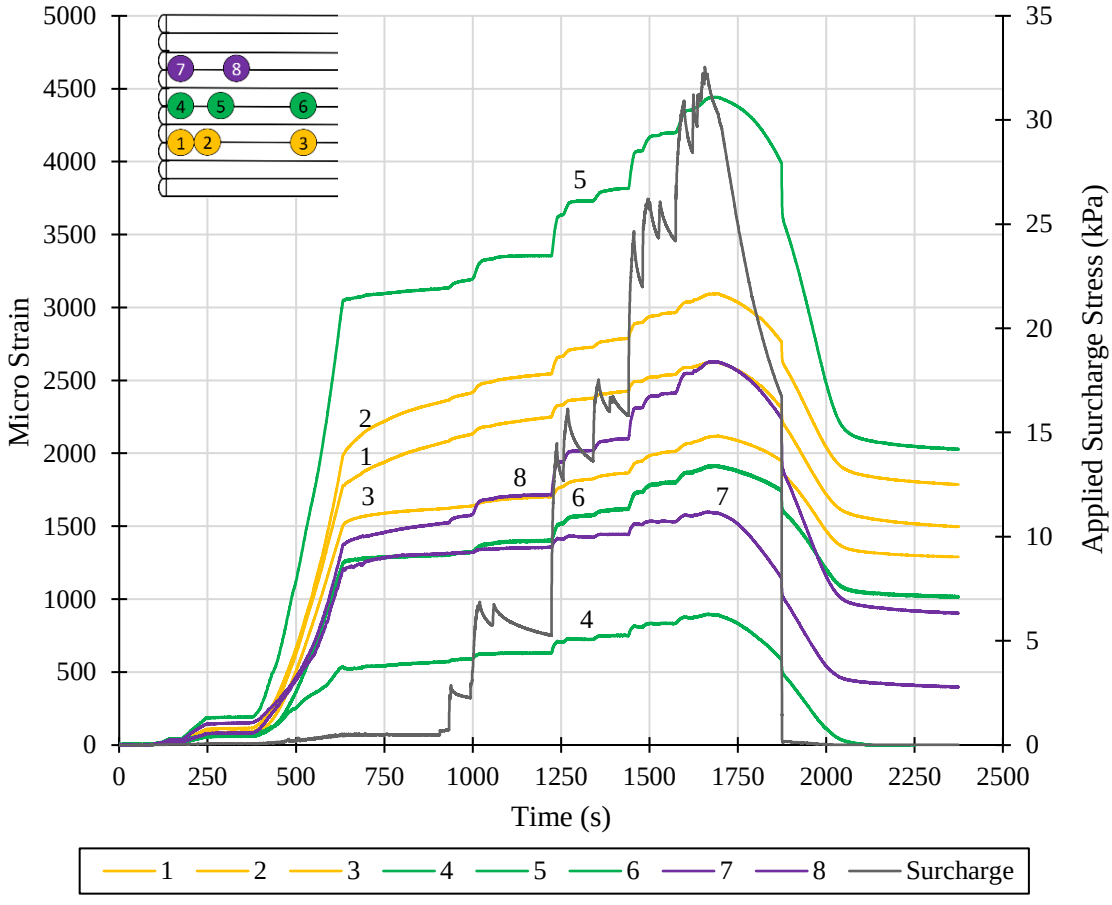

Figure 5-11. Applied surcharge stress and strain in extensible (PVC) reinforced soil wall test zeroed at 30 G.

The reinforcement strains that developed due to the application of the surface surcharge are presented in Figure 5-12. The strains are presented as a function of the stress applied. The stress-strain results were also plotted for each horizontal zone, namely:

1. Near the soil wall face (strain gauges 1, 4 and 7),
2. At the Coulomb failure plane (strain gauges 2, 5 and 8), and
3. Near the end of the reinforcement strip (strain gauges 3 and 6).

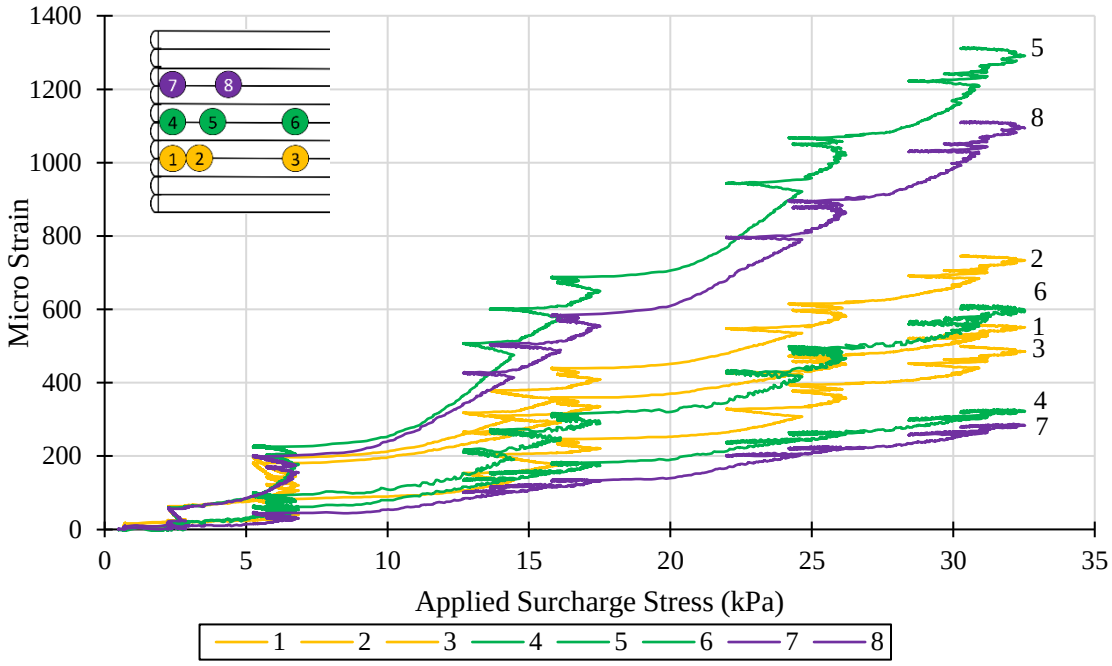

Figure 5-12. Stress-strain result in extensible (PVC) reinforced soil wall test.

It is possible to translate the measured reinforcement micro strains to tensile force, T in kN, from first principles:

$$T = \tau A \qquad \text{(Equation 5-1)}$$

And

$$\tau = E\varepsilon \qquad \text{(Equation 5-2)}$$

So that

$$T = E\varepsilon A \qquad \text{(Equation 5-3)}$$

Where:

E = 2.5 GPa and A = 0.8 mm^2 for the PVC strips.

The total tensile forces that developed along the reinforcements during the test were determined and converted to the equivalent prototype value with the scale factor n^2, where n = 30. The results are plotted for the applied surcharge stresses from 10 kPa to 30 kPa at 30 G at soil wall heights 3 m, 5 m, and 7 m in Figure 5-13, Figure 5-14, and Figure 5-15 respectively.

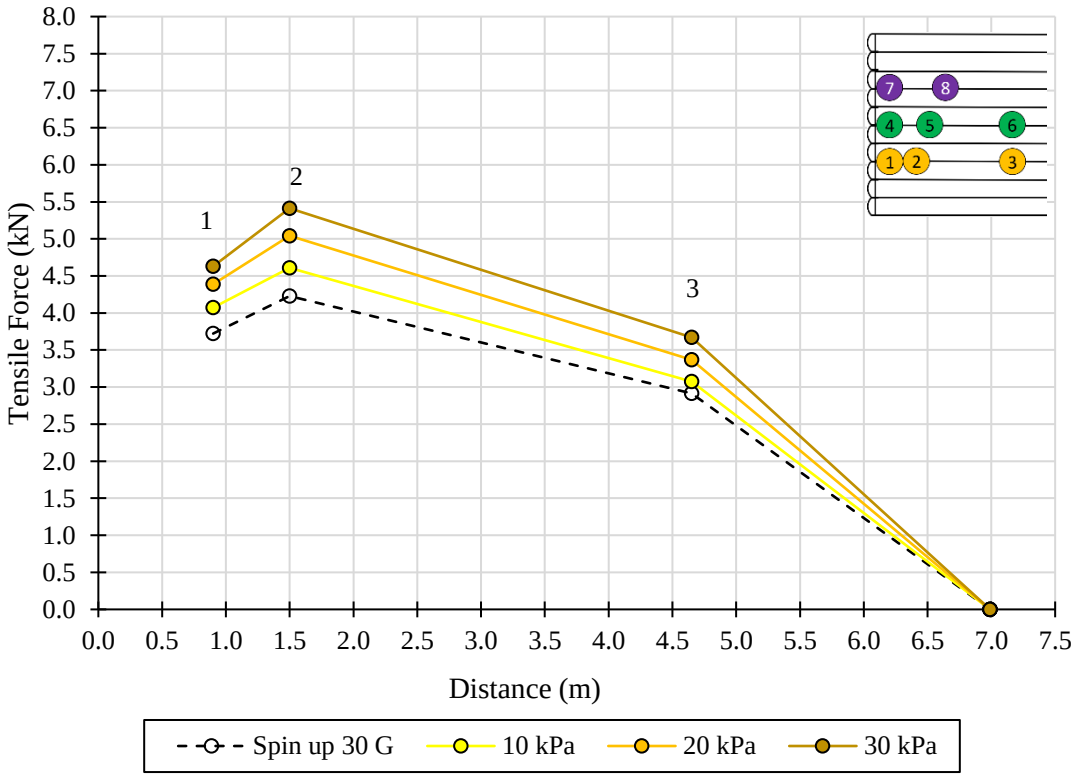

Figure 5-13. Extensible reinforcement tensile force development at 3 m soil wall height.

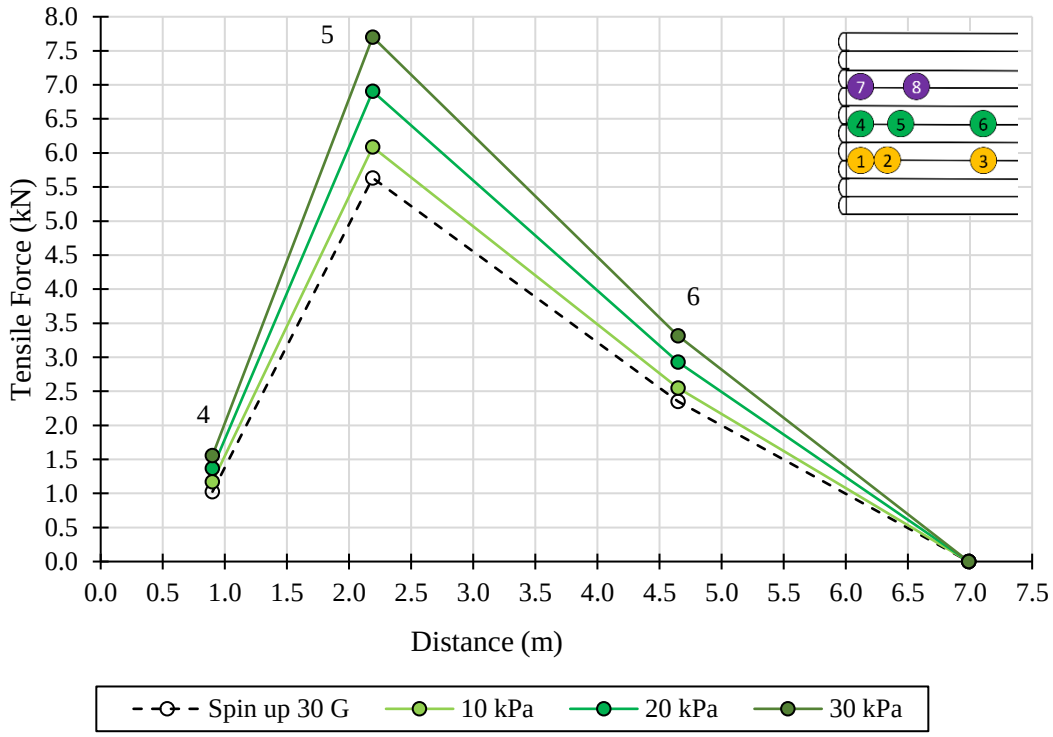

Figure 5-14. Extensible reinforcement tensile force development at 5 m soil wall height.

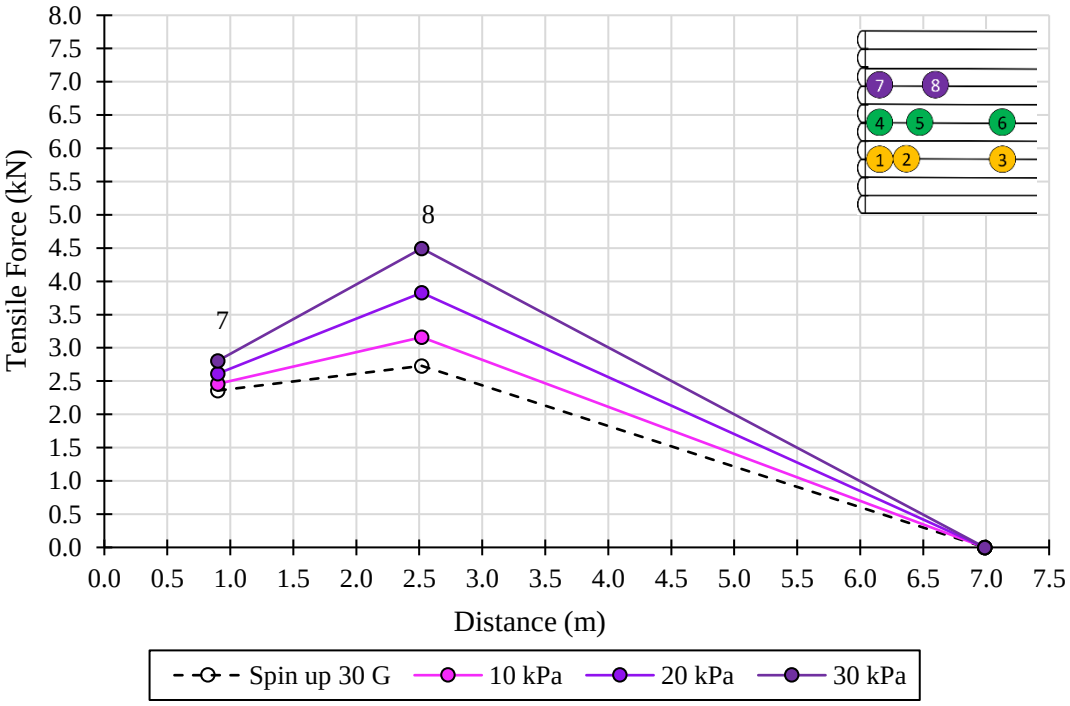

Figure 5-15. Extensible reinforcement tensile force development at 7 m soil wall height.

The largest tensile forces were recorded in the middle reinforcement along the Coulomb failure plane. The largest tensile forces due to centrifugal spin-up occurred along the Coulomb failure plane locations for all the reinforcement strips and are shown in Table 5-2. The self-weight forces calculated for the soil wall design in Chapter 3 are presented in Table 5-2 together with the tensile forces in the model reinforcements at 30 G for comparison. The theoretical tensile forces are considerably larger than the experimental results and indicate the theoretical design method is over-conservative. The maximum tension observed along the reinforcement strips at 30 kPa is shown together in Figure 5-16.

Table 5-2. Maximum tensile force at 30 G centrifugal acceleration in extensible reinforced soil wall.

Soil Wall Height	Model Max Tension (kN)	Theoretical Max Tension (kN)
3 m	4.2	29.1
5 m	5.6	21.8
7 m	2.7	14.5

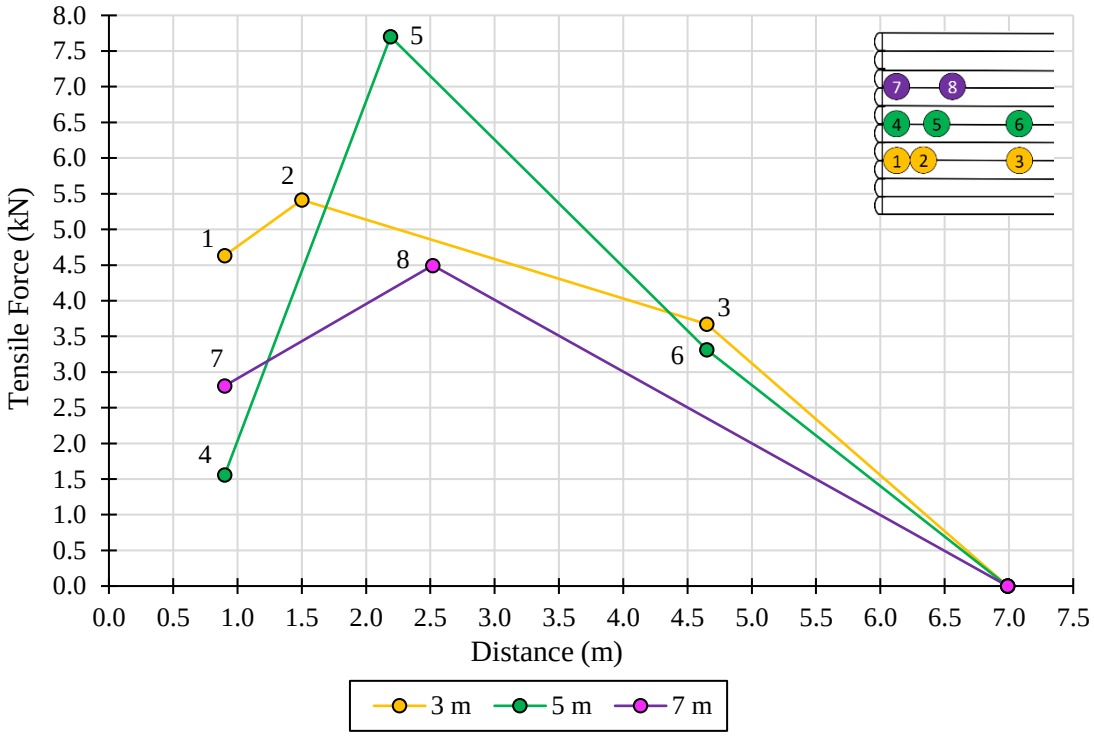

Figure 5-16. Extensible reinforcement tensile force development at 30 kPa stress.

The reinforcement strains recorded at the three soil wall heights for the three applied surcharge stresses 10 kPa, 20 kPa, and 30 kPa, are plotted together in Figure 5-17 to show the context of strain development throughout the height of the soil wall and along the length of the reinforcement strips. The soil wall heights are given for the prototype soil wall in metres.

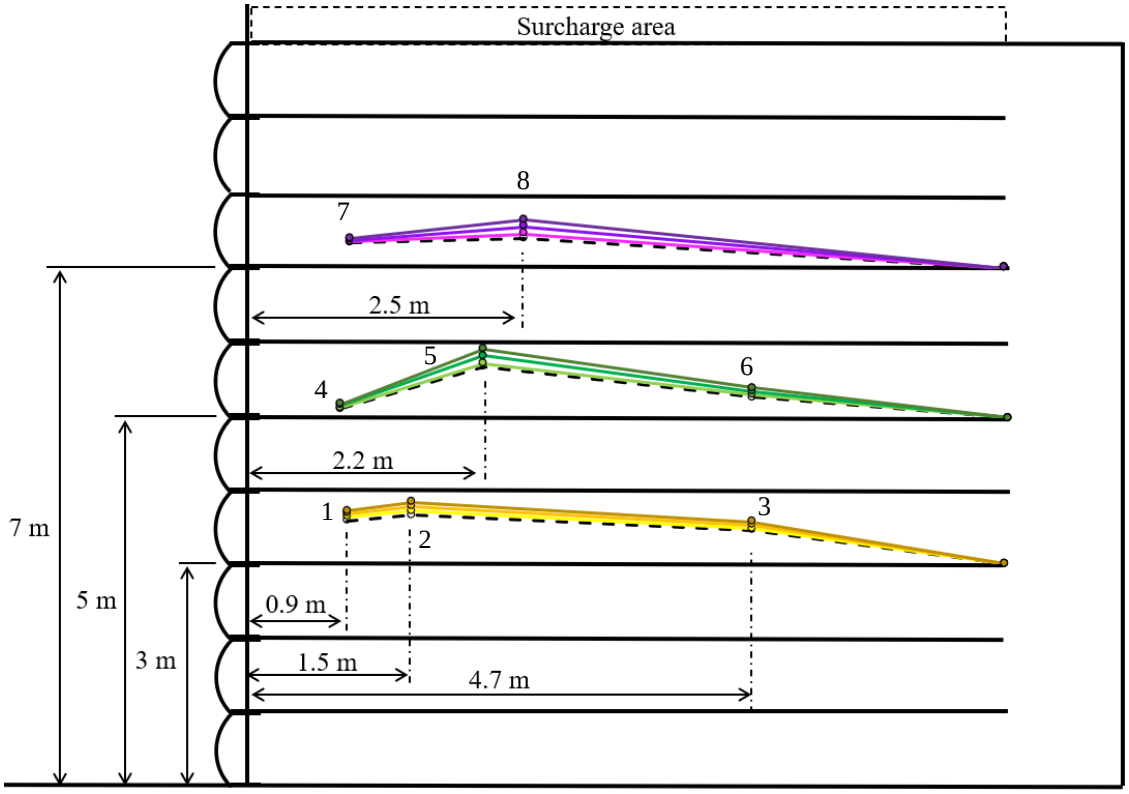

Figure 5-17. Representation of prototype soil wall cross-section with extensible reinforcement tensile force development under applied surcharge load.

5.3.2 Inextensible reinforcement

The inextensible reinforced soil wall test was conducted with the same procedure as in the extensible reinforced soil wall test. The surcharge load applied to the soil wall surface at the centrifugal acceleration of 30 G was converted to stress in kilopascals and was plotted with the strain response measured by the eight fibre Bragg gratings (FBGs) for the inextensible (brass) reinforcement test in Figure 5-18. The micro strain response was zeroed at 30 G in the figure.

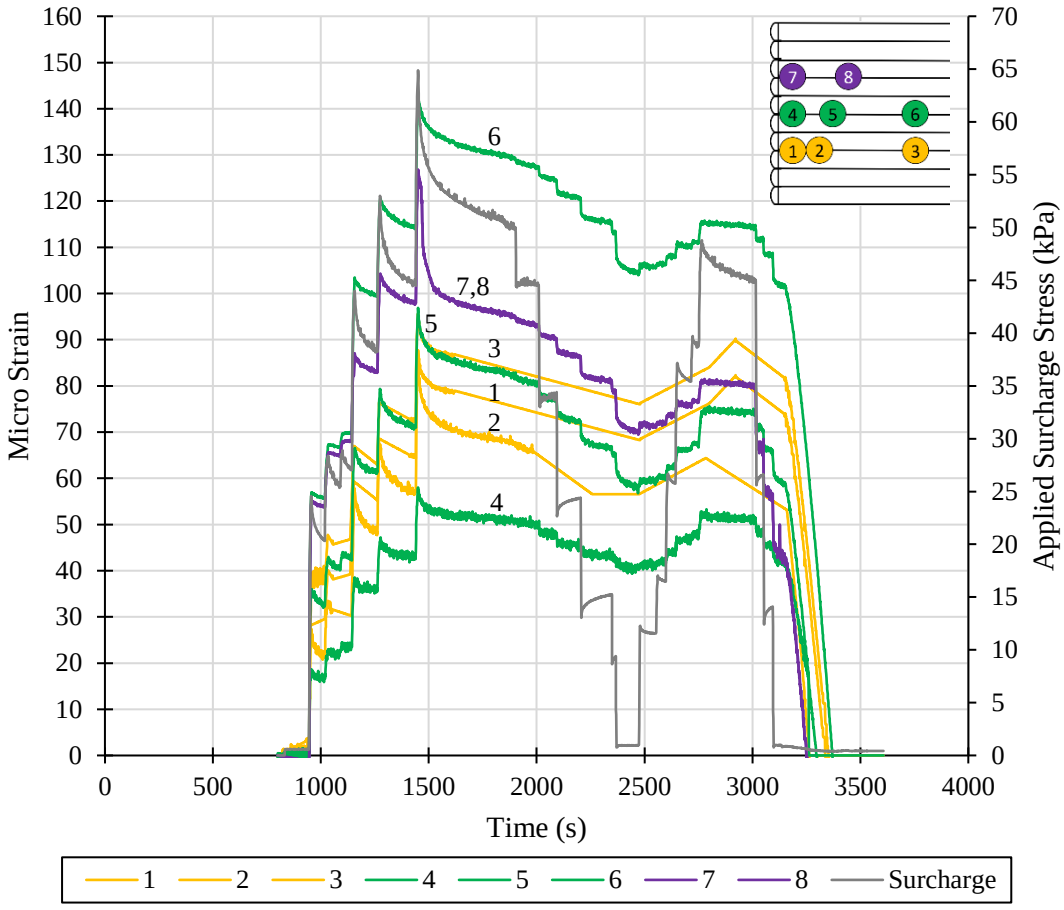

Figure 5-18. Applied surcharge stress and strain in inextensible (brass) reinforced soil wall test zeroed at 30 G.

The reinforcement strains observed as the direct result of having applied the surface surcharge are presented in Figure 5-19. The micro strain response was zeroed at 30 G in the figure. The largest strains due to the applied surcharge stress occurred at FBGs 6, 7 and 8. The strains are presented as a function of the stress applied. The stress-strain results were also plotted for each horizontal zone, namely:

1. Near the soil wall face (FBGs 1, 4 and 7),
2. At the Coulomb failure plane (FBGs 2, 5 and 8), and
3. Near the end of the reinforcement strip (FBGs 3 and 6).

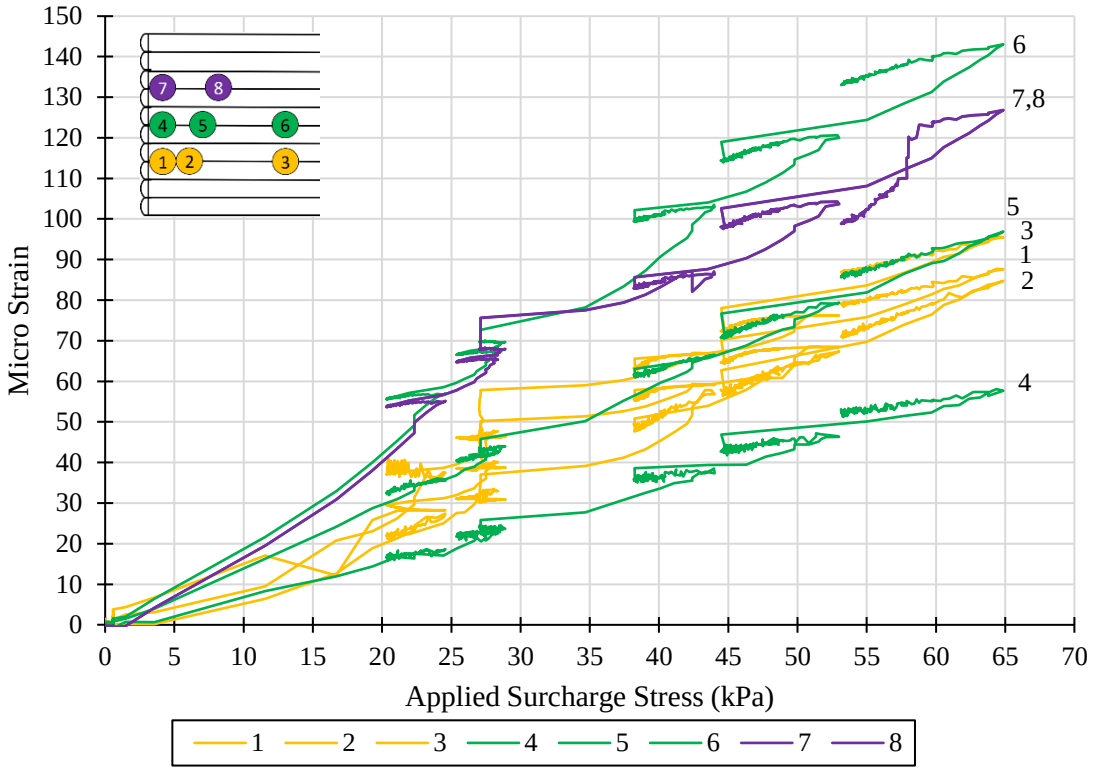

Figure 5-19. Applied stress-strain result in the inextensible (brass) reinforced soil wall test zeroed at 30 G.

The tensile forces in the inextensible reinforcements were determined using Equation 5-3, where:

E = 65 GPa and A = 0.8 mm^2 for the brass strips.

Similar to the extensible reinforce soil wall test, the total tensile forces that developed along the inextensible reinforcements were converted to the equivalent prototype value with the scale factor n^2, where n = 30. The results were plotted for the applied surcharge stresses in 10 kPa consecutive steps from 10 kPa to 60 kPa at 30 G. The results are shown in Figure 5-20, Figure 5-21, and Figure 5-22, at soil wall heights 3 m, 5 m, and 7 m respectively. Overall, similar reinforcement tensile forces were observed along the length of the reinforcement strips at each of the three soil wall heights indicating uniform resistances to strain.

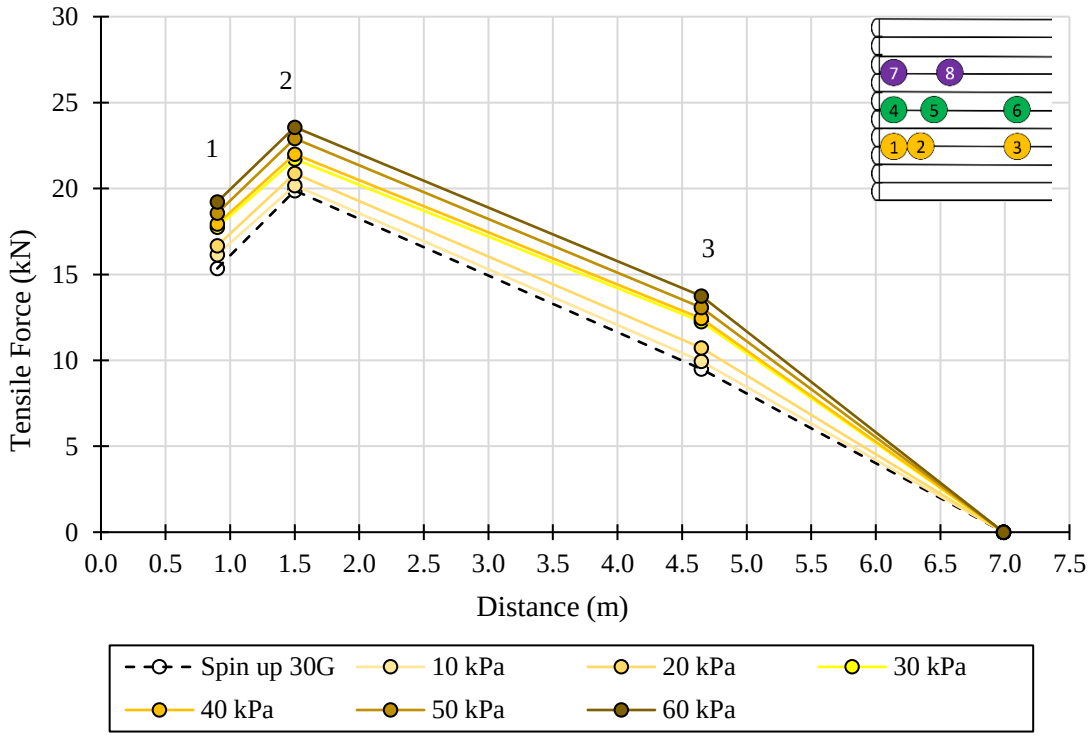

Figure 5-20. Inextensible reinforcement tensile force development at 3 m soil wall height.

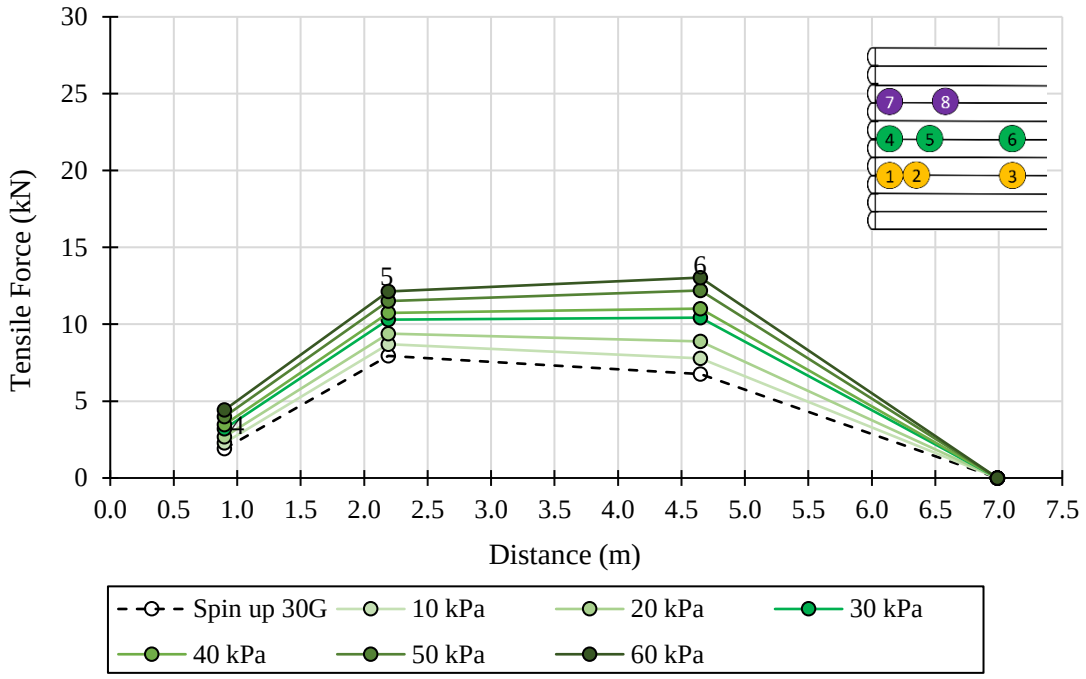

Figure 5-21. Inextensible reinforcement tensile force development at 5 m soil wall height.

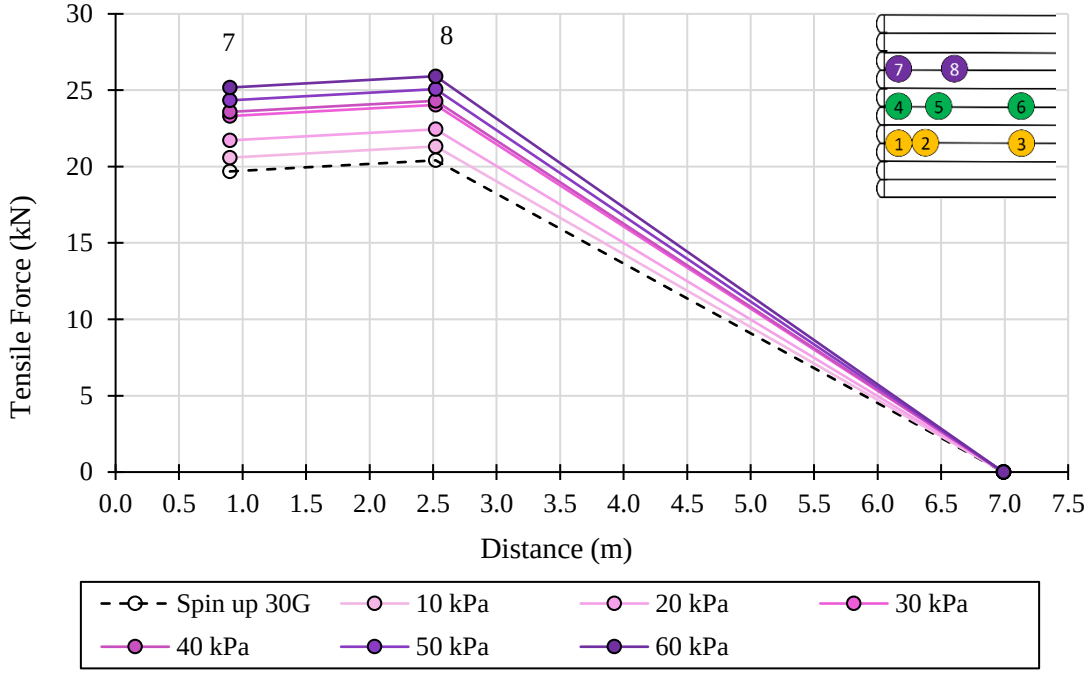

Figure 5-22. Inextensible reinforcement tensile force development at 7 m soil wall height.

The largest tensile forces overall were recorded along the Coulomb failure plane in the top reinforcement at 7 m wall height. The largest tensile forces due to centrifugal spin-up occurred along the Coulomb failure plane locations for all the reinforcement strips except at the middle of the soil wall. At 5 m soil wall height, the maximum tension occurred near the end of the reinforcement and the overall magnitudes of tension were significantly lower than at 3 m and 7 m soil wall height. The tensile forces in the reinforcements at 30 G were slightly less than the self-weight tensile forces calculated for the soil wall design in Chapter 3, except for the reinforcement at the 7 m layer. The tension in the reinforcement at 7 m soil wall height was 6 kN larger than the theoretical value and almost equal in magnitude to the tension at 3 m soil height. This indicates a consistent increase in forces across the height of the soil wall. The maximum tension at 30 G is shown in Table 5-3 and the maximum tension observed along the extensible reinforcement strips, at an applied surcharge stress of 30 kPa, are shown together in Figure 5-23.

Table 5-3. Maximum tensile force at 30 G centrifugal acceleration in inextensible reinforced soil wall.

Soil Wall Height	Model Max Tension (kN)	Theoretical Max Tension (kN)
3 m	19.9	29.1
5 m	7.9	21.8
7 m	20.4	14.5

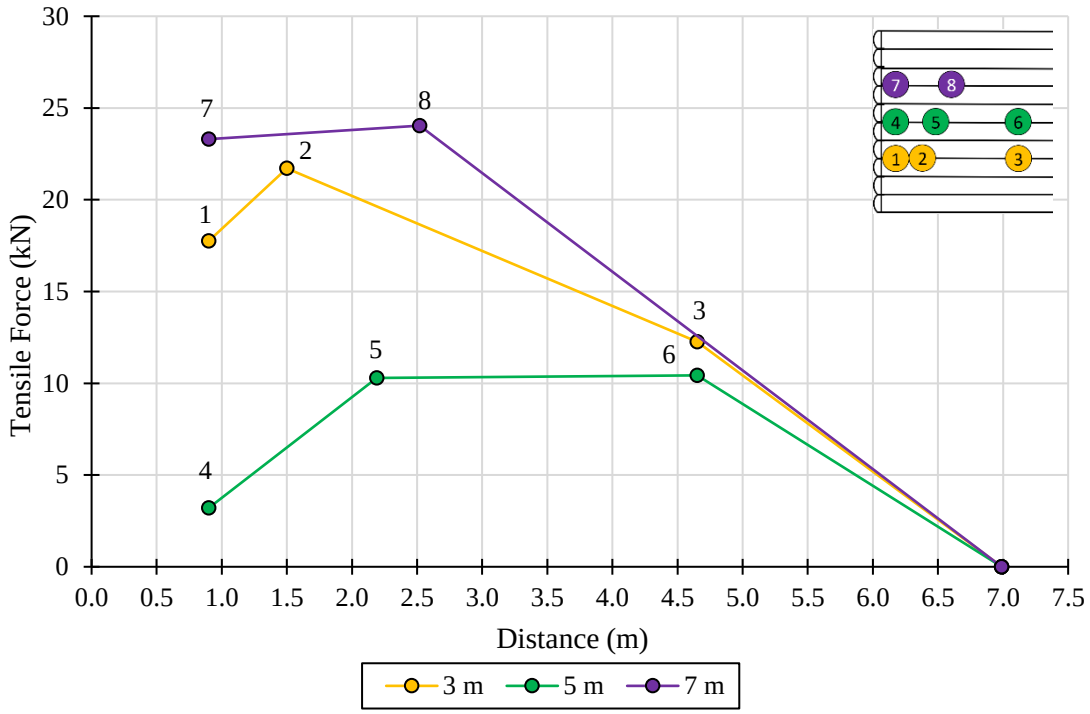

Figure 5-23. Inextensible reinforcement tensile force development at 30 kPa applied surcharge stress.

The reinforcement strains recorded at the three soil wall heights for three applied surcharge stresses at 10 kPa, 30 kPa, and 60 kPa, are plotted in cross-section in Figure 5-24**Error! Reference source not found.**. The cross-section of the soil wall shows the context of strain development throughout the height of the soil wall and along the length of the reinforcement strips. The soil wall heights are given for the prototype soil wall in metres.

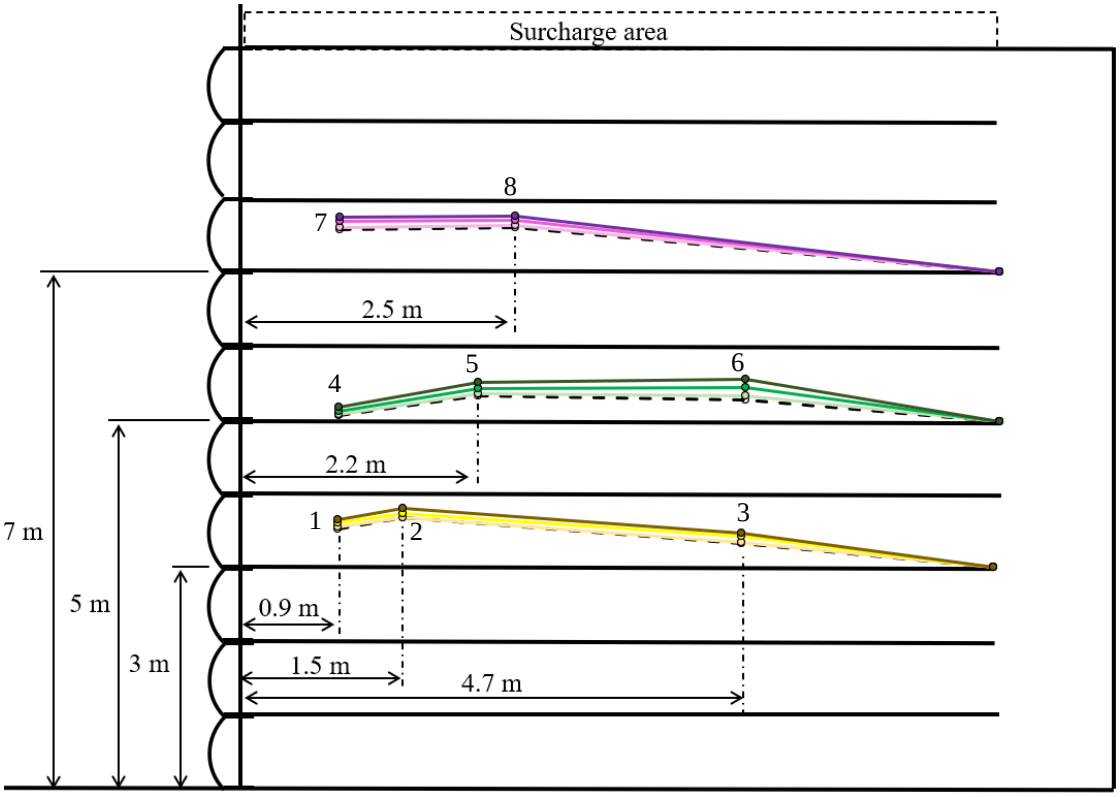

Figure 5-24. Representation of prototype soil wall cross-section with inextensible reinforcement tensile force development under applied surcharge load.

5.3.3 Extensible and inextensible reinforcement comparison

The results obtained in the extensible and inextensible tests are presented together in this section for comparison. The reinforcement strains that developed in both experiments for an applied surcharge stress from 0 kPa to 30 kPa are presented in Figure 5-25. The extensible (PVC) reinforcement strains are plotted with dashed lines for clarity. The difference in strain results between the two reinforced soil wall tests under the same applied surcharge stress is clearly observed. Overall, the extensible reinforced soil wall strained about one order of magnitude more than the soil wall reinforced with inextensible reinforcement under loading. The average of the strain results induced by the applied surcharge stress from 0 kPa to 30 kPa for both types of reinforced soil walls at each of the three soil wall layers are tabulated in Table 5-4.

Table 5-4. Average strain results for PVC and brass reinforced soil walls at applied surcharge stress from 0 kPa to 30 kPa.

Soil Wall Height	PVC Average Micro Strain	Brass Average Micro Strain
3 m	528	50
5 m	660	52
7 m	615	78

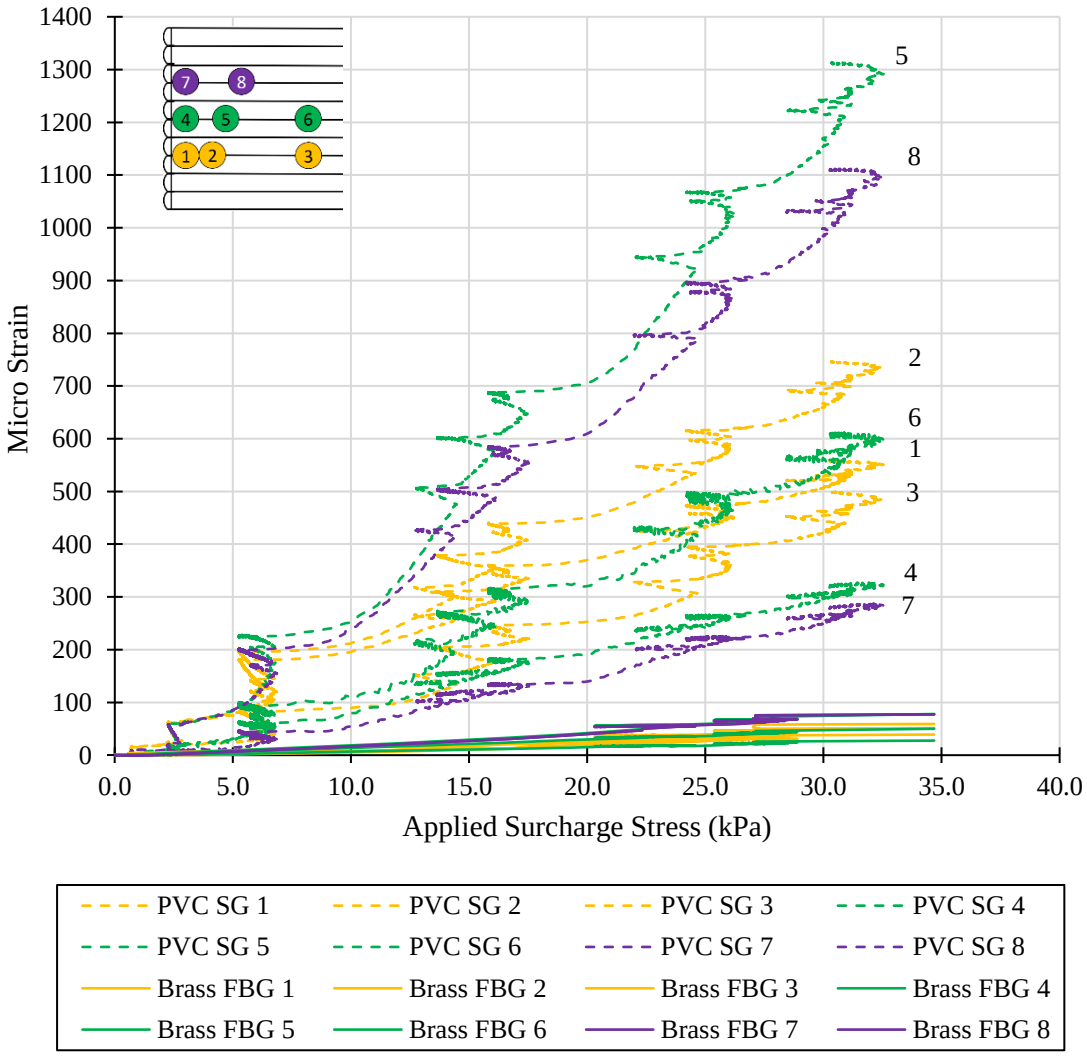

Figure 5-25. Extensible and inextensible reinforcement applied stress-strain curves.

The development of strains on the extensible and inextensible reinforcement due to the applied surcharge stress of 30 kPa is shown in Figure 5-26. Large strain peaks occurred in the PVC curves (dashed lines) at the theoretical maximum tension zones as opposed to the lower, flat strain curves in the brass results. The result demonstrates the large difference in total strain magnitude between the two soil wall types and the difference in behaviour of the two types of soil walls. Large strains developed in the PVC strips which indicated a ductile response to loading, increased deformation of the soil wall, and increased strain in the soil. Very low strains developed in the brass strips indicating brittle behaviour, caused low soil strains and wall facing deformation.

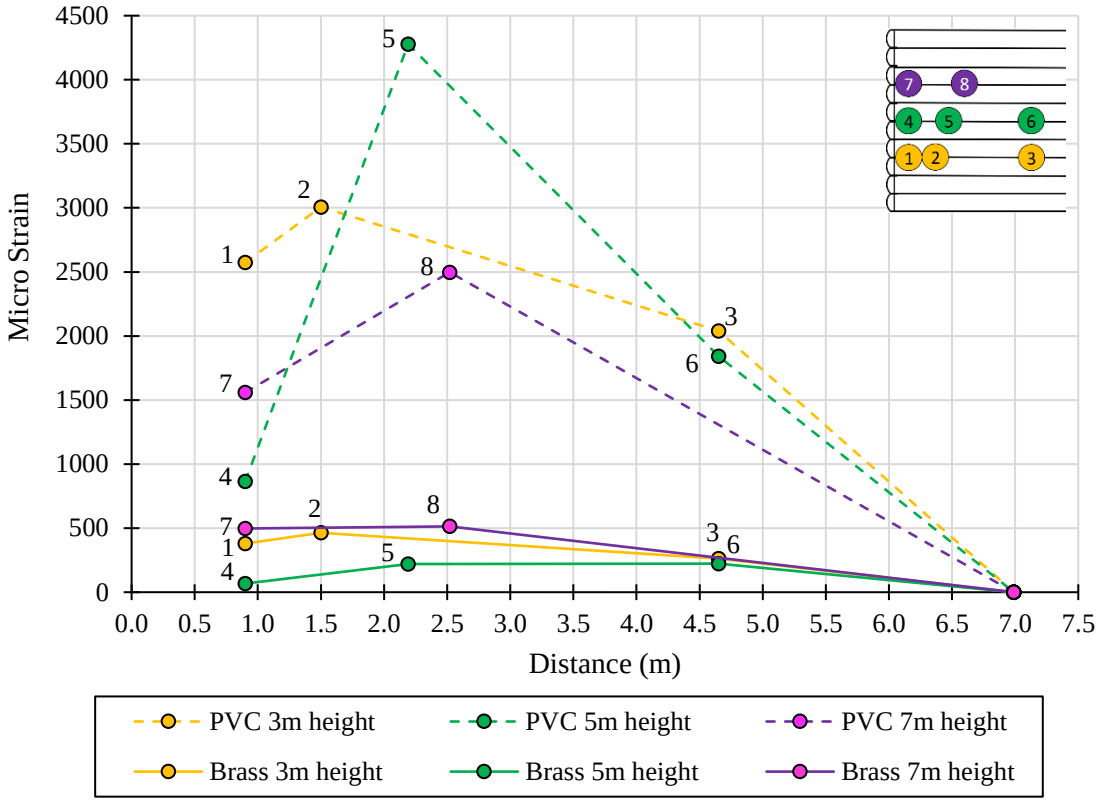

Figure 5-26. Extensible and inextensible reinforcement strain development at 30 kPa applied surcharge stress.

A similar comparison was made and presented in Figure 5-27 to show the development of the tensile forces that occurred along the reinforcement strips for both types of soil walls. It is interesting to note the inextensible brass reinforcment strips carried larger axial tensile forces than the extensible reinforcements. This is due to the higher axial stiffness of the brass reinforcement material. Larger loads were transferred to the inextensible reinforcements at the same magnitude of applied surcharge stress which resulted in lower overall soil wall strains and movement within the reinforced soil mass.

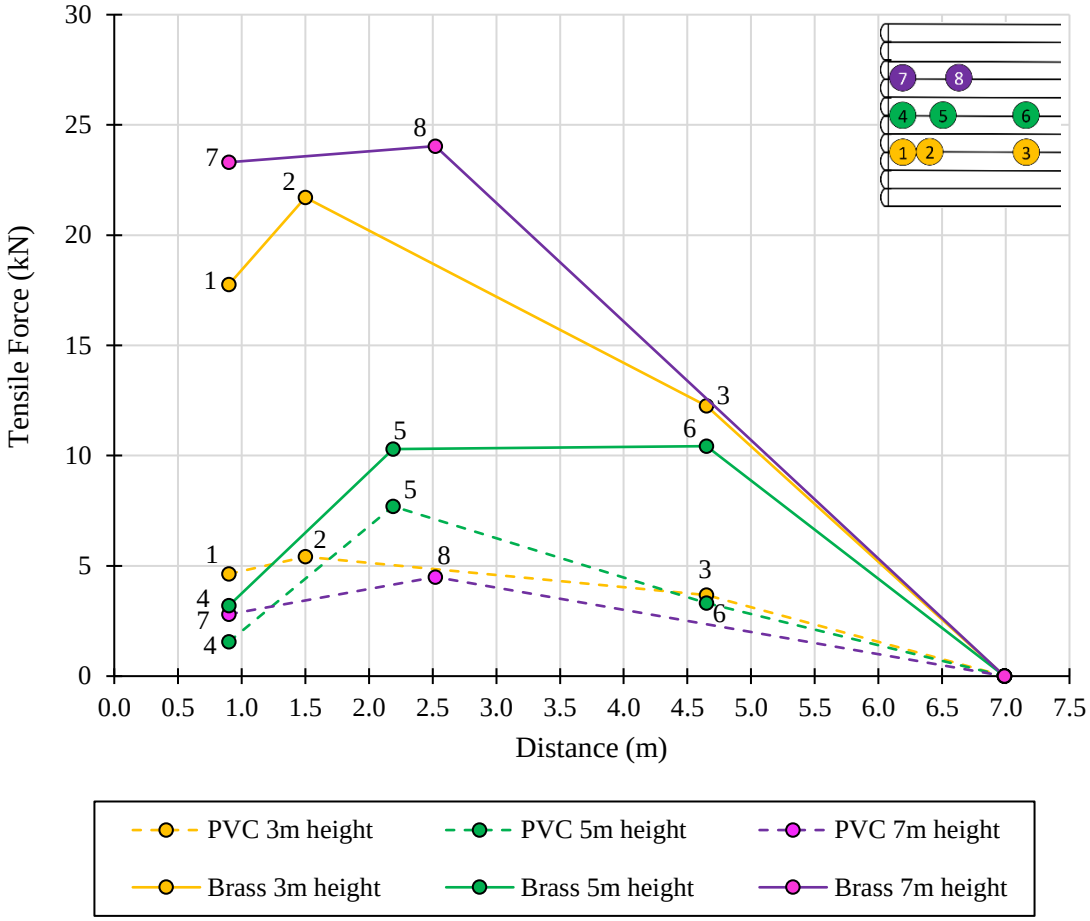

Figure 5-27. Extensible and inextensible reinforcement tension development at 30 kPa applied surcharge stress.

5.4 HORIZONTAL SOIL STRAINS USING PIV

Particle Image Velocimetry (PIV) analysis was used to track the horizontal displacement of the soil wall facing in terms of strain in the stress-strain tests. The same methodology followed in Chapter 4 for the load-displacement tests was used. Photographic images of the soil wall were taken at 5 second time intervals and photographs of the PVC reinforced soil wall and brass reinforced soil wall are shown in Figure 5-28 and Figure 5-29 respectively.

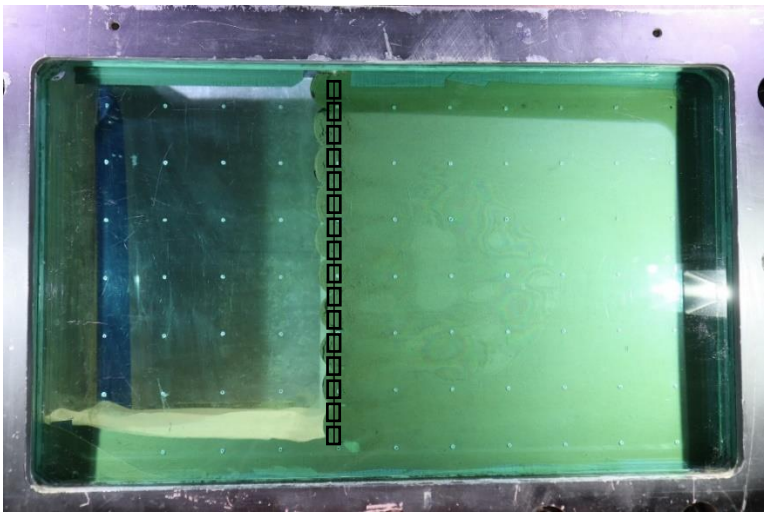

Figure 5-28. Photographic image taken during the PVC stress-strain soil wall test with PIV mesh.

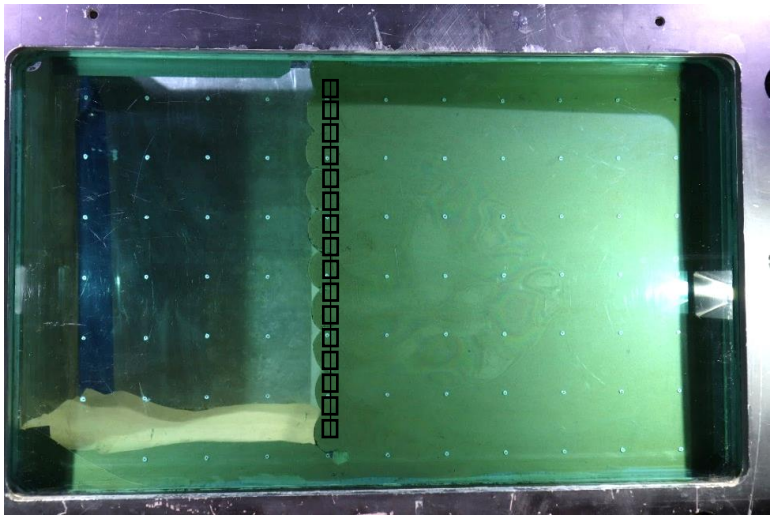

Figure 5-29. Photographic image taken during the brass stress-strain soil wall test with PIV mesh.

The test time was used to correlate the time the images were taken with the loading stage of the soil wall. Images starting at the loading stage of 0 kPa and ending at 30 kPa were analysed for horizontal strain at 5 kPa load increments. The strain analysis was done on the soil just behind the wall facing and the results are presented in Figure 5-30 and Figure 5-31 respectively. The horizontal soil strain results were plotted against the prototype wall height of 10 m and were plotted from right to left to mirror the direction of soil movement in the tests.

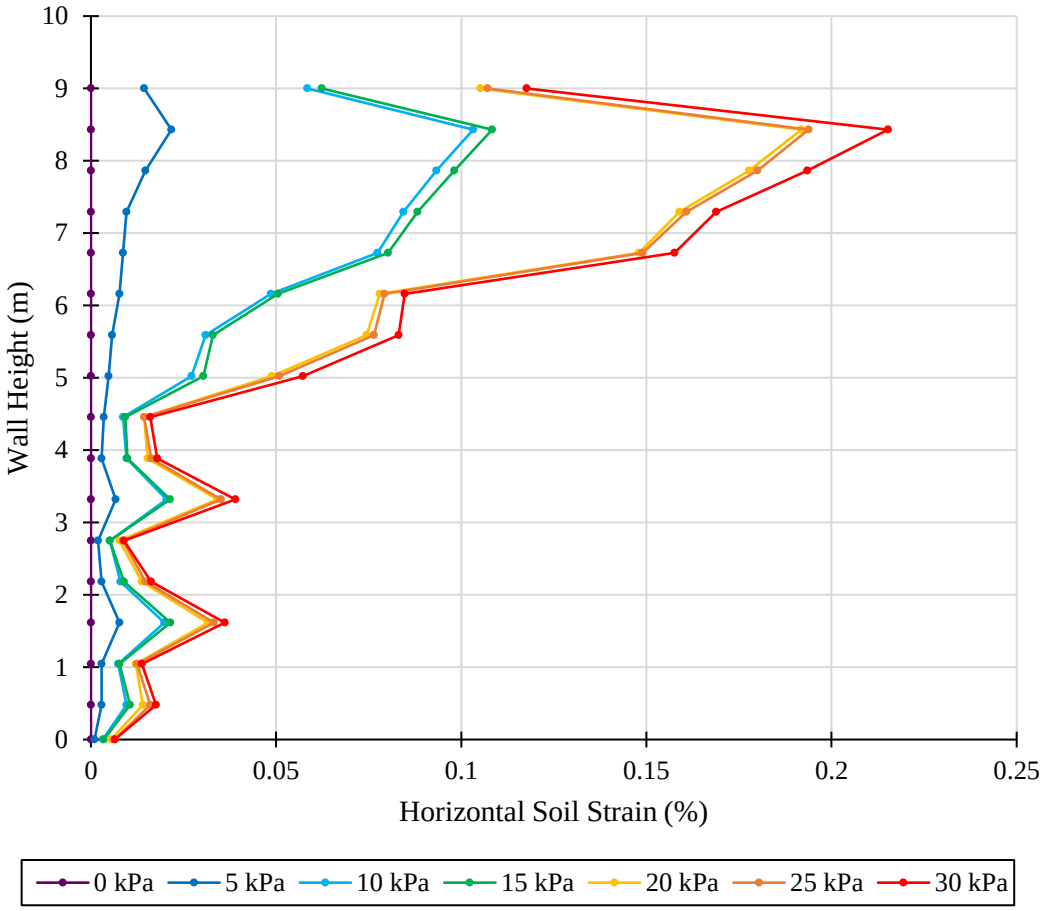

Figure 5-30. Horizontal soil strain percentage of PVC reinforced soil wall.

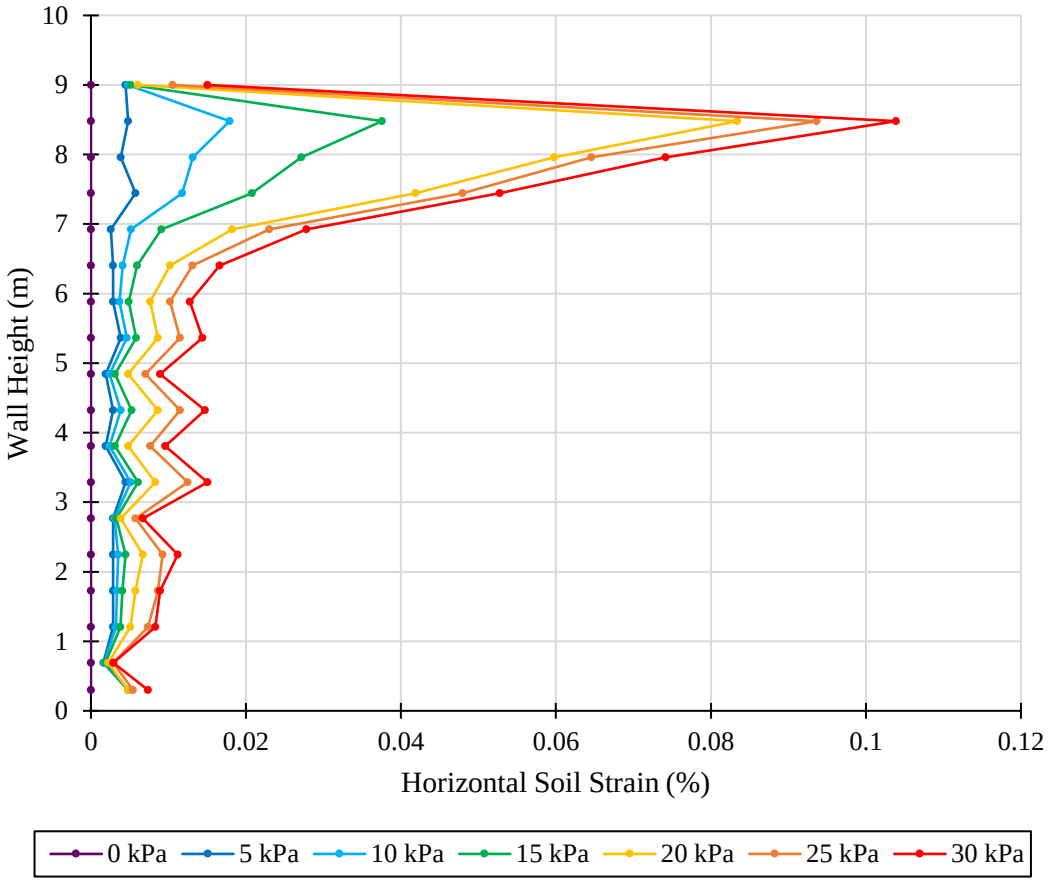

Figure 5-31. Horizontal soil strain percentage of brass reinforced soil wall.

Considering the horizontal soil strains results derived from the PIV analysis for the stress-strain tests, the following observations were made:

- The maximum horizontal soil strain occurred at 30 kPa and at 8.5 m soil wall height for both tests are presented in Table 5-5. Horizontal soil strain measured for PVC and brass at 30 kPa..Table 5-5 This is probably due to the fact that no reinforcement was installed at the top of the 10 m wall panel, which allowed excessive deformation.
- The PVC reinforced soil wall strained twice as much as the brass reinforced soil wall. This confirms the results observed in this study, that an inextensible reinforced soil wall resists displacement of the wall facing to a greater degree than a soil wall reinforced with extensible elements. The difference in strains determined by the PIV analysis was, however, not as significant as the results from the strain instruments. One possible explanation for this is the PIV analysis was done on the soil particles at the edge of the window, whereas the strain instruments were installed on the centre reinforcement strips. The soil particles may have strained less at the sides of the model.

Table 5-5. Horizontal soil strain measured for PVC and brass at 30 kPa.

Test	Max Soil Strain (%)	Normalised Strain (Δx/H)
1. PVC at 30 kPa	0.215	0.02
2. Brass at 30 kPa	0.104	0.01

- The largest increase in soil strains in the PVC reinforced soil wall started to increase from 4.5 m wall height, whereas the largest strains increased from 6.5 m height in the brass reinforced soil wall. This means more than half of the PVC soil wall facing had strained a significant amount at 30 kPa. The brass reinforced soil wall, on the other hand, remained relatively rigid under loading and only reflected larger strains at the top of the facing.
- The normalised horizontal strains correspond well with those presented in the literature from Bathurst *et al* (2010) and fall well within the FHWA (2008) and AASHTO (2009) design guidelines, as well as for the *SANS 207:2011* guideline for a safe maximum of 2% for semi-elliptical steel face walls.
- The deflected wall shapes for both types of soil wall at 15 kPa and 30 kPa are shown in Figure 5-32 in terms of horizontal strain. The brass reinforced soil wall deflected the most above 7 m wall height, whereas the PVC reinforced soil wall started to exhibit large strains from 4 m wall height. The soil wall reinforced with the PVC reinforcement strips deflected to slightly over 0.2% horizontal strain, whereas the soil wall reinforced with brass strips deflected to just over 0.1% strain at 30 kPa load.
- The soil wall reinforced with brass strips was twice as strong as the PVC reinforced soil wall at 30 kPa and both walls exhibited stronger performance compared to the results observed in the load-displacement tests at similar loading. This indicates the importance of backfill design as the soil was compacted in the stress-strain tests and resulted in stronger soil wall behaviour.

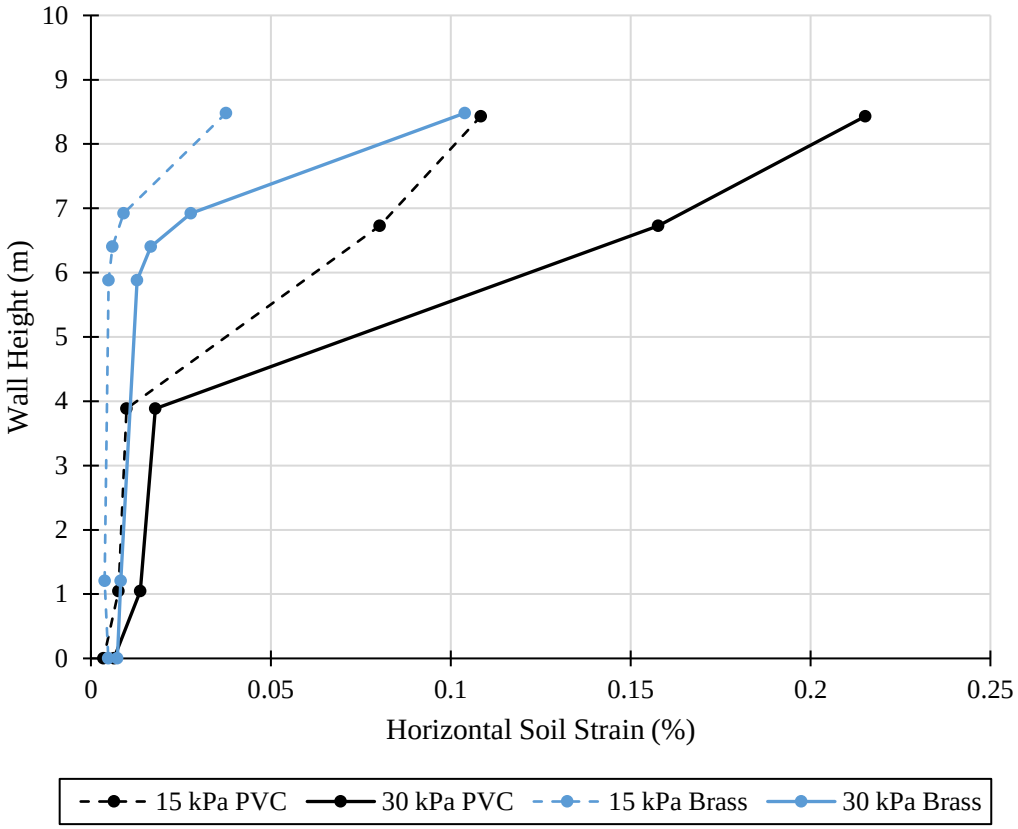

Figure 5-32. Comparison of horizontal soil strain between PVC and brass soil walls.

It is worth noting the load-displacement and stress-strain horizontal strain results could not be directly compared due to the following differences:

- Different backfill densities were used. Compacted backfill soil was used in the stress-strain tests.
- A larger load block was used in the stress-strain tests that applied the 30 kPa surcharge over a greater surface area.
- No LVDT instrumentation was used in the stress-strain tests.

5.5 CHAPTER SUMMARY

Two vertical soil wall stress-strain tests were conducted in the geotechnical centrifuge at an acceleration of 30 G. The surcharge load was applied to the top surface of the soil wall and the resulting strains that developed in the reinforcement elements were measured with strain instrumentation. The first soil wall was constructed with extensible reinforcement in the form of PVC strips and the second soil wall was reinforced with inextensible reinforcement, namely brass strips.

The stress-strain test results for the extensible (PVC) reinforced soil wall and the inextensible (brass) reinforced soil wall were presented in this chapter. The extensible reinforcement strips were instrumented with eight strain gauges and the inextensible reinforcement strips were instrumented with eight fibre Bragg gratings (FBGs). The strain instruments were fastened at 3 m, 5 m, and 7 m prototype soil wall heights and in three horizontal zones located along the lengths of the reinforcement strips. The soil walls were loaded to 30 kPa surcharge load at 30 G centrifugal acceleration and the observations are summarised as follows:

- The extensible reinforced soil wall total reinforcement micro strains ranged from 866 to 4278 and the inextensible reinforced soil wall total reinforcement micro strains ranged from 68 to 514 at an applied surcharge stress of 30 kPa.
- The reinforcement strains in the extensible reinforced soil wall were one order of magnitude larger than the strains that developed in the inextensible reinforcement elements.
- The lowest total reinforcement strains were recorded near the facing at mid-height (5 m) of the soil wall for both tests.
- The largest total reinforcement tension occurred at mid-height (0.5H) of the extensible reinforced soil wall and at the top (0.7H) of the inextensible reinforced soil wall. This finding corresponds to the maximum reinforcement tension observed at 0.6H by Holtz and Lee (2002).
- The soil wall behaviour with extensible reinforcement was classified as flexible due to the lower reinforcement axial tension forces and peak reinforcement strains at the Coulomb failure plane. The results confirm the theory that the maximum strains and maximum tension forces occur at the Coulomb failure plane locations in the soil wall.
- The soil wall behaviour with inextensible reinforcement was classified as rigid due to the higher reinforcement axial tension forces and consistently low reinforcement strains that developed along the length of the reinforcement strips. The results also confirm the theory that the maximum strains and maximum tension forces occur at the Coulomb failure plane locations in the soil wall.

- The tensile force results indicate the reinforcement tension design method was over-conservative for the extensible reinforcement and not applicable for the inextensible reinforced soil walls. The tension in the inextensible reinforced soil walls developed consistently throughout the height of the soil wall and were larger than theoretically expected. This confirms the non-plastic (rigid) behaviour expected in inextensible reinforced soil walls.
- The horizontal strains of the soil just behind the soil wall facing determined by PIV analysis showed twice as much resistance to displacement when the soil wall was reinforced with inextensible reinforcement.

6 CONCLUSIONS AND RECOMMENDATIONS

6.1 CONCLUSIONS

Four reduced scale reinforced soil walls were constructed and tested in the geotechnical centrifuge at the University of Pretoria. The models were prepared and tested to investigate the difference in performance of vertical soil walls reinforced with either extensible or inextensible reinforcement. The models were instrumented to monitor the horizontal facing displacement and the reinforcement strains that developed under loading. The experiments were separated into two groups, namely the load-displacement tests that investigated the displacement of the wall facing, and the stress-strain tests that studied the development of reinforcement strains and tensile forces. The amount of reinforcement that was selected to construct the soil walls was based on the necessary resistance to self-weight, to the common practice identified in the literature, and according to the guidelines made in the British and South African standards. The reinforcements were placed in one metre horizontal and vertical spacings, and the magnitude of axial reinforcement stiffness, provided by real-life reinforcement strips, were scaled down to the equivalent reinforcement stiffness for the soil wall models.

The following conclusions were made from the load-displacement tests:

1. The horizontal displacement of the wall facing reinforced with extensible reinforcement displaced eight times more than the wall facing reinforced with inextensible reinforcement. The maximum displacement of the prototype equivalent of the extensible soil wall was 53.2 mm at 100 kPa surcharge load, whereas the inextensible soil wall prototype equivalent displaced 6.8 mm at 100 kPa.
2. The top half of the wall facing displaced twice as much as the bottom half for both types of reinforced soil walls.
3. The soil wall reinforced with inextensible reinforcement produced four times the wall stiffness and resistance to deformation than the soil wall reinforced with extensible reinforcement.
4. The inextensible reinforced soil wall at 80 kPa surcharge displaced the same amount as the soil wall with extensible reinforcement at 15 kPa surcharge load.
5. Both soil wall types deformed the most at the top of the soil wall facing.
6. The horizontal soil strain of the loose soil reinforced with extensible reinforcement was an order of magnitude greater than the soil strains reinforced with inextensible reinforcement. The maximum horizontal soil strain of the extensible reinforced soil wall was 4.07% and 0.456% for the inextensible reinforced soil wall at 100 kPa surcharge.

7. The behaviour of the soil wall reinforced with PVC strips can be classified as flexible and extensible, whereas the behaviour of the soil wall reinforced with brass strips can be classified as rigid and inextensible.

The following conclusions were made from the stress-strain tests:

1. For both types of reinforced soil walls, the largest reinforcement strains were recorded at the Coulomb failure plane (theoretical maximum tension), followed by the strain instruments at the wall facing, and the lowest strains were measured near the end of the reinforcement strips.
2. The reinforcement strain progression along the lengths of the extensible reinforcement were adequately described by the Coulomb failure plane. The reinforcement strains peaked at the theoretical maximum tension locations in the extensible reinforcement, whereas the inextensible reinforcement strains developed relatively consistently along the full length of the reinforcement strips.
3. The extensible reinforcement strains were in most cases one order of magnitude larger than the inextensible reinforcement. At 30 kPa applied surcharge stress, the average overall extensible reinforcement micro strain was 2333, whereas the average inextensible reinforcement micro strain was only 329 for the eight strain instruments.
4. The large strains in the extensible reinforcement and tension force peaks at the Coulomb failure plane locations indicated flexible, ductile soil wall behaviour, whereas the low strains in the inextensible reinforcement and consistent tension forces along the length of the reinforcement indicated rigid, brittle soil wall behaviour.
5. Both soil wall types deformed the most at the top of the soil wall facing.
6. The largest total reinforcement tension occurred at mid-height (0.5H) of the extensible reinforced soil wall and at the top (0.7H) of the inextensible reinforced soil wall. This finding corresponds to the maximum reinforcement tension observed at 0.6H by Holtz and Lee (2002).
7. The tensile force results indicate the reinforcement tension design method was over-conservative for the extensible reinforcement and not applicable for the inextensible reinforced soil walls. The tension in the inextensible reinforced soil walls developed consistently throughout the height of the soil wall and were larger than theoretically expected. This confirms the non-plastic (rigid) behaviour expected in inextensible reinforced soil walls.
8. The maximum horizontal soil strain determined with the PIV analysis was 0.215% for the extensible reinforced soil wall and 0.104% for the inextensible reinforced soil wall at 30 kPa surcharge. One possible explanation for this is the PIV analysis was done on

the soil particles at the edge of the window, whereas the strain instruments were installed on the centre reinforcement strips. The soil particles may have strained less at the sides of the model.

6.2 RECOMMENDATIONS

6.2.1 Industry

The results concluded and presented in this study show the extensible reinforcing with flexible facing soil walls exhibit flexible behaviour and should not be used for applications where soil wall movement is not permissible. The extensible reinforced soil walls can however be used in applications with high allowable displacement, such as for storing temporary material, and where no surcharge loads are expected on top of the soil wall. It is recommended minimal surface loads are applied to soil walls with flexible facing and extensible reinforcement since the loads cause significant deformation of the wall.

Soil walls under applied loading with flexible facing and inextensible reinforcement, however, show small amounts of deformation to the soil wall. It is therefore also recommended no surcharge loads are applied to the wall unless the application allows for small amounts of soil wall deformation. The surcharge loads are then to be limited well within the design guideline limits to avoid sudden failure.

6.2.2 Future research work

There exists a multitude of variations to the work done in this study due to the possible combinations of the soil wall components, as well as the variations that exist in the design of the soil wall components themselves. One interesting future study, based on the work done in this report, would entail investigating the amount of geosynthetic reinforcement required to match the performance of the inextensible reinforced soil wall. Further possible research experiments would investigate how the wall facing and backfill soil affect the performance of the soil walls. Perhaps the geosynthetic reinforcement would provide better resistance with a fine backfill material.

7 REFERENCES

Archer, A. (2014). Using small-strain stiffness to predict the settlement of shallow foundations on sand. Masters thesis, University of Pretoria, Pretoria.

Babu, G.L. (2007). Reinforced soil retaining walls design and construction. Lecture 31, Indian Institute of Science. Bangalore.

Bagir, T. (1944). Iraq Journal, pp.5-6.

Bathurst, R.J., Miyata, Y. and Allen, T.M. (2010). Facing displacements in geosynthetic reinforced soil walls. Earth Retention Conference 3, ASCE Geo-Institute, 1-4 August 2010. Bellevue, Washington.

Bathurst, R.J., Vlachopoulos, N., Walters, D.L., Burgess, P.G. and Allen, T.M. (2006). The influence of facing stiffness on the performance of two geosynthetic reinforced soil retaining walls. Canadian Geotechnical Journal, 43(12), pp.1225.

Berry, A.D. and Byrne, G. (2008). A guide to practical geotechnical engineering in Southern Africa, 4th ed. Franki Africa (Pty) Ltd.

British Standards Institution (2010). Code of practice for strengthened/reinforced soils and other fills. BS8006:2010. British Standards Institution, London.

Bonaparte, R. and Schmertmann, G. (1988). Reinforcement extensibility in reinforced soil wall design. In: P. Jarret and A. McGown, ed., The Application of polymeric reinforcement in soil retaining structures, 1st ed. New York: Kluwer Academic Publishers, pp.409-457.

Bourgeois, E., Soyez, L., and Le Kouby, A. (2011). Experimental and numerical study of the behaviour of a reinforced-earth wall subjected to a local load. Computers and Geotechnics, 38, pp.515-525.

Coulomb, C.A. (1776). Essai sur une application des regeles des maximus et minimus a quelque problemes de statique relative a l'architecture. Memoirs Divers Savants, 7, Academie Sciences, Paris (in French).

Da Silva, T.S. (2017). Centrifuge modelling of the behaviour of geosynthetic-reinforced soils over voids. PhD thesis, University of Cambridge, Cambridge.

Da Silva, T.S., Elshafie, M.Z.E.B. and Sun, T. (2016). Fibre optic instrumentation and calibration in the geotechnical centrifuge. 3rd European Conference on Physical Modelling in Geotechnics (Eurofuge 2016), 3-6 June 2016. Nantes, France.

Gaudin, C., White, D.J., Boylan, N., Breen, J., Brown, T. and De Catania, S. (2010). A miniature high speed data acquisition system for geotechnical centrifuges. Proceedings of the

7th International Conference on Physical Modelling in Geotechnics 2010, Zurich, Switzerland, pp.229-234, Taylor and Francis Group, London.

Gaudio, D., Masini, L. and Rampello, S. (2018). A performance-based approach to design reinforced-earth retaining walls. Geotextiles and Geomembranes, 46, pp.470–485.

Holtz, R.D. and Lee, W.F. (2002). Internal stability analyses of geosynthetic reinforced retaining walls. Department of Civil and Environmental Engineering, Seattle: University of Washington.

Ingold, T. S. (1982). Reinforced Earth. 1st ed. London: Thomas Telford Ltd.

Jacobsz, S.W. (2013). Centrifuge modelling of a soil nail retaining wall. Journal of the South African Institution of Civil Engineering, 55(1), pp.85-93.

Jacobsz, S.W., Kearsley, E.P. and Kock, J.H.L. (2014). The geotechnical centrifuge facility at the University of Pretoria. 8th International Conference on Physical Modelling in Geotechnics, January 2014. Perth, Australia.

Jayashree, J., Nithesh, N., Parthiban, M., Sakthi Ganesh, C. and Sangeetha, S. (2017). Study on interface friction between sand and geotextile. International Journal of Engineering Research and Modern Education, pp.124-126.

Jones, C.J.F.P. (1985). Earth reinforcement and soil structures, 1st ed. London: Butterworth and Co. Ltd.

Juran, I. and Christopher, B. (1989). Laboratory model study on geosynthetic reinforced soil retaining walls. Journal of Geotechnical Engineering, 115(7), pp.905-926.

Juran, I. and Schlosser, F. (1978). Theoretical analysis of failure in reinforced earth structures. Proceedings of the Symposium on Earth Reinforcement, ASCE Convention. Pittsburgh, pp.528-555.

Kapogianni, E., Sakellariou, M.G., Laue, J. and Springman, S.M. (2010). The use of optical fibre sensors in a geotechnical centrifuge for reinforced slopes. 7th International Conference on Physical Modelling in Geotechnics. Zurich, Switzerland.

Kikumoto, M., Nakai, T., Hossain, S., Ishii, K., Watanabe, A. and Zhang, F. (2010). Mechanical behavior of geosynthetic-reinforced soil retaining wall. American Society of Civil Engineers, 207, pp.310-317.

Knappett, J.A. and Craig, R.F. (2012). Craig's soil mechanics, 8th ed. New York: Spon Press.

Lienhart, W., Moser, F., Schuller, H. and Schachinger, T. (2014). Reinforced earth structures at Semmering Base tunnel – construction and monitoring using fibre optic strain measurements. 10th International Conference on Geosynthetics, 21-25 September 2014. Berlin, Germany.

Masini, L., Callisto, L. and Rampello, S. (2015). An interpretation of the seismic behaviour of reinforced-earth retaining structures. Geotechnique, 65(5), pp.349–358.

McKittrick, D.P. (1978). Reinforced Earth: Applications of Theory and Research to Practice. Sydney: New South Wales Institute of Technology.

Moraci, N. and Recalcati, P. (2006). Factors affecting the pullout behaviour of extruded geogrids embedded in a compacted granular soil. Geotextiles and Geomembranes, 24, pp.220-242.

Okechukwu, S.I, Okeke, O.C, Akaolisa, C. C. Z, Jack, L. and Akinola, A.O. (2016). Reinforced earth: Principles and applications in engineering construction. International Journal of Advanced Academic Research, 2(6), pp.14-33.

South African Bureau of Standards (2011). The design and construction of reinforced soils and fills. SANS 207:2011. South African Bureau of Standards, Pretoria.

Saran, S. (2010). Reinforced Soil and its Engineering Applications, 2nd ed. New Delhi: I.K. International Publishing House Pvt. Ltd.

Schofield, A.N. (1980). Cambridge geotechnical centrifuge operation. Geotechnique, 30(3), pp.227-268.

Smith, I. (2006). Smith's Elements of Soil Mechanics, 8th ed. Edinburgh: Blackwell Publishing.

Steiner, R. S. (1975). Reinforced earth bridges highway sinkhole. Civil Engineering. American Society of Civil Engineers, pp.54-56.

Taylor, R.N. (1995). Geotechnical centrifuge technology. Blackie Academic and Professional, Glasgow.

Tatsuoka, F., Tateyama, M., Uchimura, T. and Koseki, J. (1997). Geosynthetic-Reinforced Soil Retaining Walls as Important Permanent Structures. Geosynthetics International, 4(2), pp.81-136.

Tatsuoka, F. (2019). Geosynthetic-reinforced soil structures for railways and roads: development from walls to bridges. Innovative Infrastructure Solutions, 4(1), pp.41-62.

Terzaghi, K. (1943). Theoretical Soil Mechanics. 1 ed. New York: John Wiley & Sons.

U.S. Department of Transport (2001). Mechanically stabilized earth walls and reinforced soil slopes design and construction guidelines. FHWA-NHI-00-043.

Vidal, H. (1966). La terre armee. Annles. Inst. Tech. du Batim. 19(1), pp.223-224.

Voet, M.R.H., Nancey, A. and Vlekken, J. (2005). Geodetect: a newstep for the use of Fibre Bragg Grating technology in soil engineering. 17th International Conference on Optical Fibre Sensors. Proceedings of SPIE Vol. 5855.

Watanabe, K., Munaf, Y., Koseki, J., Tateyama, M. and Kojima, K. (2003). Behaviour of several types of model retaining walls subjected to irregular excitation. Soils found, 43(5), pp.13-27.

Werneck, M.M., Allil, R.C.S.B., Ribeiro, B.A. and de Nazare, F.V.B. (2013). A guide to Fiber Bragg Grating Sensors. Current Trends in Short- and Long-period Fiber Gratings. Cuadrado-Laborde, C (ed.), IntechOpen, London.

Ziegler, M. (2016). Geosynthetic reinforcement applications. In Proceedings of the 6th European Geosynthetics Congress, pp.173-206, Ljubkjana, Slovenia.

APPENDIX A

EVALUATION FORM

UNIVERSITY OF PRETORIA
DEPARTMENT OF CIVIL ENGINEERING
MARKING SHEET FOR UNDERGRADUATE RESEARCH PROJECT REPORTS

Student:			
Minimum requirements – the project report will be referred back if it does not meet the following requirements:			
The student identified, assessed, formulated and solved a complex problem (ECSA GA1)		The report is of a professional quality and appearance (ECSA GA6)	
The student applied fundamental knowledge to solve an engineering problem (ECSA GA2)		The student is aware of the impact of engineering activities on the environment and the community (ECSA GA7)	
The student solved the complex problem systematically (ECSA GA3)		The student worked independently to submit a unique research report (ECSA GA9)	
The student designed an experiment, interpreted and derived information from data (ECSA GA4)		Project is largely the students own work. Student should clearly indicate his/her own work. (ECSA GA10)	
The student used appropriate methods and computer technology to solve the problem (ECSA GA5)		The report is submitted by the specified date. (ECSA GA10)	

❑

❑ **Marks**					
❑ 30% Very Bad	❑ 45% Bad	❑ 55% Acceptable	❑ 65% Good	❑ 75% Distinction	❑ 90% Exceptional

	Factors taken into account during evaluation:	**MAXIMUM MARKS**	**MARKS**
1	Problem definition		
2	Literature review (relevance, completeness, critical evaluation)		
3	Design of experiment		
4	Execution of experiment		
5	Presentation of results		
6	Analysis of results		
7	Evaluation of results		
8	Conclusions		
9	Recommendations		
10	Technical content		
11	Layout of report		
12	Style of writing		
13	Originality		
14	Level of difficulty		
15	Neatness of report		
16	General impression		
Final mark		100	

COMMENTS

Examiner: Date: